Argonne NATIONAL LABORATORY

ANL/RTR/TM-24/13

# PARET/ANL v7.7 Verification and Validation Report

Nuclear Science & Engineering Division

ANL/RTR/TM-24/13

# PARET/ANL v7.7 Verification and Validation Report

prepared by

A. P. Olson, M. Kalimullah, M. Sharabi, S. Yang, J. R. Rudolph, J. R. Licht, and J. W. Thomas

Nuclear Science and Engineering Division, Argonne National Laboratory

March 2025

(This page left intentionally blank)

# Abstract

This report documents the software testing which has been performed for the PARET/ANL version 7.7 software. The software testing is based on code capabilities identified by research reactor analysts as frequently used in their safety analyses. The verification and validation procedures have been performed and documented to address the steady-state capabilities of the software, as described in Chapter 2, and the transient capabilities, as described in Chapter 3. Testing based on the comparison between PARET/ANL calculations and analytical solutions, hand calculations, or other code calculations of the test cases confirms that all the identified capabilities of the software were implemented correctly. In addition, results from code comparisons against SPERT-I and SPERT-IV experiments for various flow rates are reported for the peak power, energy release and cladding surface temperature. The comparisons showed overall good agreement for the peak power and conservative predictions of the cladding surface temperature.

# Table of Contents

# List of Figures

# List of Tables

# 1 Introduction

## 1.1 Overview of Code Development

The PARET/ANL computer code was originally created in 1969 [1] at Argonne-West in Idaho, which is now part of Idaho National Laboratory (INL), to analyze accidents caused by reactivity insertion events in reactor cores cooled by light or heavy water and with fuel composed of either plates or pins. PARET/ANL can also be used to analyze reactors with fuel assemblies having curved fuel plates when the radius of curvature for each plate is large compared to the plate thickness. Development of the PARET/ANL code [2], [3] has continued at Argonne National Laboratory (ANL) for use in the U.S. Department of Energy National Nuclear Security Administration Reactor Conversion Program to analyze the expected transient behavior of a large number of reactors.

PARET/ANL models the various fueled regions of a reactor core as channels. Each of these channels consists of a single flat fuel plate or pin (including cladding and, optionally, a gap) surrounded with water coolant. In the case of plate-type fuel elements, the coolant channels on each side of the plate have identical dimensions (with mirror symmetry). There can be many channels, which are not required to have identical dimensions, but each channel is thermal hydraulically independent and coupled to the whole core only through reactivity feedback effects. PARET/ANL was originally developed to model reactors cooled by an open loop, which was adequate for rapid transients in pool-type cores.

The time-dependent differential equations that represent the system are replaced by an equivalent set of finite-difference equations in space and time. These are integrated numerically. PARET/ANL uses the solution method developed by Cohen [4] to solve the point-kinetics equations. This same numerical scheme is used to integrate the point-kinetics equations in RELAP5-3D [5]. Heat removal from each PARET/ANL channel occurs in solid materials by conduction perpendicular to the direction of coolant flow and by convection within the coolant channels using a one-dimensional, thermal hydraulics model. Material properties such as heat capacity and thermal conductivity in solid materials are temperature dependent. Coolant properties such as enthalpy, density, thermal conductivity and viscosity are temperature and pressure dependent. These parameters are used in determining friction factors and heat transfer coefficients. For any given problem, the code first determines the steady-state solution for the initial state. Then the solution of the transient is obtained by integration in time and space.

PARET/ANL contains logic models for trips on period, power, and flow. It contains a model for decay heat after shutdown, and a model for control rod reactivity versus time or position. Feedback reactivity effects from coolant density changes and temperature changes are represented by coefficients and/or tables. Feedback reactivity from fuel heat-up (Doppler Effect) is represented by a four-term polynomial in powers of fuel temperature. Delayed neutron group data are provided by tabular input. Photo-neutrons produced in beryllium or in heavy water may be included in the point-kinetics equations by using additional delayed neutron groups.

## 1.2 Code Capabilities and Verification Approaches

As shown in Table 1.1, a set of 15 capabilities were selected for verification, intended to reflect the most commonly used code features. Each code capability is verified through comparisons with analytical solutions, hand calculations, other code calculations of the test cases, and experimental

measurements. The code capabilities are organized into two general categories, general and transient. The nine general capabilities (A1 - A9) are used both in the steady-state and transient portions of a calculation; the six transient capabilities (B1 - B6) are specific to the transient portion of the calculation. In addition, integral verification and validation (V&V) of PARET/ANL's capabilities were tested by comparison to SPERT-I and SPERT-IV reactor experiments, included in Table 1.1 as "capability" C1.

Each capability identified in Table 1.1 has one or more test cases that were used to verify its functionality. Each of these test cases are listed in the third column of Table 1.1, and are described in detail in Sections 2, 3, and 4. Some test cases are used to test more than one capability, and thus may appear multiple times in the table.

Development of PARET/ANL is controlled by the Argonne RTR Software Quality Assurance Plan (SQAP), which complies with ASME NQA-1 2008 with the 2009 addenda [6]. There was an extensive effort to formalize the V&V case for PARET/ANL v7.6 and qualify it for use under the SQAP. Most of the test cases in Table 1.1, including their corresponding acceptance criteria, were established and documented in the PARET/ANL v7.6 V&V Report [7]. As part of the software development process that followed, acceptance testing is regularly performed to ensure that the modified software produces results that satisfy the acceptance criteria established for PARET/ANL v7.6. By corollary, this process ensures that PARET/ANL v7.7 maintains agreement with the original comparisons to analytical solutions, hand calculations, other code calculations, and experimental measurements. The subset of test cases used for such acceptance testing have a checkmark in the fourth column of Table 1.1. The acceptance criteria for acceptance testing—which feature tighter tolerances than the original comparisons to analytic solutions, other code calculations, and experimental measurements—are described in Appendix A .

Additional test cases have been added to the test suite since the PARET/ANL v7.6 qualification. Cases C01_01 through C01_05, which include comparisons to SPERT-I and SPERT-IV tests as described in Section 4, have been added to further strengthen the software's V&V case. Furthermore, test cases have been added to test software modifications, including A05_11 through A05_16. It may be necessary to change the acceptance criteria, i.e., if the modification fixes a bug in PARET/ANL v7.6. For PARET/ANL v7.7, there was a bug fix related to steady-state initialization for cores that feature downflow (see Section 2 of the User Guide [2]), which resulted in a test case, A05_01, that exceeded the acceptance criteria. These updates to PARET/ANL v7.6 are noted in the fifth column of Table 1.1. Blank cells in this column indicate that the test case and acceptance criteria have not changed since PARET/ANL v7.6.

Because the acceptance testing process provides reasonable assurance that PARET/ANL v7.7 code predictions are consistent with those from PARET/ANL v7.6, tables and figures in Sections 2 and 3 were not regenerated with PARET/ANL v7.7.

More information about the capabilities listed in Table 1.1 can be found in the User Guide [2].

This report is not comprehensive in the PARET/ANL V&V scope; many other exercises have been performed over its development history that are omitted here.

**Table 1.1. Code Capabilities and Test Cases Used for Verification**

| Capability | Description | | Test Case | Acceptance test | Changes Since v7.6 |
|---|---|---|---|---|---|
| **General Capabilities** | | | | | |
| **A1** | **Coolant properties** | Light water | A01_01 | ✓ | |
| | | | A01_02 | ✓ | |
| | | | A01_03 | ✓ | |
| | | | A01_04 | ✓ | |
| | | | A01_05 | ✓ | |
| | | | A01_06 | ✓ | |
| | | | A01_07 | ✓ | |
| | | | A01_08 | ✓ | |
| | | | A01_09 | ✓ | |
| | | | A01_10 | ✓ | |
| | | | A01_11 | ✓ | |
| | | Heavy water | A01_12 | ✓ | |
| | | | A01_13 | ✓ | |
| | | | A01_14 | ✓ | |
| | | | A01_15 | ✓ | |
| | | | A01_16 | ✓ | |
| | | | A01_17 | ✓ | |
| | | | A01_18 | ✓ | |
| | | | A01_19 | ✓ | |
| | | | A01_20 | ✓ | |
| | | | A01_21 | ✓ | |
| | | | A01_22 | ✓ | |
| **A2** | **Solid material thermal properties** | | A02_01 | ✓ | |
| **A3** | **Geometry options** | Fuel plate (IGEOM = 0) | A03_01 | ✓ | |
| | | Fuel rod (IGEOM = 1) | A03_02 | ✓ | |
| | | Fuel plate (IGEOM = 2) | A03_03 | ✓ | |
| **A4** | **Forced flow or buoyancy-driven flow** | IFLOW = 1 | A04_01 | ✓ | |
| | | IFLOW = 3 | A04_02 | ✓ | |
| | | IFLOW = 4 | A04_03 | ✓ | |
| | | IFLOW = 5 | A04_04 | | |
| | | | A04_05 | ✓ | |
| **A5** | **Single-phase heat transfer correlations** | Laminar | A05_01 | ✓ | Modified in v7.7 (bug fix) |
| | | | A05_02 | ✓ | |
| | | | A05_03 | ✓ | |
| | | Transition | A05_04 | ✓ | |
| | | Turbulent | A05_05 | ✓ | |
| | | | A05_06 | ✓ | |
| | | | A05_07 | ✓ | |
| | | | A05_08 | ✓ | |
| | | | A05_09 | ✓ | |
| | | | A05_10 | ✓ | |
| | | | A05_16 | ✓ | New in v7.7 |
| | | Transient Rosenthal & Miller | A05_11 | ✓ | New in v7.7 |
| | | | A05_12 | ✓ | New in v7.7 |

| | | | | | |
|---|---|---|---|---|---|
| | | | A05_13 | ✓ | New in v7.7 |
| | | | A05_14 | ✓ | New in v7.7 |
| | | | A05_15 | ✓ | New in v7.7 |
| **A6** | **Factor used for fin or bundle effect** | | A05_05 | ✓ | |
| | | | A05_06 | ✓ | |
| | | | A06_01 | ✓ | |
| | | | A06_02 | ✓ | |
| **A7** | **Boiling Heat Transfer** | Subcooled nucleate boiling heat transfer | A02_01 | ✓ | |
| | | | A07_01 | ✓ | |
| | | Transition boiling heat transfer | A07_02 | ✓ | |
| | | | A07_03 | ✓ | |
| **A8** | **Friction factor model** | Re ≤ 2000 | A08_01 | ✓ | |
| | | | A08_02 | ✓ | |
| | | 2000 < Re ≤ 100,000 | A08_03 | ✓ | |
| | | Re > 100,000 | A08_04 | ✓ | |
| **A9** | **Steady-state initialization** | | A05_01 | ✓ | |
| | | | A09_01 | | |
| **Transient Capabilities** | | | | | |
| **B1** | **Point kinetic model** | With step reactivity insertion | B01_01 | | |
| | | | B01_02 | | |
| | | | B01_03 | | |
| | | | B01_04 | | |
| | | | B01_05 | ✓ | |
| | | | B01_06 | | |
| | | | B01_07 | | |
| | | | B01_08 | | |
| | | | B01_09 | | |
| | | | B01_10 | | |
| | | | B01_11 | | |
| | | | B01_12 | | |
| | | | B01_13 | | |
| | | | B01_14 | | |
| | | | B01_15 | | |
| | | | B01_16 | | |
| | | | B01_17 | | |
| | | | B01_18 | | |
| | | | B01_19 | | |
| | | | B01_20 | | |
| | | With ramp reactivity insertion | B01_21 | ✓ | |
| | | | B01_22 | | |
| | | | B01_23 | | |
| | | | B01_24 | | |
| | | | B01_25 | | |
| | | | B01_26 | | |
| | | | B01_27 | | |
| | | | B01_28 | | |
| | | With feedback | B01_29 | ✓ | |
| **B2** | **Reactivity feedback** | Moderator | B02_01 | ✓ | |
| | | | B02_02 | | |
| | | | B02_03 | | |

| | | | | | |
|---|---|---|---|---|---|
| | | | B02_04 | | |
| | | | B02_05 | | |
| | | Doppler Effect | B02_06 | ✓ | |
| | | | B02_07 | | |
| | | | B02_08 | | |
| | | Thermal expansion | B02_09 | ✓ | |
| | | | B02_10 | | |
| | | | B02_11 | | |
| **B3** | **Reactor trips and Delay time** | Over-power trip | B03_01 | ✓ | |
| | | Period trip | B03_02 | ✓ | |
| | | Low flow trip | B03_03 | ✓ | |
| | | | B03_04 | ✓ | |
| **B4** | **Control rod reactivity** | | B04_01 | ✓ | |
| **B5** | **Decay heat** | | B05_01 | | |
| | | | B05_02 | | |
| | | | B05_03 | | |
| | | | B05_04 | | |
| | | | B05_05 | ✓ | |
| | | | B05_06 | ✓ | |
| | | | B05_07 | | |
| | | | B05_08 | | |
| **B6** | **Power-driven mode** | | B06_01 | | |
| | | | B06_02 | | |
| | | | B06_03 | ✓ | |
| **Integral V&V Exercises** | | | | | |
| **C1** | **SPERT-IV reactor experiments benchmarks** | | C01_01 | ✓ | New in v7.7 |
| | | | C01_02 | ✓ | New in v7.7 |
| | | | C01_03 | ✓ | New in v7.7 |
| | | | C01_04 | ✓ | New in v7.7 |
| | | | C01_05 | ✓ | New in v7.7 |

The acceptance criteria used in test cases for validation of PARET/ANL results require engineering judgement. They depend on the complexity of the modeled physical phenomena, the geometrical simplification of the reactor, and the accuracy of the data used in the comparisons. The adopted acceptance criteria used in the V&V of PARET/ANL test cases are listed in Table 1.2.

For problems with simple thermal hydraulics, neutronics and geometries, for which analytical solutions are available, an acceptance criterion between 0.1-1% is adopted. For comparisons with hand calculations, larger acceptance criteria are adopted because the physical properties used in such verification are approximate and they slightly differ than those used in the code. For code-to-code comparisons where only single-phase flow is involved, a relatively small difference can be assumed between the two codes. On the other hand, when two-phase flow is involved, a larger acceptance criterion is used due to the high uncertainty in predicting two-phase flow between different codes. For comparing physical properties of water, when pressures are below 5 bar, typical of most research reactor applications, a relatively small difference is used. However, for larger pressures, a larger difference between the code output and other references for estimating water physical properties can be tolerated.

**Table 1.2. Acceptance Criteria for Test Cases**

| Case Type | Acceptance criteria, agreement with reference results |
|---|---|
| Comparing a specific capability with analytic solutions | 0.1-1% |
| Comparing code results with hand calculations | 1-3% |
| Comparing code results against other codes for single phase flow | 3-5% |
| Comparing code results against other codes for two-phase flow | 5-20% |
| Comparing temperature distributions with other codes using variable solid material properties | 1-2% |
| Comparing physical properties of water with NIST database for pressures up to 5 bar | 3-7% |
| Comparing physical properties of water with NIST database for pressures greater than 5 bar | 7-25% |

As presented below, Sections 2 , 3, and 4 describe the verification of general and transient capabilities, respectively. Conclusions are presented in Section 5. Acceptance testing, which ensures that future software development activities do not inadvertently reduce the accuracy of results compared to this evaluation, is described in Appendix A .

# 2 Verification of General Capabilities

## 2.1 Capability A1 - Coolant Properties

PARET/ANL uses FORTRAN subprograms that use fitted equations to generate temperature-dependent and pressure-dependent properties of both light water and heavy water [8]. The User option IFLUID described in Section 5.1 of the User Guide selects the coolant [2]. This report only verifies the IFLUID options of 0 (light water) and 1 (heavy water). The properties needed to be checked are saturation temperature ($T_{sat}$), enthalpy ($H$), thermal conductivity ($k$), specific heat capacity ($Cp$), density ($\rho$), and viscosity ($\mu$). This capability is verified by comparing the code calculated data of a series of test cases with corresponding results published on the National Institute of Standards and Technology (NIST) website [9]. As discussed below, it can be concluded that the coolant properties generated by the code are adequate for the current safety analyses of the research reactors.

Because the code generates tables of coolant properties before performing the main calculation, the input settings for geometry, material, and reactor kinetic aspects do not impact the consideration of this capability. Therefore, very simple test cases with short transient time (0.1 s) are used for the comparison. Two series of test cases were run for light and heavy water coolants at 11 different inlet pressures ranging from 1 bar to 125 bar, by changing (i) the input value of inlet pressure, PRESUR, i.e., PRESUR = 1, 2, …, 125 bar, and (ii) the input value of coolant reference density, RHOREF, i.e., the coolant density at inlet pressure and temperature.

### 2.1.1 Coolant Saturation Temperature

The comparison of obtained data is first performed for the saturation temperatures. As shown in Table 2.1, the calculated saturation temperatures over the pressure range from 1 to 125 bar agree very well with NIST values for both light and heavy water. The percentage differences are well below the acceptance criteria defined in Table 1.2 for physical properties of water in comparison with NIST database.

**Table 2.1. Comparison of Saturation Temperature Data between PARET/ANL and NIST**

| Pressure, Bar | Saturation Temperature, °C | | | | | | | |
|---|---|---|---|---|---|---|---|---|
| | Light Water | | | | Heavy Water | | | |
| | Test Case | PARET/ANL | NIST | Diff., % | Test Case | PARET/ANL | NIST | Diff., % |
| 1 | A01_01 | 99.632 | 99.606 | 0.026 | A01_12 | 101.07 | 101.05 | 0.015 |
| 2 | A01_02 | 120.23 | 120.21 | 0.017 | A01_13 | 121.41 | 121.41 | 0.002 |
| 5 | A01_03 | 151.85 | 151.83 | 0.012 | A01_14 | 152.64 | 152.65 | 0.005 |
| 10 | A01_04 | 179.88 | 179.88 | 0.002 | A01_15 | 180.37 | 180.38 | 0.007 |
| 20 | A01_05 | 212.37 | 212.38 | 0.004 | A01_16 | 212.52 | 212.51 | 0.003 |
| 30 | A01_06 | 233.84 | 233.85 | 0.006 | A01_17 | 233.77 | 233.75 | 0.008 |
| 40 | A01_07 | 250.33 | 250.35 | 0.008 | A01_18 | 250.10 | 250.07 | 0.011 |
| 50 | A01_08 | 263.91 | 263.94 | 0.010 | A01_19 | 263.54 | 263.51 | 0.012 |
| 75 | A01_09 | 290.51 | 290.54 | 0.008 | A01_20 | 289.85 | 289.81 | 0.012 |
| 100 | A01_10 | 310.96 | 311.00 | 0.012 | A01_21 | 310.07 | 310.04 | 0.011 |
| 125 | A01_11 | 327.78 | 327.81 | 0.010 | A01_22 | 326.69 | 326.67 | 0.006 |

Checking of remaining fluid properties is performed for both liquid and vapor states and presented in the following subsections.

### 2.1.2 Light Water Properties

The maximum differences in light water properties between PARET/ANL and NIST for all tested temperatures are presented in Table 2.2, while the detailed results for each property are shown in Figure 2.1 to Figure 2.5. Generally, PARET/ANL results agree quite well with the NIST data but there are differences between the two, especially at pressures > 5 bar. Note that the code tracks enthalpy and deduces temperature from enthalpy. Changes in enthalpy are not computed based on *Cp*. Consequently, the larger errors shown in *Cp* for light water at some specific state points such as in the plot at 30 bar do not affect overall results. Specific heat capacity is supplied by equations with fitted coefficients derived from experimentally measured data. It stems from the subroutine taking the derivative of enthalpy to find *Cp*. This process is correct as long as the derivative is smooth. There is a break point in the equations for the fit to enthalpy that causes the local error as shown in Figure 2.3. This discontinuity results from two fitting functions for H(p,T) that are used for different pressure ranges, and they have a discontinuous slope at the intersection point. So, it shows up only when it happens to be very close to this point. This break point is less pronounced at lower pressures, and it can be avoided and may be corrected in the future. Nevertheless, the code is currently applied in the analyses of research reactors with operation pressures that are typically lower than 5 bar. The percentage differences shown in Table 2.2 are below the acceptance criteria defined in Table 1.2 for physical properties of water in comparison with NIST database for pressures in the range 1 to 5 bar, which is the relevant range for most research reactor applications. Therefore, the light water properties generated by PARET/ANL are adequate for the current applications.

Above 5 bar, the *Cp* for vapor begins to deviate but the effect on fuel and cladding temperatures is expected to be minor for the reasons mentioned above, so larger differences of up to 23% are tolerated and lies within the acceptance criteria in Table 1.2 for this pressure range.

**Table 2.2. Maximum Difference in $H_2O$ Properties between PARET/ANL and NIST Data**

| Phase & Pressure | Maximum Difference for all Tested Temperatures, % | | | | |
|---|---|---|---|---|---|
| | ***H*** | ***k*** | ***Cp*** | ***ρ*** | ***μ*** |
| Liquid, 1 bar | 0.53 | 2.14 | 1.18 | 0.07 | 3.02 |
| Vapor, 1 bar | 0.22 | 0.93 | 3.79 | 0.62 | 1.92 |
| Liquid, 2 bar | 0.52 | 2.06 | 1.07 | 0.10 | 3.59 |
| Vapor, 2 bar | 0.24 | 2.70 | 3.83 | 0.64 | 1.22 |
| Liquid, 5 bar | 0.51 | 2.02 | 1.00 | 0.11 | 3.51 |
| Vapor, 5 bar | 0.26 | 5.08 | 5.29 | 0.68 | 0.65 |
| Liquid, 10 bar | 0.50 | 2.09 | 0.99 | 0.11 | 3.38 |
| Vapor, 10 bar | 1.27 | 5.84 | 14.84 | 4.14 | 0.65 |
| Liquid, 20 bar | 0.46 | 1.97 | 2.99 | 0.11 | 3.09 |
| Vapor, 20 bar | 0.41 | 6.02 | 6.16 | 1.27 | 1.77 |
| Liquid, 30 bar | 0.43 | 1.85 | 14.77 | 0.11 | 3.42 |
| Vapor, 30 bar | 0.09 | 5.11 | 13.26 | 0.23 | 2.90 |
| Liquid, 40 bar | 0.39 | 1.73 | 3.28 | 0.11 | 3.85 |
| Vapor, 40 bar | 0.34 | 3.95 | 17.31 | 0.99 | 4.02 |
| Liquid, 50 bar | 0.36 | 1.67 | 2.98 | 0.11 | 4.05 |
| Vapor, 50 bar | 0.51 | 2.80 | 20.06 | 1.52 | 5.14 |
| Liquid, 75 bar | 0.30 | 1.57 | 2.76 | 0.11 | 4.42 |
| Vapor, 75 bar | 0.64 | 0.82 | 23.43 | 1.99 | 8.04 |
| Liquid, 100 bar | 0.26 | 1.47 | 2.09 | 0.11 | 6.75 |
| Vapor, 100 bar | 0.47 | 3.13 | 23.87 | 1.52 | 10.99 |
| Liquid, 125 bar | 0.21 | 1.37 | 1.30 | 0.11 | 14.33 |
| Vapor, 125 bar | 0.41 | 4.49 | 17.51 | 0.86 | 14.01 |

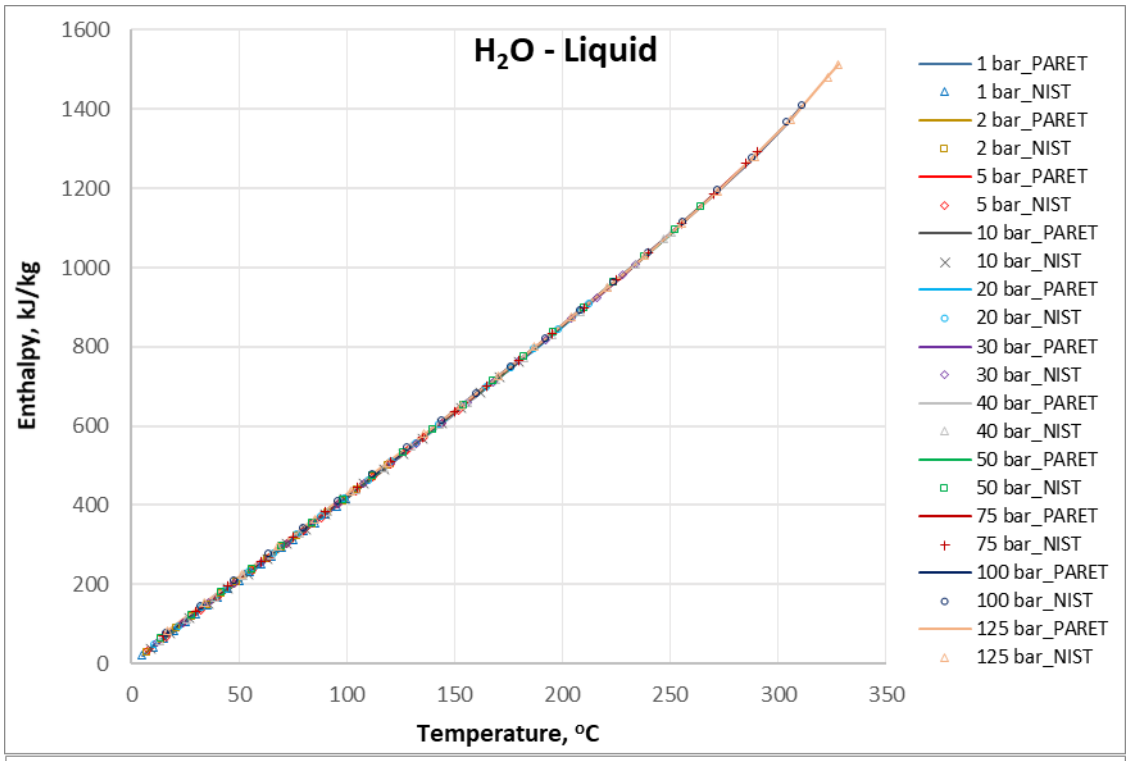


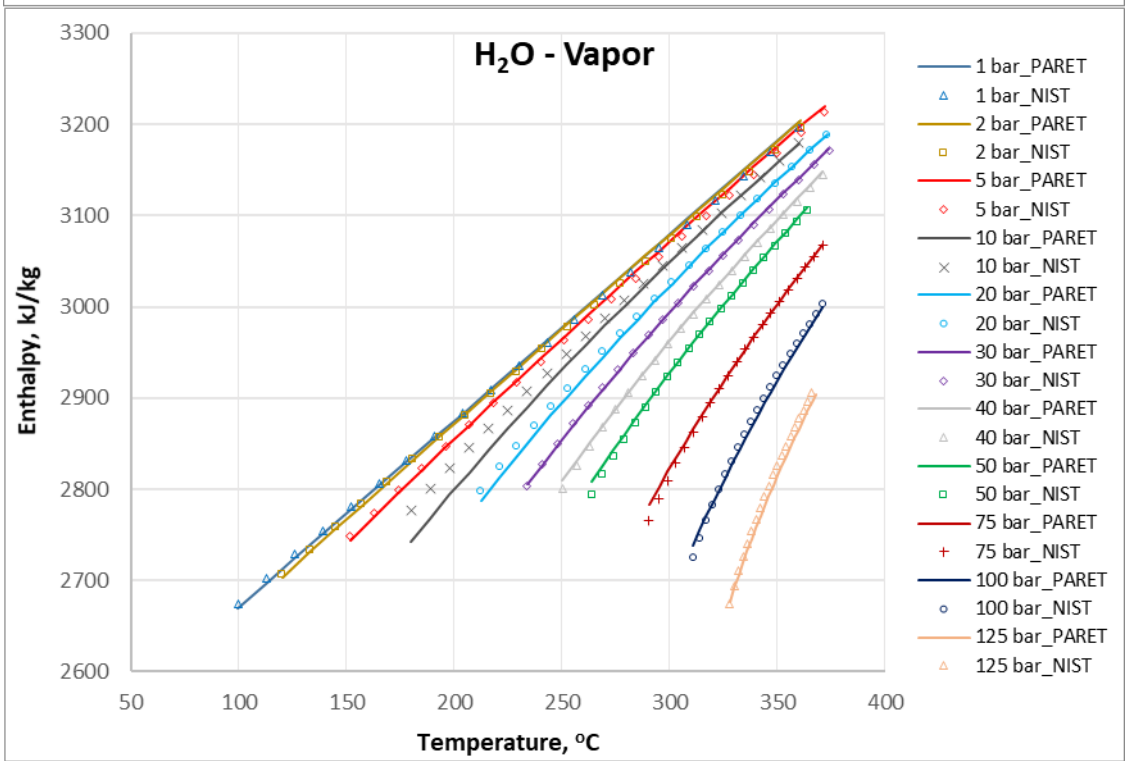


**Figure 2.1. Comparison of $H_2O$ Enthalpy between PARET/ANL and NIST Data**

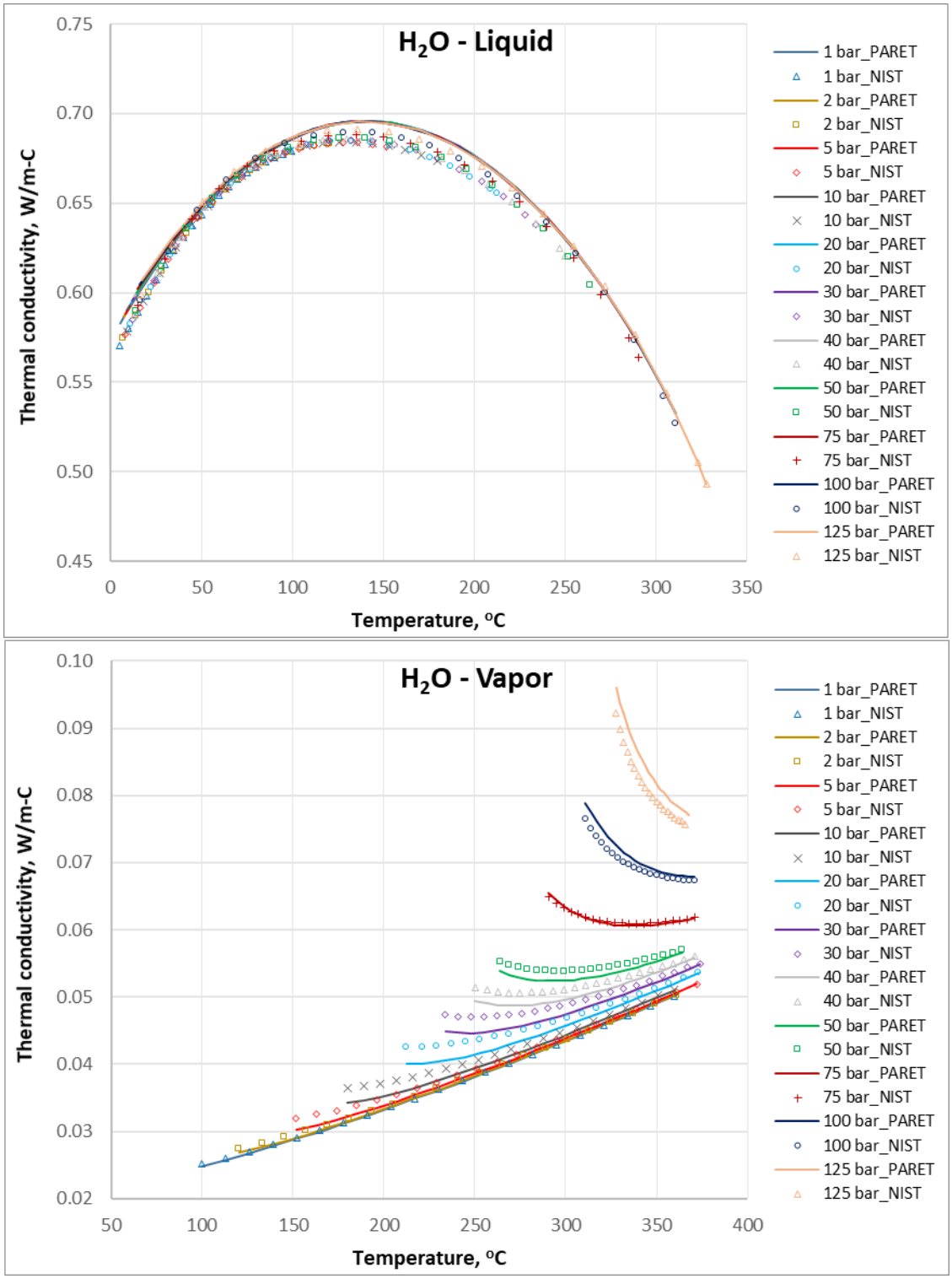


**Figure 2.2. Comparison of $H_2O$ Thermal Conductivity between PARET/ANL and NIST Data**

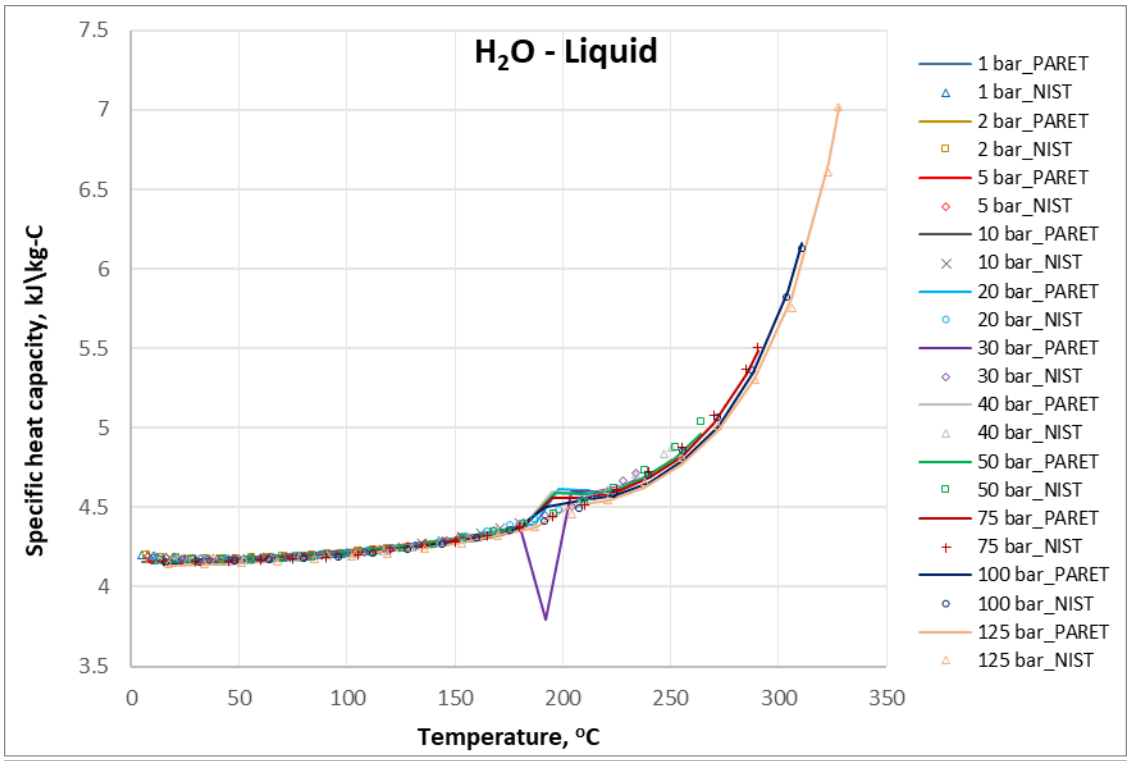


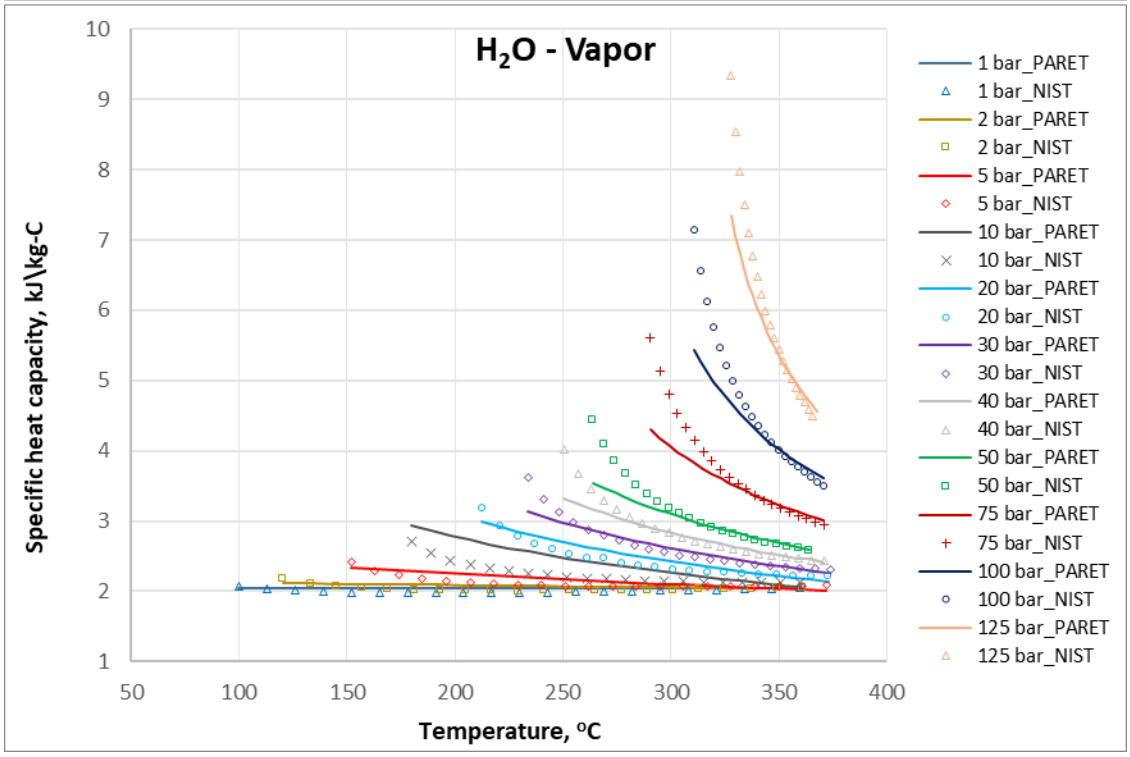


**Figure 2.3. Comparison of $H_2O$ Specific Heat Capacity between PARET/ANL and NIST Data**

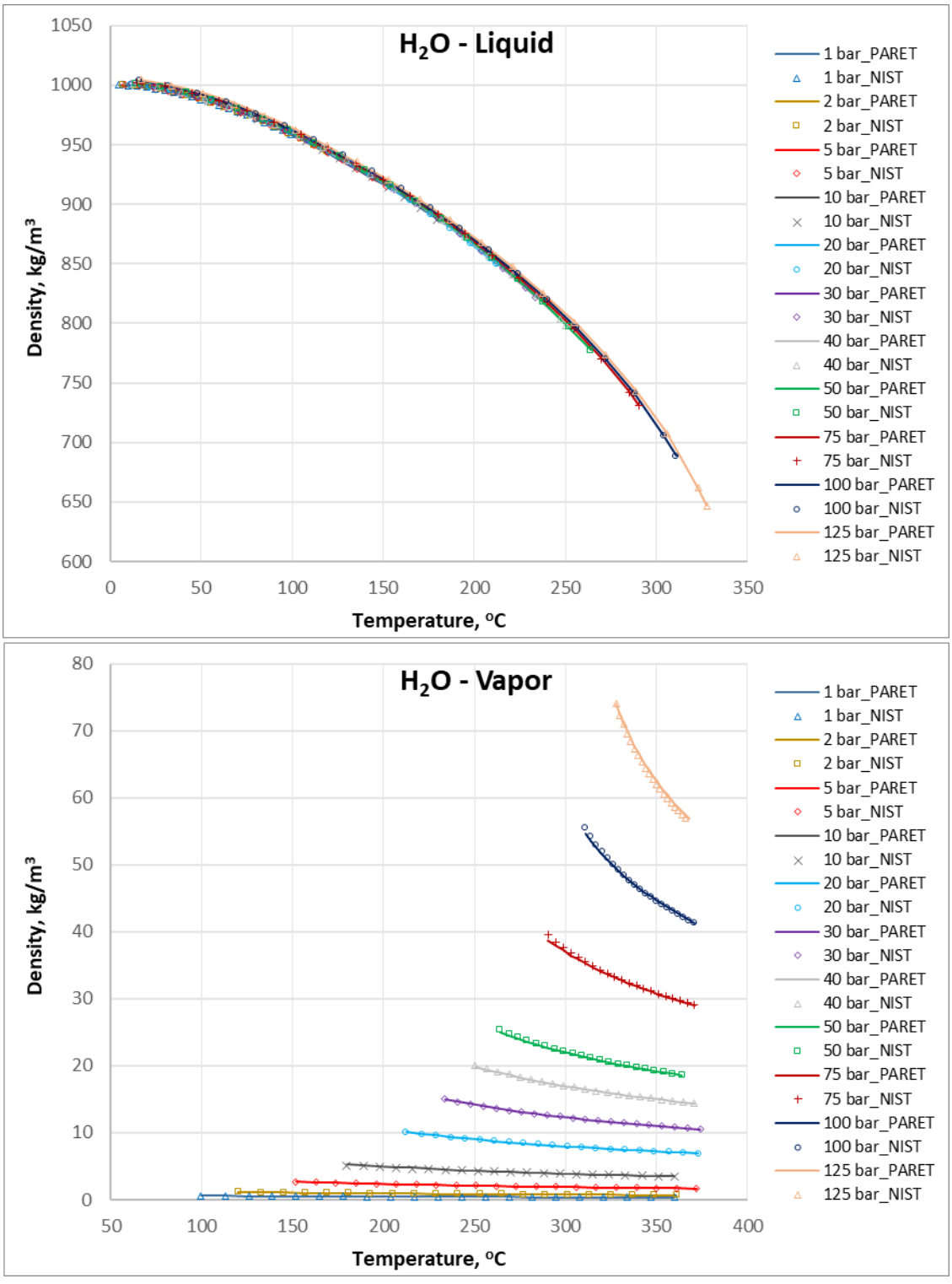


**Figure 2.4. Comparison of $H_2O$ Density between PARET/ANL and NIST Data**

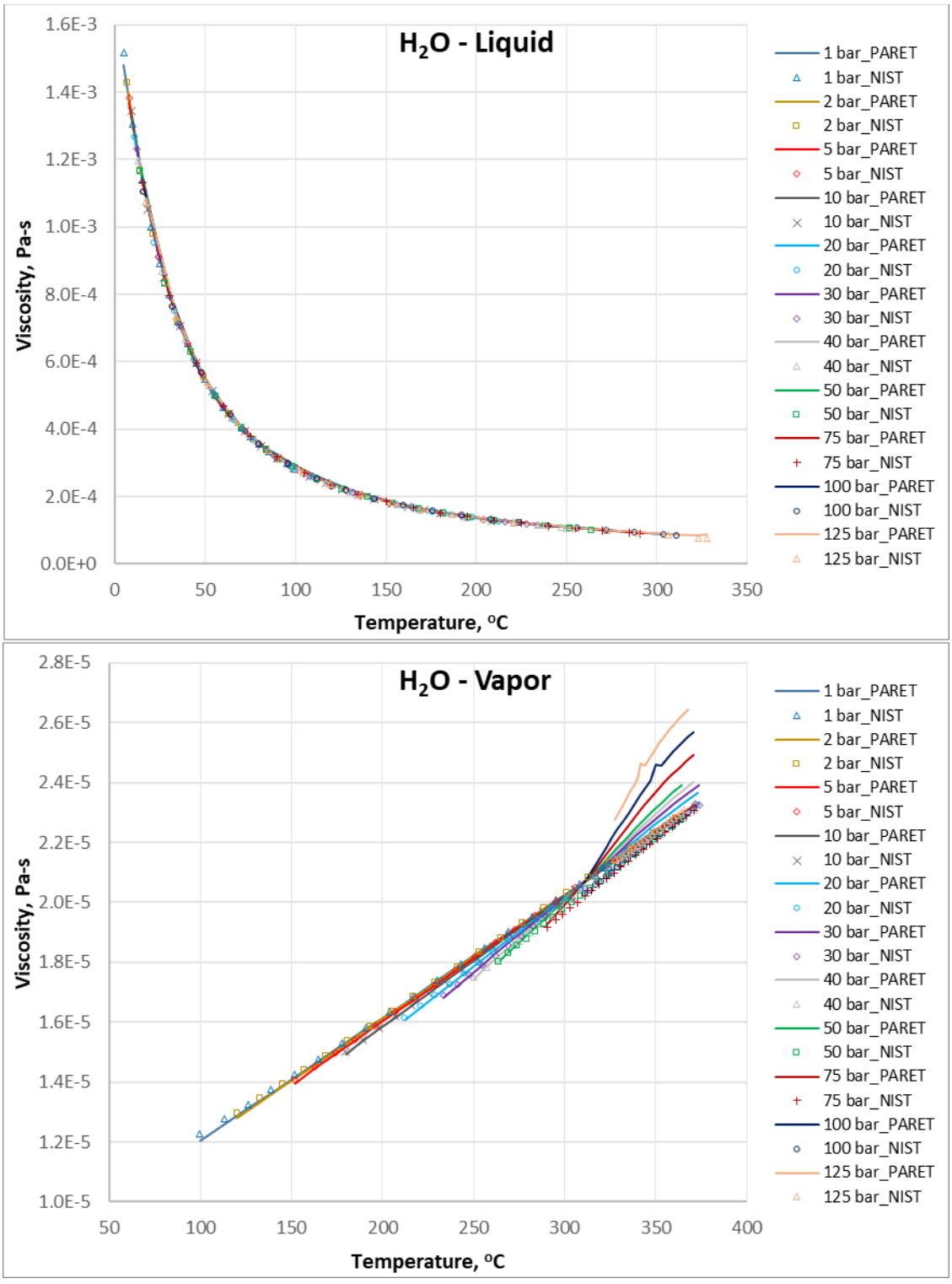


**Figure 2.5. Comparison of $H_2O$ Viscosity between PARET/ANL and NIST Data**

## 2.1.3 Heavy Water Properties

The maximum differences in heavy water properties between PARET/ANL and NIST for all tested temperatures are presented in Table 2.3, while the detailed results for each property are showed in Figure 2.6 to Figure 2.10. It is seen that PARET/ANL results agree quite well with the NIST data for the pressures up to 50 bar. Also, the percentages differences calculated in Table 2.3 are well below the acceptance criteria defined in Table 1.2. It is concluded that the heavy water properties generated by PARET/ANL are adequate for the current applications to research and test reactors.

**Table 2.3. Maximum difference in $D_2O$ properties between PARET/ANL and NIST Data**

| Phase & Pressure | Maximum Difference for all Tested Temperatures, % | | | | |
|---|---|---|---|---|---|
| | ***H*** | ***K*** | ***Cp*** | ***ρ*** | ***μ*** |
| Liquid, 1 bar | 2.725 | 1.855 | 3.285 | 0.463 | 1.363 |
| Vapor, 1 bar | 0.284 | 3.613 | 1.098 | 0.021 | 1.892 |
| Liquid, 2 bar | 2.718 | 1.773 | 3.170 | 0.453 | 0.986 |
| Vapor, 2 bar | 0.283 | 3.331 | 0.424 | 0.040 | 2.262 |
| Liquid, 5 bar | 2.724 | 1.533 | 2.882 | 0.412 | 0.622 |
| Vapor, 5 bar | 0.241 | 2.604 | 0.893 | 0.179 | 2.181 |
| Liquid, 10 bar | 2.765 | 1.452 | 2.796 | 0.394 | 0.615 |
| Vapor, 10 bar | 0.160 | 2.147 | 0.877 | 0.412 | 1.556 |
| Liquid, 20 bar | 2.776 | 1.375 | 2.718 | 0.384 | 0.571 |
| Vapor, 20 bar | 0.169 | 1.999 | 2.234 | 0.386 | 1.015 |
| Liquid, 30 bar | 2.791 | 1.298 | 2.646 | 0.371 | 0.629 |
| Vapor, 30 bar | 0.150 | 2.724 | 3.798 | 0.473 | 0.627 |
| Liquid, 40 bar | 2.791 | 1.298 | 2.646 | 0.371 | 0.629 |
| Vapor, 40 bar | 0.150 | 2.724 | 3.798 | 0.473 | 0.627 |
| Liquid, 50 bar | 2.790 | 1.225 | 2.632 | 0.356 | 0.754 |
| Vapor, 50 bar | 0.150 | 2.724 | 3.798 | 0.473 | 0.627 |
| Liquid, 75 bar | 2.805 | 1.146 | 2.621 | 0.338 | 0.823 |
| Vapor, 75 bar | 0.156 | 3.456 | 6.799 | 0.753 | 0.932 |
| Liquid, 100 bar | 2.798 | 1.068 | 2.596 | 0.326 | 0.821 |
| Vapor, 100 bar | 0.248 | 1.328 | 7.704 | 0.927 | 1.310 |
| Liquid, 125 bar | 2.787 | 2.694 | 2.559 | 0.311 | 0.892 |
| Vapor, 125 bar | 0.336 | 1.575 | 8.019 | 1.001 | 1.611 |

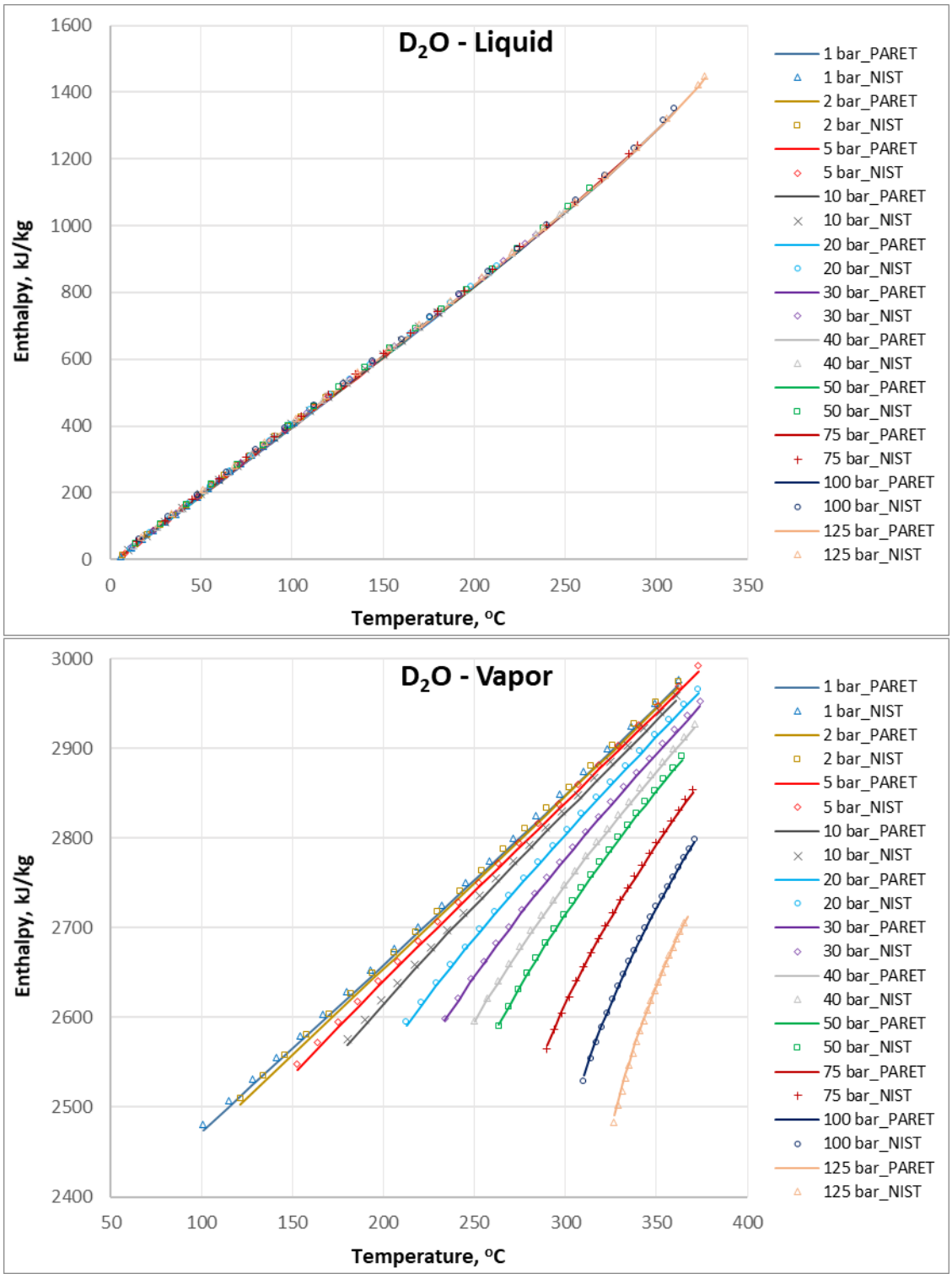


**Figure 2.6. Comparison of $D_2O$ Enthalpy between PARET/ANL and NIST Data**

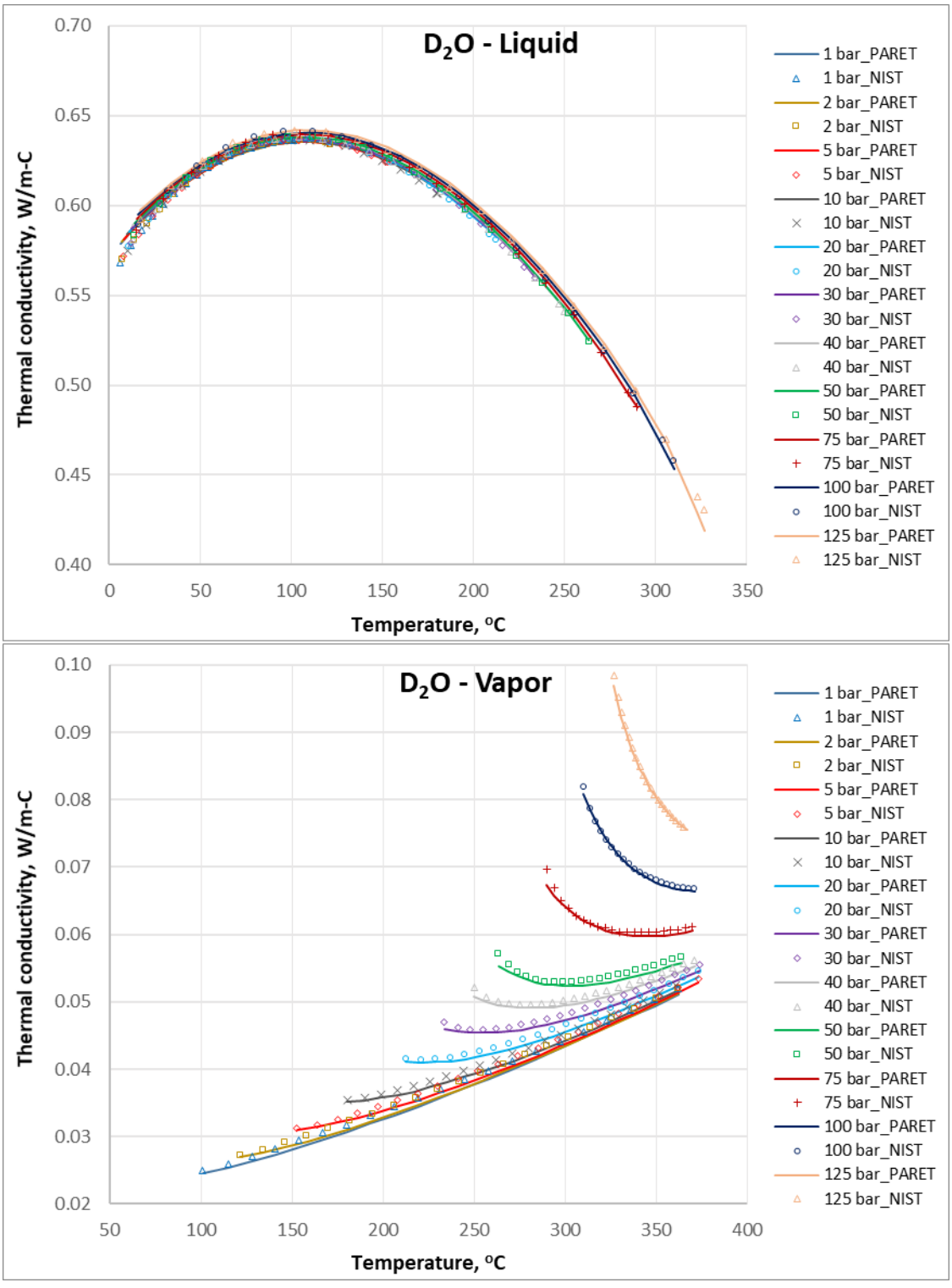


**Figure 2.7. Comparison of $D_2O$ Thermal Conductivity between PARET/ANL and NIST Data**

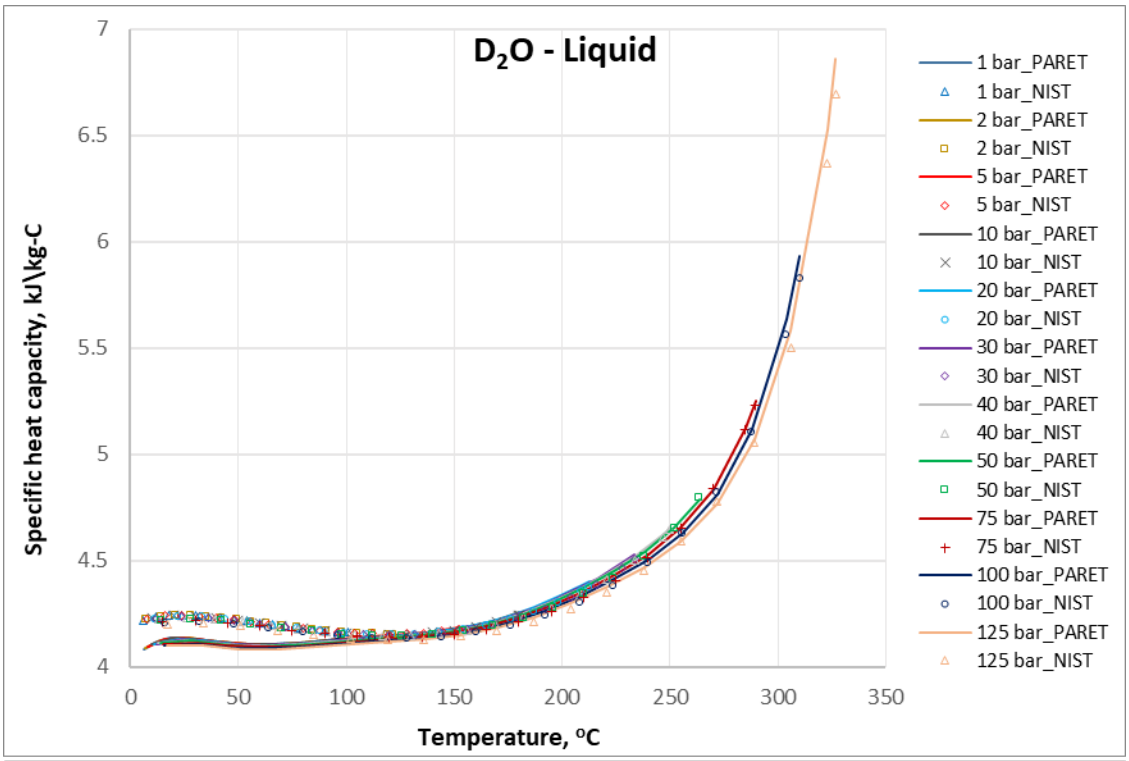


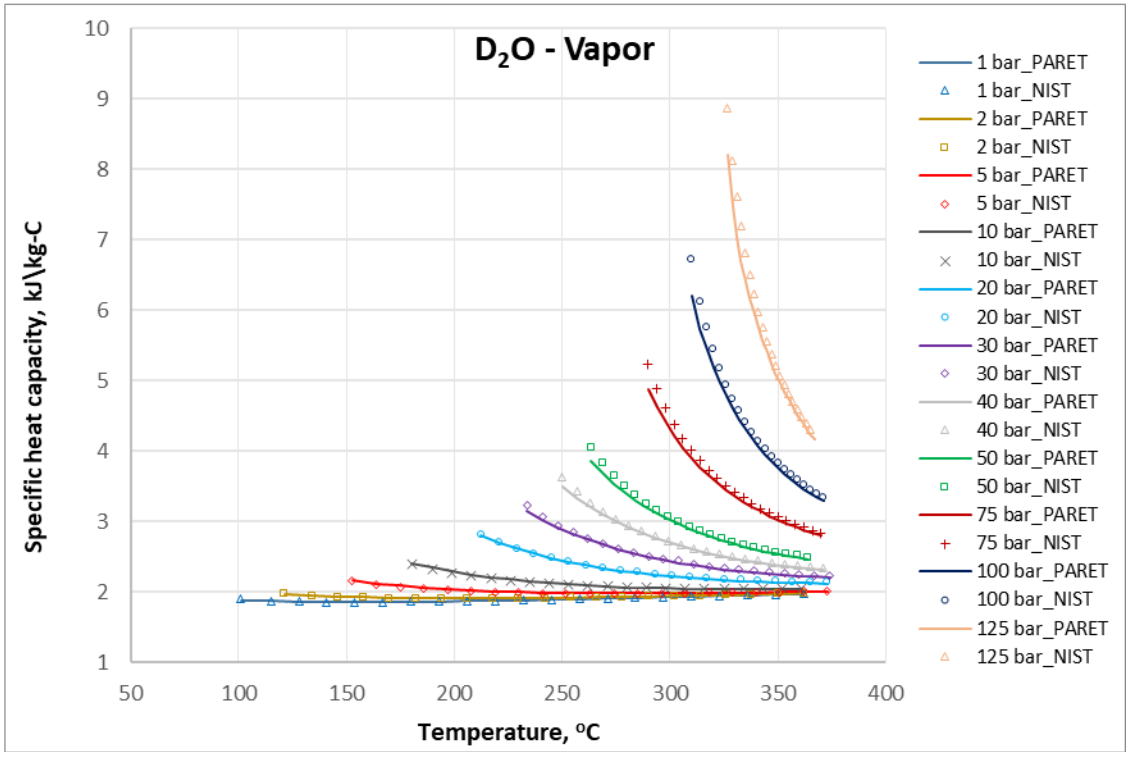


**Figure 2.8. Comparison of $D_2O$ Specific Heat Capacity between PARET/ANL and NIST Data**

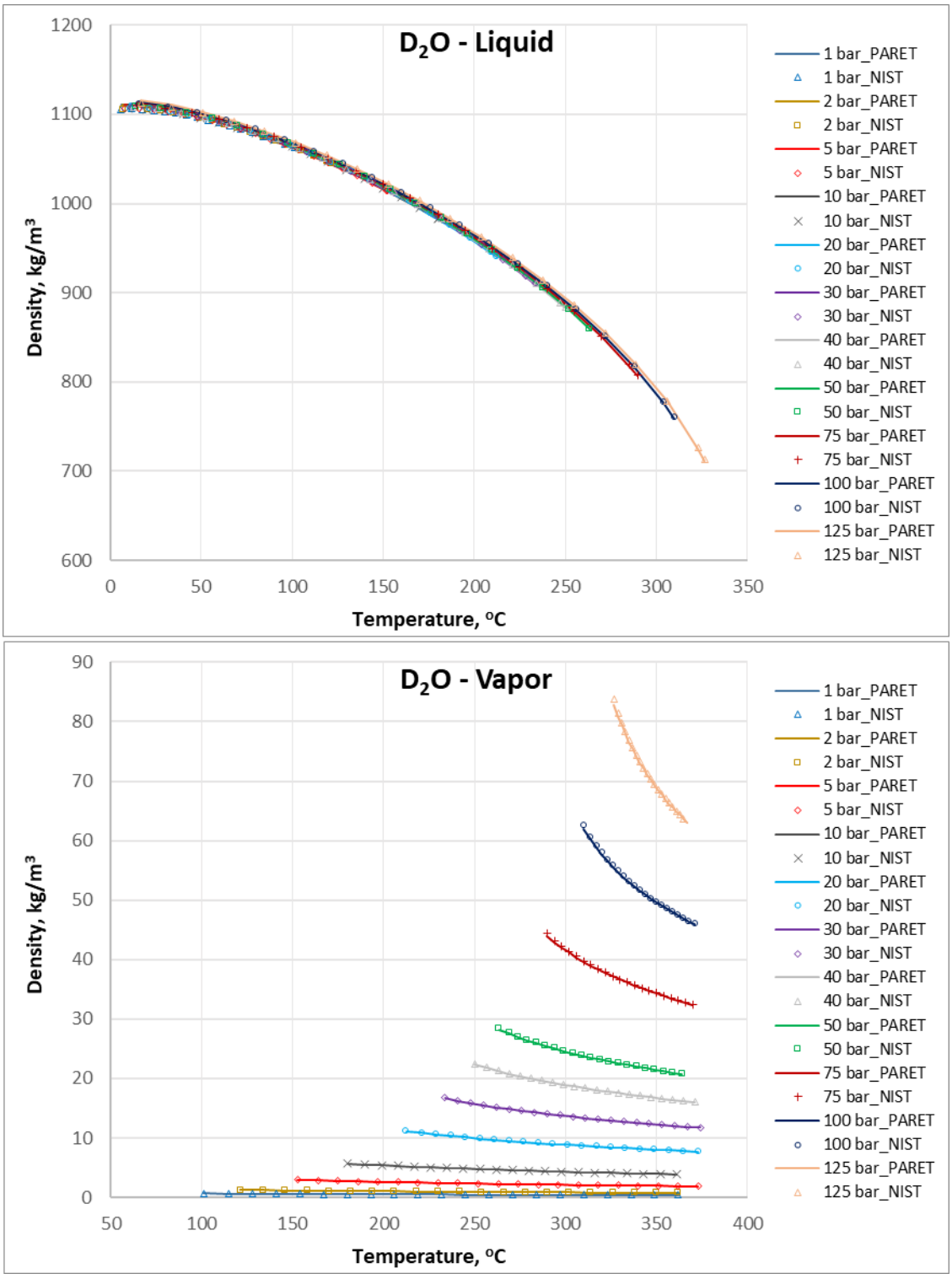


**Figure 2.9. Comparison of $D_2O$ Density between PARET/ANL and NIST Data**

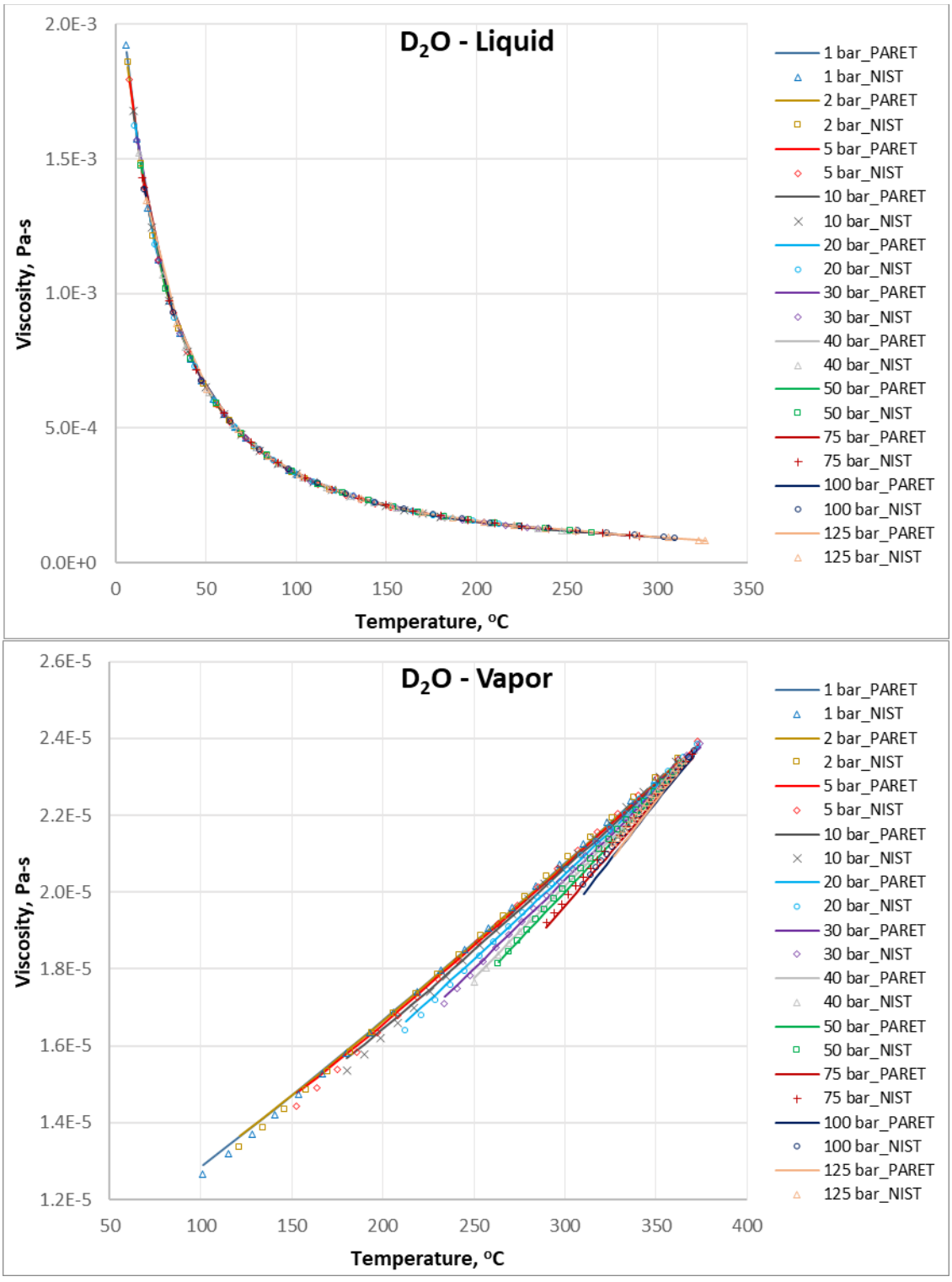


**Figure 2.10. Comparison of $D_2O$ Viscosity between PARET/ANL and NIST Data**

## 2.2 Capability A2 - Solid Material Thermal Properties

PARET/ANL requires input of thermal conductivity ($k$) and volumetric heat capacity ($\rho C_p$) in order to model the temperature and energy content everywhere at any time in the solid materials comprising the fuel plate or pin. As indicated by the User Guide Section 5.5.1 [2], both parameters are specified using the following relationship:

$$X = \alpha_1 T^2 + \alpha_2 T + \alpha_3 + \alpha_4 T^{-1}$$

where X: thermal conductivity or volumetric heat capacity; T: solid temperature; and α: coefficients.

Verification of this capability is based on a code-to-code comparison between PARET/ANL and RELAP5/MOD3.3 calculations of a power-driven test. Obtained data at steady-state conditions are used to check the material thermal conductivities, while the volumetric heat capacities are evaluated by transient data because there are significant changes in temperatures of fuel and cladding.

Test case A02_01 is selected to represent the fuel used by a typical 12-MW U.S. research reactor that goes through a transient characterized by a given power history of 2.0 sec. The relationship between power and transient time (Figure 2.11a) is extracted from previous simulation results for a reactivity insertion scenario in this reactor. The test case consists of two channels (one average channel and one hot channel) having the same axial relative power distribution showed by Figure 2.11b and the main input data presented in Table 2.4.

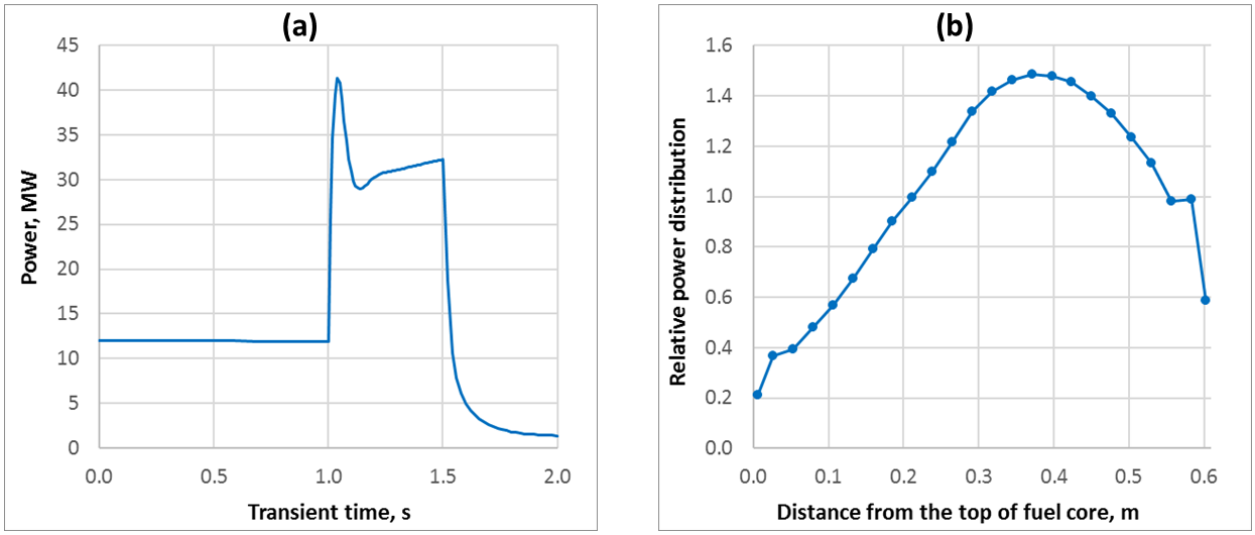


**Figure 2.11. Input Data of (a) Power History and (b) Axial Power Distribution**

**Table 2.4. Specifications of Test Case A02_01**

| Group | Input Parameters | | Channel | |
|---|---|---|---|---|
| | | | Average | Hot |
| Geometry | Active fuel length, m | | 0.6096 | |
| | Volume of fuel meat, $m^3$ | | 7.28400E-02 | 4.99682E-03 |
| | Fuel thickness, m | | 4.79287E-04 | 4.31800E-04 |
| | Zirconium thickness (one side), m | | 2.54000E-05 | |
| | Cladding thickness (one side), m | | 2.96517E-04 | 3.81000E-04 |
| | Oxide thickness (one side), m | | 1.49860E-05 | 1.00000E-10 |
| | Coolant flow area, m | | 3.25933E-02 | 1.19778E-05 |
| | Channel hydraulic diameter, m | | 4.49820E-03 | 4.57160E-03 |
| Flow condition | Coolant flowrate, kg/s | | 2.17812E+02 | 8.00250E-02 |
| | Inlet temperature, °C | | 5.44000E+01 | |
| | Outlet pressure, Pa | | 4.39000E+05 | |
| Material thermal property | Thermal conductivity, W/m*K (Temperature T is in Kelvin) | Fuel meat | 11.0 + 0.025*T | 14.0 + 0.030*T |
| | | Zirconium | 9.0+0.007*T | |
| | | Cladding | 150.0 + 0.18*T - 0.00025*$T^2$ | |
| | | Oxide | 2.25 | |
| | Rho*Cp, J/$m^3$*K (Temperature T is in Kelvin) | Fuel meat | 2.0E6 + 1200*T | |
| | | Zirconium | 1.8E+6 + 700*T | |
| | | Cladding | 4.3E+6-2700*T+2.2*$T^2$ | |
| | | Oxide | 1.00 | |
| Power | Total steady-state core power, MW | | 12.0 | |
| | Channel power distribution, % | | 99.9326 | 0.0674 |

It should be noticed that there are differences in the meshing systems used by the RELAP5 and PARET/ANL codes as well as in the locations at which the temperatures are reported. As can be seen in Figure 2.12a, PARET/ANL has an optimized solid and coolant nodalization in which the temperatures are calculated at the center of solid nodes and at the boundary of coolant nodes. In this figure, T stands for temperature and P stands for power density. In contrast, the RELAP5 calculations use the temperatures at the outlet of both solid and coolant nodes. Therefore, in order to enable a direct code-to-code comparison, the fuel plate in RELAP5 model is discretized as shown in Figure 2.12b so that the temperatures $T_2$, $T_4$, $T_6$… correspond to the temperatures $T_2$, $T_3$, $T_4$… reported by the PARET/ANL model.

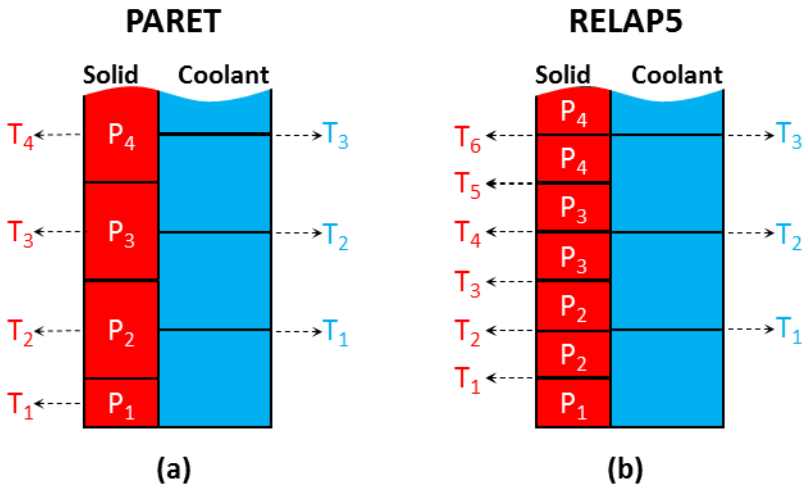


**Figure 2.12. Axial Meshing Systems of (a) PARET/ANL and (b) RELAP5 Codes**

The implementation of solid material thermal conductivity is evaluated by comparing steady-state data obtained from PARET/ANL to the same data from RELAP5/MOD3.3, which is extensively validated, and its results are used here as a reference for code validations. The detailed axial profiles of all important thermal hydraulics parameters at 0.9 s are considered. Figure 2.13 shows excellent agreement between the steady-state data for both average and hot channels. This agreement verifies that the PARET/ANL code has implemented the temperature-dependent thermal properties of solid materials correctly.

In order to evaluate the implementation of volumetric heat capacity, results obtained during the transient are compared. Specifically, the peak temperatures of the fuel, clad, and coolant are compared at many time steps. Notice that PARET/ANL calculates the peak temperature as the maximum of all axial nodes and prints it out as an output parameter, while RELAP5 does not. Therefore, a spreadsheet is used to calculate the peak temperature from the RELAP5 output data at every time step. As can be seen in Figure 2.14, there is excellent agreement between the transient temperature data for the average channel. The same data obtained for the hot channel show differences of up to 3.7 ˚C (1.6%) in the peak temperatures (Table 2.5). These differences, however, are considered acceptable because the heat transfer mode in the hot channel is changed from single-phase liquid to the more complicated subcooled nucleate boiling at ~1.03 sec. Also, the calculated differences are lower than the acceptance criteria defined in Table 1.2.

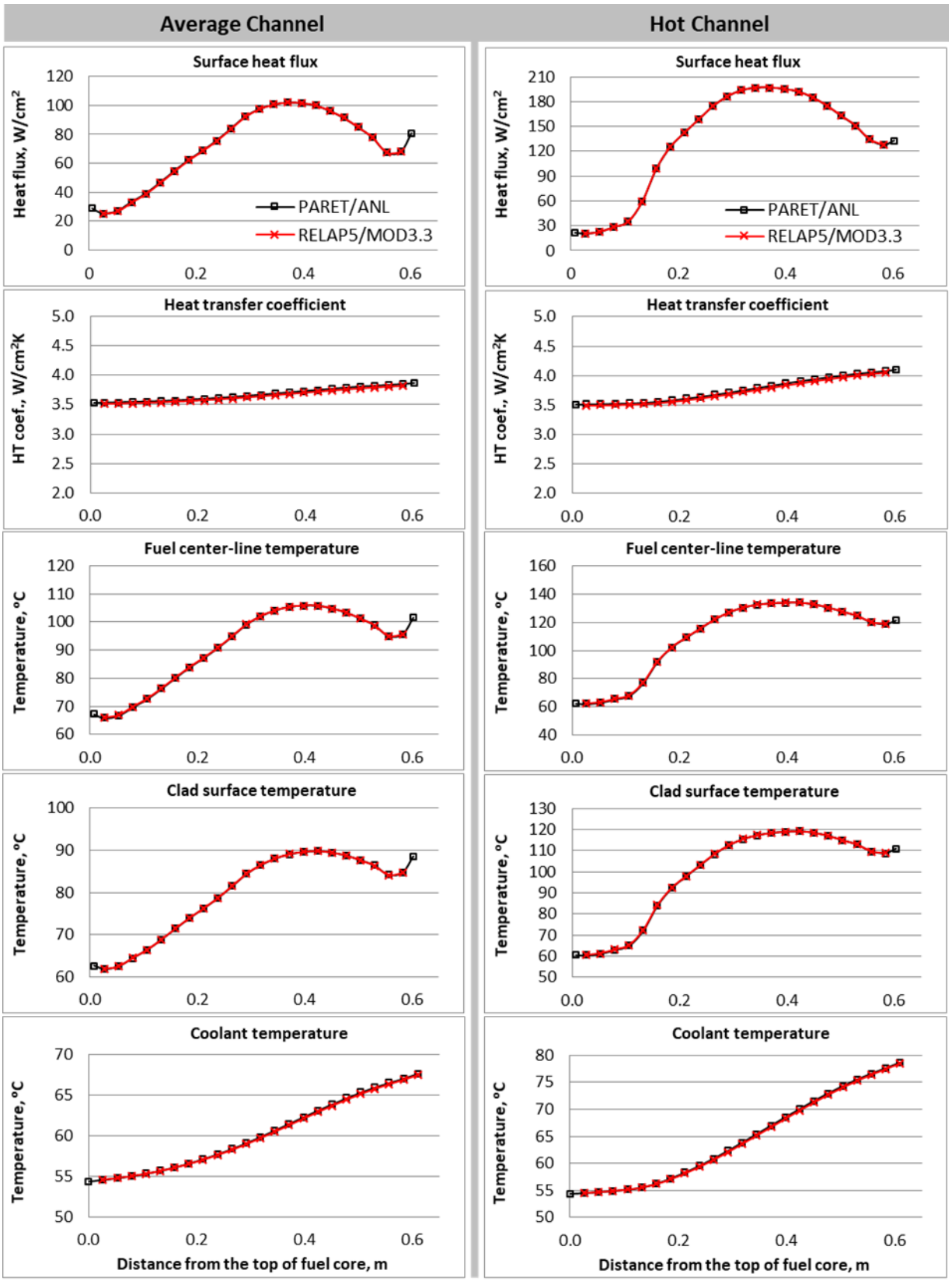


**Figure 2.13. Comparison of Steady-State Data**

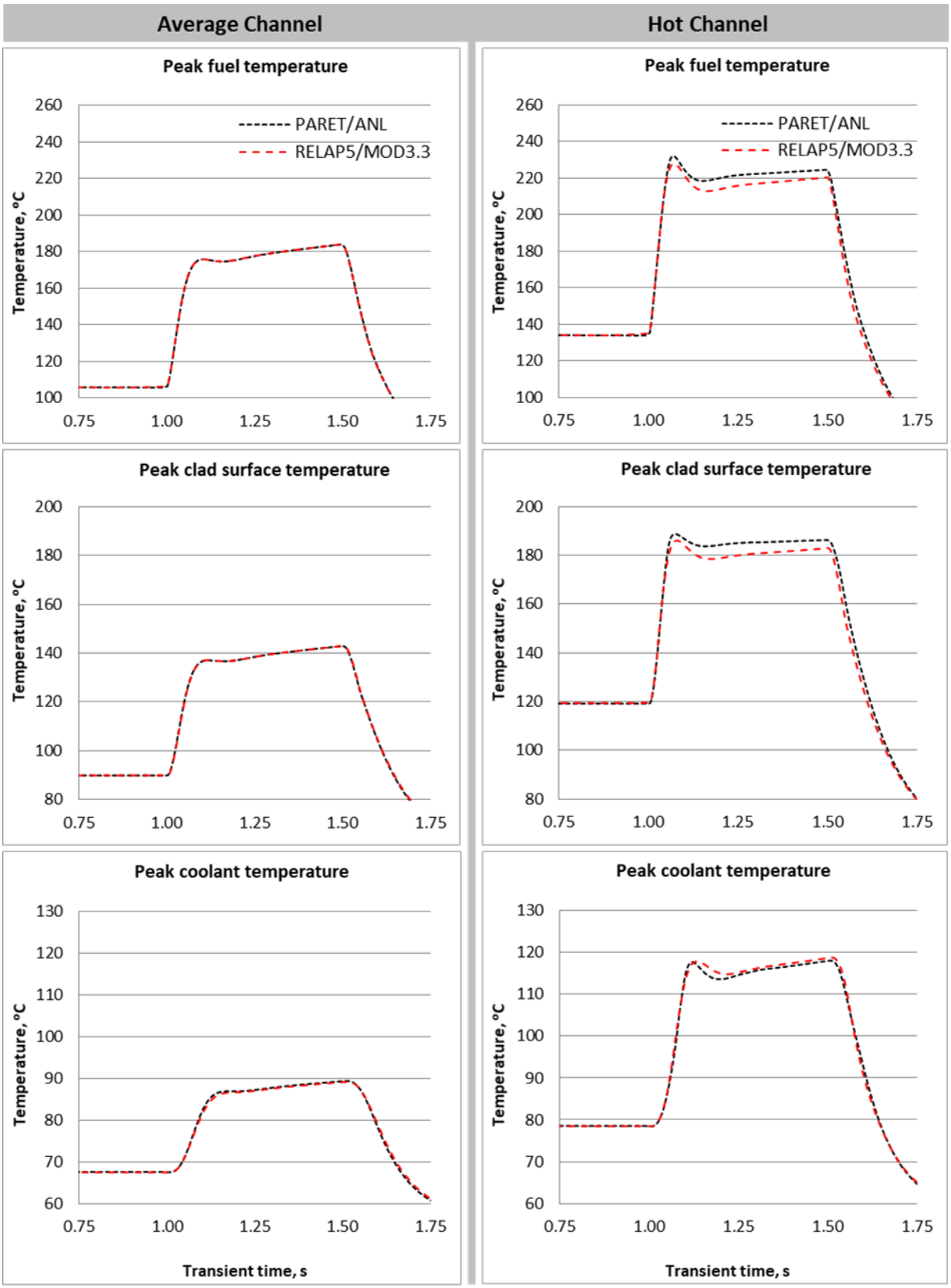


**Figure 2.14. Comparison of Transient Data**

**Table 2.5. Comparison of Transient Peak Temperatures**

| Peak Temperature, °C | | PARET/ANL | RELAP5/MOD3.3 |
|---|---|---|---|
| **Fuel meat** | **Average** | 184.0 | 184.2 |
| | **Hot** | 231.8 | 228.1 |
| **Cladding** | **Average** | 142.8 | 142.9 |
| | **Hot** | 188.9 | 186.0 |
| **Coolant** | **Average** | 89.4 | 89.1 |
| | **Hot** | 118.0 | 118.9 |

## 2.3 Capability A3 – Geometry Options

PARET/ANL has three geometry options regarding the type of fueled components that can be analyzed:

- Fuel in the form of plates, all having the same dimensions and materials (IGEOM=0),
- Fuel in the form of pins, all having the same dimensions and materials (IGEOM=1),
- Fuel in the form of plates with some optional variability for the dimensions and composition of each channel (IGEOM=2).

A channel consists of a single fuel element (rod or plate) together with associated coolant on each side (if a plate) or surrounding it (if a rod). It is generally necessary and reasonable to simplify the analysis of reactor transients by clustering fuel elements of the same physical dimensions and nominally at the same average power density to be represented as a single channel. The point of the IGEOM=2 option is to enable different channels to be unique in certain aspects of their geometry and/or composition. For example, two channels may be identical except that the average burnup is unique in each one. Alternatively, the cladding materials may differ. Or the radial dimensions of meat, gap, clad, and crud layer may be unique. The code can model up to 120 channels.

Verification is performed for each geometry option (IGEOM) as follows:

### 2.3.1 Fuel Plate (IGEOM = 0)

Test case A03_01 is set up using the geometry shown in Figure 2.15 and a flat axial power distribution. This test model consists of two classes of channels which together represent a full core: the first class has three identical channels, and the second class has one channel with the same fuel and cladding thickness but a coolant channel with half thickness.

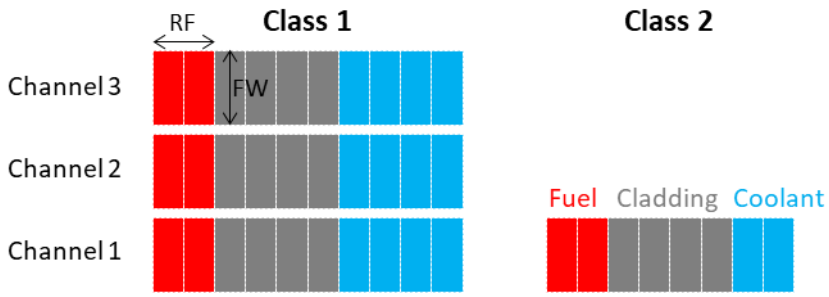


**Figure 2.15. Cross-Section of Test Model Using IGEOM= 0**

To simplify the hand calculation process, the input parameters (Table 2.6) are determined with the following constraints:

- Same power deposited to each channel: POWER1 = 3 * POWER2
- Same heat flux at all plate surfaces: PFQ1 = PFQ2

**Table 2.6. Input Parameters of Test Problem with IGEOM = 0**

| | | |
|---|---|---|
| Model power, MW | 1.0 | |
| Total fuel volume, $m^3$ | 0.00192 | |
| Active fuel length, m | 0.6 | |
| Coolant mass flux, $kg/m^2s$ | 10000 | |
| Inlet coolant temperature, °C | 20.0 | |
| Fuel half thickness (RF), mm | 4.0 | |
| Cladding thickness, mm | 8.0 | |
| Channel fuel width (FW), m | 0.1 | |
| - | Class 1 | Class 2 |
| Number of channels | 3 | 1 |
| Coolant half thickness, mm | 8.0 | 4.0 |
| Fuel volume fraction (BM) | 0.75 | 0.25 |
| Axial source description for all node (PFQ) | 1.000 | 1.000 |

**Table 2.7. Comparison between Hand and PARET/ANL Calculations with IGEOM = 0**

| Calculated Data | | Class 1 | | Class 2 | | Full Core | Max. diff., % |
|---|---|---|---|---|---|---|---|
| | | Channel | Class | Channel | Class | | |
| Power, MW | Hand Calc. | 0.25 | 0.75 | 0.25 | 0.25 | 1.0 | 0 |
| | PARET/ANL | 0.25 | 0.75 | 0.25 | 0.25 | 1.0 | |
| Flowrate, kg/s | Hand Calc. | 16.0 | 48.0 | 8.0 | 8.0 | 56.0 | 0 |
| | PARET/ANL | 16.0 | 48.0 | 8.0 | 8.0 | 56.0 | |
| Coolant temperature rise, °C | Hand Calc. | 3.737 | - | 7.474 | - | - | 0.42 |
| | PARET/ANL | 3.753 | - | 7.504 | - | - | |
| Surface heat flux, $MW/m^2$ | Hand Calc. | 2.083 | - | 2.083 | - | - | 0 |
| | PARET/ANL | 2.083 | - | 2.083 | - | - | |

The results obtained, as presented in Table 2.7, show a very good agreement between PARET/ANL and hand calculations. The maximum difference is 0.42%, which is less than the acceptance criteria defined in Table 1.2 for comparisons with hand calculations. Therefore, it is confirmed that the geometry option IGEOM = 0 works correctly.

## 2.3.2 Fuel Rod (IGEOM = 1)

Test case A03_02 is set up using the geometry shown in Figure 2.16 and a flat axial power distribution. This test model consists of two classes of channels, which together represent a full core: the first class has three identical channels, and the second class has one channel with the same fuel and cladding radii but a coolant channel with half thickness.

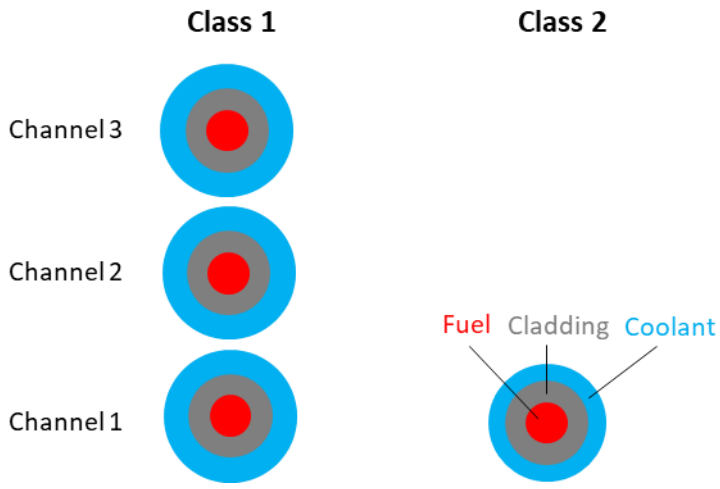


**Figure 2.16. Cross-Section of Test Model Using IGEOM = 1**

To simplify the hand calculation process, the input parameters (Table 2.8) are determined with the following constraints:

- Same power deposited to each channel: POWER1 = 3 * POWER2
- Same heat flux at all pin surfaces: PFQ1 = PFQ2

**Table 2.8. Input Parameters of Test Problem with IGEOM = 1**

| | | |
|---|---|---|
| Model power, MW | 0.2 | |
| Total fuel volume, $m^3$ | 4.825E-04 | |
| Active fuel length, m | 0.6 | |
| Coolant mass flux, $kg/m^2s$ | 10000 | |
| Inlet coolant temperature, °C | 20 | |
| Fuel radius, mm | 8 | |
| Cladding thickness, mm | 4 | |
| Model power, MW | 0.2 | |
| - | Class 1 | Class 2 |
| Number of channels | 3 | 1 |
| Coolant thickness, mm | 4 | 2 |
| Fuel volume fraction (BM) | 0.75 | 0.25 |
| Axial source description for all node (PFQ) | 1 | 1 |

**Table 2.9. Comparison between Hand and PARET/ANL Calculations with IGEOM = 1**

| Calculated Data | | Class 1 | | Class 2 | | Full Core | Max. diff., % |
|---|---|---|---|---|---|---|---|
| | | Channel | Class | Channel | Class | | |
| Power, MW | Hand Calc. | 0.05 | 0.15 | 0.05 | 0.05 | 0.2 | 0 |
| | PARET/ANL | 0.05 | 0.15 | 0.05 | 0.05 | 0.2 | |
| Flowrate, kg/s | Hand Calc. | 3.519 | 10.556 | 1.634 | 1.634 | 12.189 | 0.01 |
| | PARET/ANL | 3.519 | 10.555 | 1.634 | 1.634 | 12.188 | |
| Coolant temperature rise, °C | Hand Calc. | 3.399 | - | 7.320 | - | - | 0.44 |
| | PARET/ANL | 3.414 | - | 7.350 | - | - | |
| Surface heat flux, $MW/m^2$ | Hand Calc. | 1.105 | - | 1.105 | - | - | 0 |
| | PARET/ANL | 1.105 | - | 1.105 | - | - | |

The results obtained, as presented in Table 2.9, show a very good agreement between PARET/ANL and hand calculations. The maximum difference is 0.44%, which is less than the acceptance criteria defined in Table 1.2 for comparisons with hand calculations. Therefore, it is confirmed that the geometry option IGEOM = 1 works correctly.

## 2.3.3 Fuel Plate with Different Channel Geometries (IGEOM = 2)

Test case A03_03 is set up using the geometry shown in Figure 2.17 and a flat axial power distribution. This test model consists of two classes of channels which together represent a full core: the first class has three identical channels, and the second class has one channel with different radial dimensions for fuel, cladding and coolant.

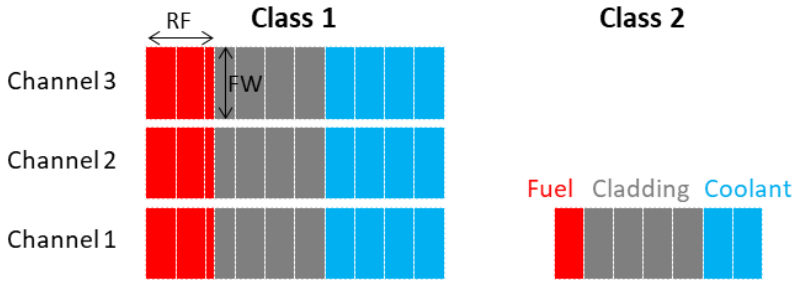


**Figure 2.17. Cross-Section of Test Model Using IGEOM = 2**

To simplify the hand calculation process, the input parameters (Table 2.10) are determined with following constraints:

- Same power deposited to each channel: POWER1 = 3 * POWER2
- Same heat flux at all plate surfaces: PFQ1 * RF1 = PFQ2 * RF2
- Averaged PFQ = 1.0: PFQ1 * BM1 + PFQ2 * BM2 = 1.0

**Table 2.10. Input Parameters of Test Problem with IGEOM = 2**

| | | |
|---|---|---|
| Model power, MW | 1.0 | |
| Total fuel volume, $m^3$ | 0.00192 | |
| Active fuel length, m | 0.6 | |
| Coolant mass flux, $kg/m^2s$ | 10000 | |
| Inlet coolant temperature, °C | 20.0 | |
| - | Class 1 | Class 2 |
| Number of channels | 3 | 1 |
| Fuel half thickness (RF), mm | 4.66 | 2.00 |
| Cladding thickness, mm | 7.34 | 10 |
| Fuel width (FW), m | 0.1 | 0.1 |
| Coolant half thickness, mm | 8.0 | 4.0 |
| Fuel volume fraction (BM) | 0.875 | 0.125 |
| Axial source description for all node (PFQ) | 0.857 | 2.000 |

**Table 2.11. Comparison between Hand and PARET/ANL Calculations with IGEOM = 2**

| Calculated Data | | Class 1 | | Class 2 | | Full Core | Max. diff., % |
|---|---|---|---|---|---|---|---|
| | | Channel | Class | Channel | Class | | |
| Channel power, MW | Hand Calc. | 0.25 | 0.75 | 0.25 | 0.25 | 1.0 | 0 |
| | PARET/ANL | 0.25 | 0.75 | 0.25 | 0.25 | 1.0 | |
| Flowrate, kg/s | Hand Calc. | 16.0 | 48.0 | 8.0 | 8.0 | 56.0 | 0 |
| | PARET/ANL | 16.0 | 48.0 | 8.0 | 8.0 | 56.0 | |
| Coolant temperature rise, °C | Hand Calc. | 3.737 | - | 7.474 | - | - | 0.43 |
| | PARET/ANL | 3.753 | - | 7.505 | - | - | |
| Surface heat flux, $MW/m^2$ | Hand Calc. | 2.083 | - | 2.083 | - | - | 0.05 |
| | PARET/ANL | 2.083 | - | 2.084 | - | - | |

The results obtained, as presented in Table 2.11, show a very good agreement between PARET/ANL and hand calculations. The maximum difference is 0.43%, which is less than the acceptance criteria defined in Table 1.2 for comparisons with hand calculations. Therefore, it is confirmed that the very large differences in all varied input parameters are processed correctly. Note that this test case uses the relative fuel and plate widths (RFW and RPW) equaling to 1.0 as requested by the current code version. The results obtained confirm that the geometry option IGEOM = 2 works correctly when RFW = RPW = 1.0.

## 2.4 Capability A4 – Flow Options (Forced or Buoyancy-Driven Flow)

The flow options used to simulate forced or buoyancy-driven flow can be selected by the input parameter IFLOW as presented in Table 2.12.

**Table 2.12. Flow Options and Test Case**

| Input Setting | Description | | Test Case |
|---|---|---|---|
| IFLOW = 1 | Forced flow specified by Input Cards 10xxx | | A04_01 |
| IFLOW = 2 | (Not available in current code version) | | |
| IFLOW = 3 | Buoyant forced flow (in all channels) with pump coast down superimposed from Input Cards 17xxx. Initial flow rate is computed from friction pressure drop given in next entry (parameter DELP). | | A04_02 |
| IFLOW = 4 | Same as IFLOW = 3 but initial flow specified by Input Card 10xxx. | | A04_03 |
| IFLOW = 5 | Buoyancy only (no pump) | Test case without unfueled part | A04_04 |
| | | Test case with unfueled part | A04_05 |

The verification of this capability is started with the checking of option IFLOW = 5 using a *Mathematica* notebook developed to solve the test problem of natural circulation as given by Table 2.13. The Mathematica calculations applied the same energy conservation equation and thermal properties for the coolant flow as implemented in PARET/ANL. The *Mathematica* calculations required starting with an assumed flow rate in the coolant channel. That flow rate was manually adjusted to reach convergence such that the buoyancy pressure drop equaled the frictional pressure drop in the channel. Note that PARET/ANL will use a nominal friction factor of 96/Re in slab geometry as a starting value but will correct it when there is heating as described in the User Guide [2]. This friction model is implemented in the *Mathematica* program for the comparison.

**Table 2.13. Input Parameters of Test Problem IFLOW = 5 (test case A04_04)**

| | |
|---|---|
| Model power, MW | 0.1 |
| Inlet coolant temperature, °C | 25.0 |
| Inlet pressure, bar | 5.0 |
| Active fuel length, m | 0.75 |
| Channel thickness, m | 0.003 |
| Channel width, m | 0.30 |
| Hydraulic diameter, m | 0.00594 |
| Inlet K-loss | 0.0 |
| Outlet K-loss | 0.0 |
| Gravity constant, $m/s^2$ | 9.8 |

**Table 2.14. Results of Test Problem with IFLOW = 5 (test case A04_04)**

| Output Parameter | PARET/ANL | Mathematica |
|---|---|---|
| Channel mass flux, kg/m$^2$s | 132.77 | 132.77 |
| Outlet coolant temperature, °C | 75.02 | 75.02 |
| $\Delta P_{Buoyancy}$, Pa | 66.766 | 66.0 |
| $\Delta P_{Friction}$, Pa | 66.378 | 66.4 |

The results obtained, as presented in Table 2.14, show a very good agreement between PARET/ANL run using IFLOW = 5 and the independent Mathematica notebook. In other words, it is confirmed that the option IFLOW = 5 handles natural circulation correctly. $\Delta P_{Buoyancy}$ is an upward pressure drop acting on mass flux to promote upward flow. $\Delta P_{Friction}$ is the friction loss pressure drop that resists flow. When the upward pressure drop from buoyancy is equal to the friction pressure drop, the flow is balanced and is in steady-state.

The verification of remaining IFLOW options 1, 3, and 4 are performed by comparing their calculation results with the final steady-state natural circulation data obtained with IFLOW = 5 of a test model. To be more general, the test case A04_04 mentioned above is modified to include unfueled parts and the K-loss at the channel inlet and outlet shown in Table 2.15. This forms a new test case A04_05 which is used as the reference case for the checking of other IFLOW options as follows:

- Test case A04_01 is to check IFLOW = 1. The output natural circulation mass flux calculated by test case A04_05 is used as the forced mass flux at the input cards 10xxx.

- Test case A04_02 is to check IFLOW = 3. The initial friction pressure drop calculated by test case A04_05 (IFLOW = 5) is used as the parameter DELP on the input card 5xxx. The code searches for the mass flux yielding this pressure drop. The result from the search process initializes the mass flux at time zero for the transient solution to follow.

- Test case A04_03 is to check IFLOW = 4. It begins with forced downflow stabilized at time zero, continuing through a loss-of-flow event specified by input cards 17xxx to zero flow at 30 s, continuing on to a steady-state upflow solution driven by buoyancy forces.

Together with comparison between the option IFLOW = 5 and *Mathematica* notebook (Table 2.14), good agreement between the IFLOW options presented in Table 2.16 confirm that the flow options corresponding to IFLOW = 1, 3, 4, and 5 have been implemented correctly. The percentage differences shown in Table 2.16 are extremely small and they are less than the acceptance criteria defined in Table 1.2. The following observations support the verification of the hydraulic model:

- The resulting $\Delta P_{friction}$ for test case A04_01 matches test case A04_05 within five significant figures.

- The resulting $\Delta P_{buoyancy}$ for test case A04_02 matches test case A04_05 within five significant figures.

- For test case A04_03, there is excellent agreement with test case A04_05 for the channel mass flux, $\Delta P_{friction}$, and $\Delta P_{buoyancy}$.

**Table 2.15. Input Parameters of Test Problem of IFLOW = 1, 3, 4, and 5 (cases A04_01, A04_02, A04_03, and A04_05)**

| | |
|---|---|
| Power, MW | 0.1 |
| Inlet coolant temperature, °C | 25.0 |
| Inlet pressure, bar | 5.0 |
| Unfueled length at top, m | 0.15 |
| Active fuel length, m | 0.75 |
| Unfueled length at bottom, m | 0.15 |
| Channel thickness, m | 0.003 |
| Channel width, m | 0.30 |
| Hydraulic diameter, m | 0.00594 |
| Inlet K-loss | 0.5 |
| Outlet K-loss | 1.0 |
| Gravity constant, $m/s^2$ | 9.8 |

**Table 2.16. Comparison of Calculation Results**

| Test case | A04_01 | A04_02 | A04_03 | A04_05 |
|---|---|---|---|---|
| **IFLOW option** | **1** | **3** | **4** | **5** |
| Channel mass flux, $kg/m^2s$ | (input) | 127.89 | 127.89 | 127.89 |
| Outlet coolant temperature, °C | 76.92 | 76.92 | 76.92 | 76.92 |
| $\Delta P_{friction}$, Pa | 103.09 | (input) | 103.09 | 103.09 |
| $\Delta P_{buoyancy}$, Pa | (not edited) | 100.13 | 100.12 | 100.13 |
| Difference in Buoyancy between the value of $\Delta P_{buoyancy}$ and its average for cases A04_02,_A04_03, and A04_05, Pa | | +0.003 | -0.006 | +0.003 |

The percentage differences shown in Table 2.16 are extremely small and they are less than the acceptance criteria defined in Table 1.2.

# 2.5 Capability A5 – Single-Phase Heat Transfer Correlations

## 2.5.1 Description of Code Calculation Method

As shown in Table 2.17, the heat transfer from fuel plate to single-phase coolant takes place in three flow regimes, i.e., laminar, transition, and turbulent which are separated by the input Reynolds numbers of REL_T and RET_T. The current V&V will use the default input values of REL_T = 2300 and RET_T = 3700 and therefore, the flow regimes to be considered are

- Laminar (Re < 2300): The calculation is controlled by input IHT options of 0, 1, and 2.

- Transition ($2300 \leq \text{Re} \leq 3700$): Interpolation is performed between laminar and turbulent regimes.

- Turbulent (Re > 3700): The calculation is controlled by input parameter IONEP.

- Transient (Rosenthal & Miller): The heat transfer coefficient calculated based on Rosenthal & Miller correlation ($h_{TRAN}$) may be used if it is higher than the heat transfer coefficient calculated for natural convection ($h_{NC}$) or the heat transfer coefficient for fully turbulent forced convection flow ($h_{TURB}$). Rosenthal & Miller correlation will not be considered in the selection if IONEP<0.

**Table 2.17. Single-Phase Heat Transfer Correlation [2]**

| Flow Regime | Input Setting | Single-Phase Heat Transfer Correlation |
|---|---|---|
| Laminar | IHT=0 | Heat transfer coefficient: $h_{NC}= \frac{1.02\,K\,Re^{0.45}\,Pr^{1/3}}{D_e^{0.6}\,L_h^{0.4}} \times \left(\frac{\mu_b}{\mu_w}\right)^{0.14} \times \delta\,(T_w - T_b)^n$ where $\delta$ and $n$ are specified by input HTTCON and HTTEXP |
| | IHT=1 | Without entrance effect: $h_{NC}= Nu*k/D_e$ where Nu is specified by input HTTCON |
| | IHT=2 | With entrance effect: $h_{NC}= (Nu+X)*k/D_e$ where Nu is specified by input HTTCON, and $X$ is obtained using a lookup table of Graetz number: Gz = $\frac{D_e \mathrm{RePr}}{z}$, with z is the distance from inlet |
| Transition | IHT & IONEP | Heat transfer coefficient: $h_{TRANSIT} = h_{NC} * (1-x) + h_{TURB} * x$ where $h_{NC}$ and $h_{TURB}$ are obtained by applying laminar and turbulent correlations to the Re under consideration and $x = (Re - REL\_T)/(RET\_T - REL\_T)$ |
| Turbulent | IONEP=0 | Dittus-Boelter: $Nu = 0.023 Re^{0.8} Pr^{0.4}$ |
| | IONEP=1 | Sieder-Tate : $Nu = 0.027 Re^{0.8} Pr^{1/3} \left(\frac{\mu_b}{\mu_w}\right)^{0.14}$ |
| | IONEP=2 | Petukhov-Popov: $h_{TURB} = \frac{\frac{k_b f_D}{\mathrm{De}\ 8}\mathrm{RePr}\left(\frac{\mu_b}{\mu_w}\right)^{0.11}}{(1+3.4 f_D)+\left(11.7+\frac{1.8}{\mathrm{Pr}^{1/3}}\right)\left(\frac{f_D}{8}\right)^{\frac{1}{2}}\left(\mathrm{Pr}^{2/3}-1.0\right)}$ where $f_D = \frac{1.0875-0.1125(\frac{b}{s})}{(1.82\log \mathrm{Re}-1.64)^2}$; $b$ and $s$ are the thickness and span or the larger side of the rectangular cross section of the channel. |
| | IONEP=3 | Colburn: $Nu = 0.023 Re^{0.8} Pr^{0.3}$ with fluid properties calculated at film temperature $T_{film} = (T_{clad} + T_b)/2$ |
| | IONEP=4 | Russian: $Nu = 0.021 Re^{0.8} Pr^{0.43} \left(\frac{\mu_b}{\mu_w}\right)^{0.25}$ |
| | IONEP=6 | Dittus-Boelter modified by ANL: $Nu = 0.023 Re^{0.8} Pr^{0.4} \left(\frac{\mu_b}{\mu_w}\right)^{0.11}$ |
| | IONEP=8 | Dittus-Boelter: $Nu = 0.023 Re^{0.8} Pr^{0.4}$ |
| Transient, Rosenthal & Miller | IONEP>=0 | $h_{TRAN} = \sqrt{\frac{k\rho C_p}{T}}$ , where $h_{TRAN}$ is the heat transfer coefficient, $k$ is coolant thermal conductivity, $C_p$ is the specific heat of the coolant, and $T$ is the period of the power rise (reactor period). |

*Note:*

- *Option IONEP = 5 corresponding to China Inst. of Atomic Energy MNSR correlation is currently not used and therefore, it is not considered under this V&V.*
- *Using the positive values of IONEP as shown in this table will activate the Rosenthal & Miller correlation. The code, however, only uses this correlation in the case of extremely rapid power increase and very low flow rate which is not considered under the current V&V.*

The user can find an identifier (JHT) for the flow and heat transfer regime printed in the major edits for each axial node. The value of the identifier is defined as follows:

1. Laminar
2. Natural convection
3. Turbulent
4. Transient (Rosental & Miller)
5. Nucleate boiling
6. Transition boiling
7. Film boiling

## 2.5.2 Verification Approach for Laminar, Transition, and Turbulent Flows

A single-channel base model using slab geometry and flat power distribution with four axial nodes is set up for the comparison between PARET/ANL and hand calculations (Table 2.18). Then, the test cases are created by specifying the IHT and IONEP, as well as by adjusting the mass flux and total reactor power to achieve the single-phase flow conditions corresponding to laminar, transition, and turbulent regimes (Table 2.19). Rosenthal and Miller correlation was not selected during the simulations in any of the tested cases in Table 2.19.

**Table 2.18. Base Model Specifications**

| | |
|---|---|
| Total fuel volume, $m^3$ | 0.00144 |
| Active fuel length, m | 0.6 |
| Inlet coolant temperature, °C | 20.0 |
| Fuel thickness, mm | 4.0 |
| Plate thickness, mm | 12.0 |
| Channel fuel width, m | 0.1 |
| Axial source description for all node (PFQ) | 1.000 |

**Table 2.19. Input Setting for Test Cases**

| Flow Regime | Input Setting | Mass Flux, $kg/m^2s$ | Total Power, MW | Input Constant | | Test Case |
|---|---|---|---|---|---|---|
| | | | | HTTCON | HTTEXP | |
| Laminar | IHT=0 | 100 | 0.02 | 1.4 | 0.33 | A05_01 |
| | IHT=1 | 100 | 0.02 | 30 | - | A05_02 |
| | IHT=2 | 100 | 0.02 | 30 | - | A05_03 |
| Transition | IHT=0<br>IONEP=0 | 180 | 0.02 | 1.4 | 0.33 | A05_04 |
| Turbulent | IONEP=0 | 2000 | 0.2 | - | - | A05_05 |
| | IONEP=1 | 2000 | 0.2 | - | - | A05_06 |
| | IONEP=2 | 2000 | 0.2 | - | - | A05_07 |
| | IONEP=3 | 2000 | 0.2 | - | - | A05_08 |
| | IONEP=4 | 2000 | 0.2 | - | - | A05_09 |
| | IONEP=6 | 2000 | 0.2 | - | - | A05_10 |

Using a spreadsheet, the hand calculation of each of these test cases implements the corresponding heat transfer correlation as follows:

- If the Dittus-Boelter correlation is used (turbulent regime and IONEP = 0),
  - Obtain bulk temperature $T_b$ and surface heat flux from PARET/ANL output
  - Use NIST table add-on for Excel [10] to determine coolant properties at bulk temperature $T_b$ and input pressure
  - Calculate the Re, Pr, Nu, and $h$

- If a laminar or turbulent correlation other than the Dittus-Boelter is used, the calculation involving the cladding surface temperature is performed iteratively:
  - Obtain bulk temperature $T_b$ and surface heat flux from PARET/ANL output. These values are constant during the iteration.
  - Assume an axial profile of cladding surface temperatures, $T_{clad\_A}$
  - Calculate reference coolant temperature $T_{film}$ from $T_b$ and $T_{clad\_A}$
  - Determine coolant properties at $T_{film}$
  - Calculate the Re, Pr, Nu, and $h$
  - Calculate new $T_{clad}$ using $h$ and PARET/ANL's output surface heat flux
  - Using a spreadsheet solver, adjust $T_{clad\_A}$ until $\sum\left(T_{clad} - T_{clad\_A}\right)^2 < 1\text{E-}10$

- In the case of the transition flow regime ($2300 \leq \text{Re} \leq 3700$), as shown in Table 2.17, the heat transfer coefficients $h_{NC}$ and $h_{TURB}$ must be calculated simultaneously using a single wall temperature that is the actual wall temperature corresponding to the heat transfer coefficient in the transition flow regime, $h_{TRANSIT}$. This is done on spreadsheet by performing the following calculation steps iteratively for a local axial node:
  - Obtain bulk temperature $T_b$ and surface heat flux from PARET/ANL output. These values are constant during the iteration.
  - Assume an axial profile of cladding surface temperatures ($T_{clad\_A}$)
  - Determine coolant properties at $T_b$ and $T_{clad\_A}$
  - Calculate Re, Pr, Nu
  - Calculate $h_{NC}$ by applying the laminar correlation to the obtained Re
  - Calculate $h_{TURB}$ by applying the turbulent correlation to the obtained Re
  - Calculate $x$ and $h_{TRANSIT}$
  - Calculate new $T_{clad}$ using $h_{TRANSIT}$ and PARET/ANL's output surface heat flux
  - Using a spreadsheet solver, adjust $T_{clad\_A}$ until $\sum\left(T_{clad} - T_{clad\_A}\right)^2 < 1\text{E-}10$

## 2.5.3 Calculation Results for Laminar, Transition, and Turbulent Flows

The comparison between PARET/ANL and hand calculations for all flow regimes is presented in Table 2.20. Good agreements are obtained for the heat transfer coefficients shown for all test cases. Those with the largest differences in Reynolds numbers and in heat transfer coefficients are A5_02, A5_03, and A5_04 (1.34%). The relative differences in Reynolds numbers in all cases come from the differences in water properties calculated by the NIST Table add-on for Excel and by the PARET/ANL code.

As shown in Table 2.17, the heat transfer coefficient in cases A5_02 and A5_03 is calculated directly from the input Nusselt number (input parameter HTTCON) and coolant thermal conductivity. Therefore, the difference in coolant thermal conductivity will show up in the heat transfer coefficient.

The difference in coolant properties has the strongest impact on the transition flow regime (test case A5_04) because the Reynolds number is used for the interpolation between the laminar and turbulent heat transfer correlations.

Overall, the differences in heat transfer coefficients obtained by PARET/ANL and hand calculations using water properties from NIST Tables are accepted for the application. The maximum difference is 2.6%, which is lower than the acceptance criteria defined in Table 1.2 for comparisons against hand calculations.

**Table 2.20. Comparison of PARET/ANL and Hand Calculations**

| Flow Regime | Test Case | Setting | | Axial Location | Reynolds Number* | | | Heat Transfer Coefficient, W/m$^2$.K | | |
|---|---|---|---|---|---|---|---|---|---|---|
| | | IHT | IONEP | | PARET/ ANL | Hand Calc. | Diff., % | PARET/ ANL | Hand Calc. | Diff., % |
| Laminar | A05_01 | 0 | - | Inlet | 1575.5 | 1596.7 | 1.34 | 2409.9 | 2419.9 | 0.42 |
| | | | | Outlet | 1987.0 | 2006.2 | 0.97 | 2475.7 | 2484.4 | 0.35 |
| | A05_02 | 1 | - | Inlet | 1575.5 | 1596.7 | 1.34 | 1138.5 | 1121.3 | 1.51 |
| | | | | Outlet | 1987.0 | 2006.2 | 0.97 | 1165.8 | 1152.0 | 1.18 |
| | A05_03 | 2 | - | Inlet | 1575.5 | 1596.7 | 1.34 | 1473.0 | 1454.0 | 1.29 |
| | | | | Outlet | 1987.0 | 2006.2 | 0.97 | 1414.2 | 1400.0 | 1.01 |
| Transition | A05_04 | 0 | 0 | Inlet | 2835.9 | 2874.0 | 1.34 | 2369.9 | 2335.0 | 1.47 |
| | | | | Outlet | 3233.6 | 3275.7 | 1.30 | 1936.9 | 1886.6 | 2.60 |
| Turbulent | A05_05 | - | 0 | Inlet | 31510.0 | 31933.6 | 1.34 | 7529.1 | 7516.7 | 0.16 |
| | | | | Outlet | 35464.8 | 35940.2 | 1.34 | 7950.7 | 7945.7 | 0.06 |
| | A05_06 | - | 1 | Inlet | 31510.0 | 31933.6 | 1.34 | 9016.3 | 8992.1 | 0.27 |
| | | | | Outlet | 35464.8 | 35940.2 | 1.34 | 9475.3 | 9463.5 | 0.12 |
| | A05_07 | - | 2 | Inlet | 31510.0 | 31933.6 | 1.34 | 9823.2 | 9852.9 | 0.30 |
| | | | | Outlet | 35464.8 | 35940.2 | 1.34 | 10269.8 | 10315.2 | 0.44 |
| | A05_08 | - | 3 | Inlet | 59931.6 | 59754.4 | 0.30 | 8964.6 | 8892.5 | 0.80 |
| | | | | Outlet | 63884.6 | 63650.4 | 0.36 | 9294.8 | 9220.3 | 0.81 |
| | A05_09 | - | 4 | Inlet | 31510.0 | 31933.6 | 1.34 | 9438.8 | 9408.5 | 0.32 |
| | | | | Outlet | 35464.8 | 35940.2 | 1.34 | 9725.8 | 9712.1 | 0.14 |
| | A05_10 | - | 6 | Inlet | 31510.0 | 31933.6 | 1.34 | 8502.1 | 8489.5 | 0.15 |
| | | | | Outlet | 35464.8 | 35940.2 | 1.34 | 8884.1 | 8884.9 | 0.01 |

** The Reynolds numbers are calculated using bulk temperature except for the test case A5_08 where the film temperature is used.*

### 2.5.4 Verification of the Transient Heat Transfer (Rosenthal & Miller) Option

If the input value of IONEP is zero or positive, then the Rosenthal & Miller transient heat transfer correlation will be considered in the selection of the heat transfer coefficient for natural convection and forced convection fully turbulent flows. The code will compare the values of the heat transfer coefficient from the Rosenthal & Miller correlation against the other value obtained from the correlation relevant to the flow regime. It will eventually use the largest value of the heat transfer coefficient in the calculations of the cladding temperature. If IONEP is negative, then the Rosenthal & Miller transient correlation is never selected. The JHT flag is listed in the main output file at each major edit, for each axial node. If the heat transfer coefficient from the Rosenthal & Miller correlation

is used, then the JHT identifier will be set to value 4 at the corresponding axial node.

For the verification of the implementation of the Rosenthal & Miller correlation, test cases from the SPERT-IV [11] experiments were selected because they have shown that this correlation is used under certain conditions (i.e., for very fast transients). SPERT-IV D-12/25 consists of 25 fuel assemblies in a rectangular grid structure. The reactor was cooled and moderated by light water. The experiments aim to determine the consequences of accidental reactivity insertion produced in the core by rapidly ejecting the transient rod starting from low initial power levels. Power excursion is initially limited by reactivity feedback and the event is terminated by control rod insertion. The experiments were conducted with zero forced flow, as well as with coolant flow provided by a coolant pump operating at various mass flow rates ranged between 0 and 5000 US GPM. The PARET/ANL model consists of two parallel channels and 20 axial nodes. Table 2.21 summarizes the cases considered to test the selection of Rosenthal & Miller correlation inlet flow rates at time zero and code options selection:

**Table 2.21. Cases Description for Verification of the Rosenthal & Miller Option**

| Case | Flow rate [GPM] | IHT | IONEP | Flow Regime |
|---|---|---|---|---|
| **A05_11** | 1000 | 2 | 0 | Fully turbulent flow |
| **A05_12** | 1000 | 0 | 8 | Fully turbulent flow |
| **A05_13** | 1000 | 0 | -8 | Fully turbulent flow |
| **A05_14** | 500 | 2 | 0 | Transition flow |
| **A05_15** | 0 | 0 | 0 | Natural convection |

In these cases, the PARET/ANL output from the first node of channel 1 is used for comparisons against hand calculations. The results are extracted at time t=0.201 s for all cases except for case A05_15 where the results are extracted at time t=0.099 s. The comparisons are provided in Table 2.22, along with the heat transfer coefficient selected for each case ($h_{selected}$).

Cases A05_11, A05_12, and A05_13 have the same flow rate of 1000 GPM and they are in the fully turbulent flow regime. For IHT=2 and IONEP=0 (Case A05_11), the original Dittus-Boelter correlation is used to calculate $h_{TURB}$ and the Rosenthal & Miller correlation is used to calculate $h_{TRAN}$. In this case, the $h_{TRAN}$ is selected because it is larger than $h_{TURB}$. As expected, case A05_12 with IHT=0 and IONEP=8 gives identical results with case A05_11 because IONEP=8 option adopts the same original formulation of the Dittus-Boelter correlation. In case A05_13, where IONEP=-8, the selected heat transfer coefficient is $h_{TURB}$, since the Rosenthal & Miller correlation is never selected for negative values of IONEP. (Although IONEP=8 is redundant with IONEP=0, the option was created to allow users to avoid using the Rosenthal & Miller correlation along with the selection of the original Dittus-Boelter by setting IONEP=-8.)

Case A05_14 has Re number in the transition flow range. In this case, the transition flow heat transfer coefficient ($h_{TRANSIT}$) is calculated using linear interpolation between the laminar and turbulent heat transfer coefficients based on the Re number ratio between the limits REL_T=2300 and RET_T=3700. $h_{TRANSIT}$ is the selected heat transfer coefficient although it is smaller than $h_{TRAN}$, because the Rosenthal & Miller correlation is not used for forced flow when Re<RET_T.

Case A05_15 has no pump, and the reactor is cooled by natural convection. It is seen from Table 2.22 that the calculated natural convection heat transfer coefficient ($h_{NC}$) is much smaller than $h_{TRAN}$, and therefore $h_{TRAN}$ is selected.

**Table 2.22. Comparisons of PARET/ANL and Hand Calculations for the Rosenthal & Miller Option**

| Case | Re | $h_{TURB}$ [W/m².K] | $h_{TRANSIT}$ [W/m².K] | $h_{NC}$ [W/m².K] | $h_{TRAN}$ [W/m².K] | $h_{selected}$ | $h_{PARET}$ [W/m².K] | Diff % |
|---|---|---|---|---|---|---|---|---|
| **A05_11** | 6129.39 | 3816.98 | - | - | 10149.56 | $h_{TRAN}$ | 10267.59 | 1.15 |
| **A05_12** | 6129.39 | 3816.98 | - | - | 10149.56 | $h_{TRAN}$ | 10267.59 | 1.15 |
| **A05_13** | 6129.39 | 3816.98 | - | - | 10149.56 | $h_{TURB}$ | 3810.74 | 0.16 |
| **A05_14** | 3064.71 | - | 1625.83 | - | 11602.77 | $h_{TRANSIT}$ | 1623.87 | 0.12 |
| **A05_15** | 15.17 | - | - | 337.80 | 27236.36 | $h_{TRAN}$ | 27304.54 | 0.25 |

It is found from these comparisons that the code logic for selection of the Rosenthal & Miller correlation performs appropriately. The percentage differences between the hand calculations and the PARET/ANL outputs ($h_{PARET}$) are acceptably small. The small differences between PARET/ANL output and hand calculations are mostly attributed to a small difference in the evaluation of physical properties used in hand calculations compared to those used internally in the code calculations. The maximum difference is 1.15%, which is smaller than the acceptance criteria defined in Table 1.2 for comparisons against hand calculations.

It should be noted that the Rosenthal & Miller correlation was implemented in the PARET/ANL code because the natural convection heat transfer coefficient (used when Re<REL_T, and IHT=0) predictions were too low for very fast transients. The heat transfer coefficient from the Rosenthal & Miller correlation may be used with both natural convection and forced convection fully turbulent flows, if this value is larger than those computed from the original correlations. The user can avoid using Rosenthal & Miller correlations if IONEP<0 is selected.

## 2.6 Capability A6 – Factor Used for Fin or Bundle Effect

Through the input parameter FINF, the PARET/ANL code allows the user to specify a scaling factor to account for the effect of the fuel bundles or the fins (on the cladding surface) on the turbulent heat transfer. This scaling factor is applied to the heat transfer coefficient which in turn is used to calculate the cladding temperature during the iterative calculation scheme.

The verification of this scaling process is performed through the comparison between the code and hand calculations. The spreadsheet used for the hand calculation of heat transfer presented in Section 2.5 is modified to include the input scale factor to the calculation of heat transfer coefficient. Two test cases used in the Section 2.5, A05_05 (Dittus-Boelter correlation) and A05_06 (Sieder-Tate correlation), are also modified to be A06_01 and A06_02, respectively, by changing the input FINF from 1.0 to 2.5 for the comparison purpose. The test cases and obtained calculation results are presented in Table 2.23.

**Table 2.23. Comparison of PARET/ANL and Hand Calculations**

| Test Case | Input Setting | | Description | Axial Location | Heat Transfer Coefficient, W/m$^2$.K | | Diff., % |
|---|---|---|---|---|---|---|---|
| | IONEP | FINF | | | PARET/ ANL | Hand Calc. | |
| A05_05 | 0 | 1.0 | Dittus-Boelter correlation without scaling | Inlet | 7529.1 | 7516.7 | 0.16 |
| | | | | Outlet | 7950.7 | 7945.7 | 0.06 |
| A06_01 | 0 | 2.5 | Dittus-Boelter correlation with scaling | Inlet | 18822.7 | 18791.8 | 0.16 |
| | | | | Outlet | 19876.6 | 19864.2 | 0.06 |
| A05_06 | 1 | 1.0 | Sieder-Tate correlation without scaling | Inlet | 9016.3 | 8992.1 | 0.27 |
| | | | | Outlet | 9475.3 | 9463.5 | 0.12 |
| A06_02 | 1 | 2.5 | Sieder-Tate correlation with scaling | Inlet | 21010.7 | 20916.2 | 0.45 |
| | | | | Outlet | 22208.4 | 22127.8 | 0.36 |

Table 2.23 shows that the PARET/ANL results agree well with hand calculations for all test cases. It should be noted that the calculated heat transfer coefficient is scaled by a factor of 2.5 in the case of Dittus-Boelter correlation and by a factor of 2.33 in the case of Sieder-Tate correlation, although both cases have the same input of FINF=2.5. The reason is that the Dittus-Boelter correlation does not use the cladding temperature to calculate the heat transfer coefficient, while the Sieder-Tate correlation does, because the latter has the correction factor $(\mu_b/\mu_w)^{0.14}$. So, the cladding temperatures predicted in A05_06 with FINF=1 are higher than those predicted in A06_02 with FINF=2.5, which leads to deviation of the heat transfer coefficients ratio from 2.5. In fact, the heat transfer calculation using Sieder-Tate or a correlation other than Dittus-Boelter requires iteration between the heat transfer coefficient and cladding temperature. As mentioned in Section 2.5, the spreadsheet was designed to use a solver capability to perform this iteration. Overall, the very good agreement between code and hand calculations confirms that the implementation of the scaling factor FINF in the code is correct. The maximum difference is 0.45%, which is lower than the acceptance criteria defined in Table 1.2 for comparisons against hand calculations.

## 2.7 Capability A7 – Boiling Heat Transfer

PARET/ANL includes two-phase heat transfer correlation options to model nucleate boiling (input parameter ITWOP), transient two-phase scheme (IMODE), and departure from nucleate boiling and flow instability (ICHF). The current work considers flow regimes up to transition boiling (liquid, nucleate boiling and transition boiling regimes) controlled by the input parameter ITWOP as presented in Table 2.24. The two-phase heat transfer involving boiling beyond the nucleate transition boiling has not been evaluated. Users can inspect the code output to determine if film boiling is occurring and may wish to further evaluate their application for these conditions.

## Table 2.24. Subcooled and Transition Boiling Heat Transfer Correlations [2]

| Flow Regime | Input Setting | Heat Transfer Correlation | Test Case |
|---|---|---|---|
| Subcooled Nucleate Boiling | ITWOP=0 | Heat flux boundary condition: $(q''_{\text{NB}})^{m+1} = (q''_{\text{NB}})^{m}\left[1+\frac{4(u_s^{m+1}-u_s^{\prime m})}{u_s^{\prime m}-u_{\text{sat}}}\right]$ where $m$ refers to the m$^{th}$ time node, subscript $s$ denotes cladding surface, and subscript *sat* denotes saturation conditions. Variable $u_s$ is the cladding surface temperature and $u_s'$ is two-phase temperature at the cladding surface. This boundary condition is based on the Jens-Lottes correlation: $$u'_s = u_{\text{sat}} + 60\exp\left(-\frac{p}{900}\right)\left(\frac{q''}{10^6}\right)^{\frac{1}{4}}$$ The numerical values of 60, 900, $10^6$, and ¼ are all fitted. US Customary units are used. | A02_01 |
| | ITWOP=1 | McAdams correlation $q''_{\text{nb}} = 0.074(U_w - U_{sat})^{3.86}$ Parameters used are 3.86 and 0.074. The 0.074 value shown varies with the extent of degassing of the water. It was found to be 0.074 at 0.06 ml. of air at standard conditions per liter of water. Temperature $U_w$ is the wall temperature (cladding surface temperature) and $U_{sat}$ is saturation temperature of the bulk coolant. US Customary units are used. | A07_01 |
| Transition Boiling Heat Transfer | ITWOP=1 ICHF=0 and ICHF=1 | For ICHF=0, Tong correlation is used to calculate the DNB heat flux as follows: $$q''_{\text{DNB}} = (0.23\times10^6 + 0.094G)\,[3.0 + 0.01(u_{\text{sat}} - u_b)] * \left[0.435 + 1.23\exp\left(-0.0093\frac{L}{D_e}\right)\right]\,[1.7 - 1.4e^{-a}]$$ where, $$a = 0.532\left[\frac{H_f - H_I}{H_{fg}}\right]^{\frac{3}{4}}\left(\frac{\rho_f}{\rho_g}\right)^{\frac{1}{3}}$$ G is the mass flux (Ib/hr.ft$^2$), $u_{sat}$ is saturation temperature (°F), $u_b$ is the bulk temperature (°F), L is the length (ft), $D_e$ is the hydraulic diameter (ft), $H_f$ is the enthalpy of saturated liquid (Btu/Ib), $H_I$ is the enthalpy at inlet temperature (Btu/Ib), $H_{fg}$ is the enthalpy difference (Btu/Ib), $\rho_f$ is the density of saturated liquid (Ib/ft$^3$), $\rho_g$ is the density of saturated vapor(Ib/ft$^3$). For ICHF=1, Bernath correlation is used to calculate the DNB heat flux, and the DNB surface temperature as follows: $$q_c = h_c[(U_w)_c - (U_b)_c]$$ $$h_c = \frac{0.067D_e}{D_e + \frac{\xi}{\pi}} + 0.65\times10^{-4}\frac{V}{{D_e}^{0.6}}$$ $$(U_w)_c = 57\ln(14.5P) - \frac{54P}{P+1.034214} - \frac{V}{1.2192}$$ where, $h_c$ is the (critical) heat transfer coefficient at burnout (MW/m$^2$-K), $(U_w)_c$ is the (critical) wall temperature (°C), $(U_b)_c$ is the (critical) bulk coolant temperature (°C), $D_e$ is the hydraulic diameter (m), $\xi$ is the | A07_02, A07_03 |

| | | | |
|---|---|---|---|
| | | heated perimeter (m), V is the coolant velocity (m/s), P is the absolute pressure (bar).<br>This correlation is valid for 0<V≤ 54 ft/s; 23 < P < 3000 psia; 0.143 < $D_e$ < 0.66 in.<br><br>Two-phase nucleate boiling heat flux is calculated from McAdams correlation:<br><br>$q'' = 0.074(U_w - U_{sat})^{3.86}$<br><br>where, q'' in Btu/hr/ft2. and temperatures in °F<br><br>Nucleate boiling boundary is calculated from:<br><br>$(q''_{\mathrm{NB}})^{m+1} = (q''_{\mathrm{NB}})^{m}\left[1 + \frac{4(u_s^{m+1} - u_s'^{m})}{u_s'^{m} - u_{\mathrm{sat}}}\right]$<br><br>where $m$ refers to the m[th] time node, subscript *s* denotes cladding surface, and subscript *sat* denotes saturation conditions. The variable $u_s$ is the cladding surface temperature and $u_s'$ is the two-phase temperature at the cladding surface.<br><br>Transition boiling heat flux is calculated from:<br><br>$q''_{\mathrm{TB}} = q''_{\mathrm{DNB}} - K_{TB}(u_s - (u_s)_{DNB})$, where $K_{TB}$ is a constant. | |

## 2.7.1 Nucleate Boiling Heat Transfer

The verification of these subcooled heat transfer correlations is based on code-to-code comparisons between PARET/ANL and RELAP5. It should be noted that RELAP5 does not use the Jens-Lottes or the McAdams correlations. Instead, the subcooled nucleate boiling is handled by the Chen correlation [12]. The difference in heat transfer correlations used by the codes would affect the validity of the current V&V. However, the code-to-code comparison still provides strong evidence on the performance of each code.

As mentioned in section 2.2, the test case A02_01 was previously created for the code-to-code comparison, and it uses ITWOP = 0. This case is modified using ITWOP = 1 to form a new test case A07_01. Results from these two test cases are presented in Figure 2.18 and Table 2.25. As the heat transfer mode is changed from single-phase liquid to subcooled nucleate boiling at ~1.03 sec, the application of different heat transfer correlations leads to differences in the calculated temperatures. It should be noted that the average channels of both ITWOP=0 and ITWOP=1 cases do not present subcooled boiling, and the boiling only occurs in the hot channel. The results obtained by PARET/ANL bound those by RELAP5 and the use of ITWOP=1 is more conservative for peak fuel and peak cladding temperatures. Peak coolant temperatures are essentially the same for all results. Given the complexity of the nucleate boiling heat transfer, it can be concluded that the codes' calculations agree with each other, and they give consistent results, which gives confidence about the code performance for subcooled nucleate boiling conditions. Additional verification case of subcooled nucleate boiling is provided in the next subsection along with subcooled transition boiling verification using hand calculations to further confirm the accuracy of the predicted results.

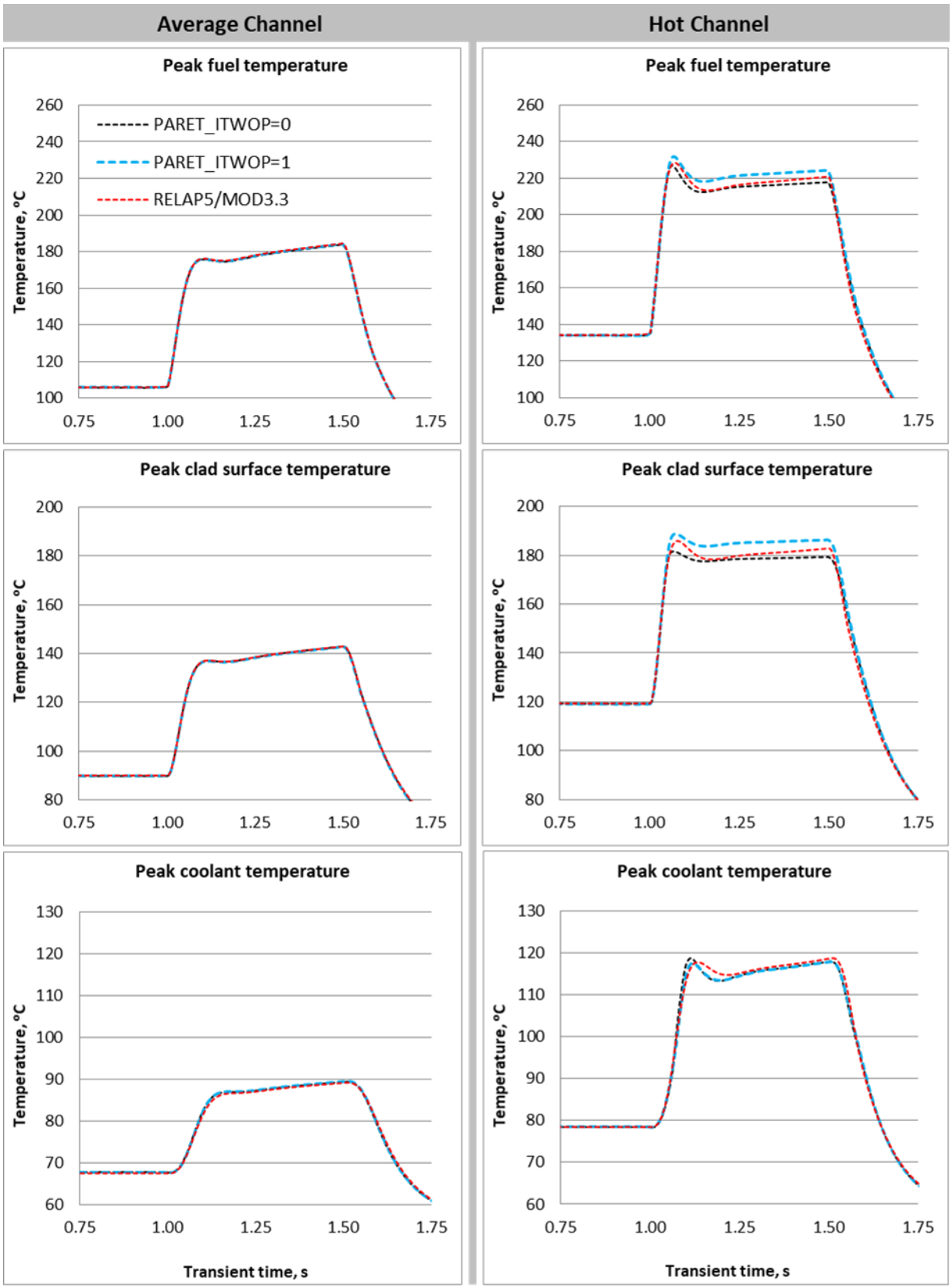


**Figure 2.18. Comparison of Transient Data**

**Table 2.25. Comparison of Transient Peak Temperatures (°C)**

| Component | Channel | PARET/ANL | | RELAP5/MOD3.3 |
|---|---|---|---|---|
| | | ITWOP=0 | ITWOP=1 | |
| Fuel meat | Average | 184.0 | 184.0 | 184.2 |
| | Hot | 226.5 | 231.8 | 228.1 |
| Cladding | Average | 142.8 | 142.8 | 142.9 |
| | Hot | 181.5 | 188.9 | 186.1 |
| Coolant | Average | 89.4 | 89.4 | 89.1 |
| | Hot | 118.8 | 118.0 | 118.9 |

## 2.7.2 Transition Boiling Heat Transfer

Test cases A07_02 and A07_03 were derived from a case from SPERT-III E-core reactor experiments [13] for the verification of heat transfer in single-phase liquid, nucleate boiling, and transition boiling modes. The SPERT-III E-core represents a pressurized water reactor core consisting of 64 assemblies with eight control rods and a centrally located transient rod. For the case considered, the reactor pressure is 103.42 bar, and the inlet temperature is 262.5 °C. The reactor was initially operating at a low power of 0.015 MW and then the transient is initiated by ejection of transient rod resulting in a reactivity insertion of 1.29 $ with a ramp rate of 15 $/s.

The reactor core is modeled in PARET/ANL using five channels with 20 axial nodes in each channel. The axial power distribution varies asymmetrically with minimum power towards the top and bottom, and the maximum power below the center of the channel. To simplify the verification process, the model is run in power-driven mode, with the input power evolution determined as follows:

- For $0 \le t \le t_{max}$, where $t_{max}$ is the time of the peak power in the modeled reactivity insertion transient, the power evolution matches that of a prior PARET/ANL analysis in reactivity-driven mode,
- For $t > t_{max}$, the power is held fixed to the peak power.

Having the problem run in power-driven mode provides flexible control over the transient to reach the desired heat transfer modes needed in this verification process. Power distribution changes axially with minimum power towards the channel inlet and outlet and the maximum power is in the lower half of the channel.

The following heat transfer options are adopted in this case, see Table 2.17 and Table 2.24 for a description of each correlation:

- IONEP=0 (Dittus-Boelter correlation is used for single-phase turbulent heat transfer)
- ITWOP=1 (McAdams two-phase nucleate boiling correlation)
- IMODE=0 (original PARET/ANL transient two-phase scheme)
- ICHF=1 (Bernath DNB correlation) & ICHF=0 (Tong DNB correlation)
- IHT =2 (single-phase heat transfer is calculated from subroutine htran2)

Cases A07_02 and A07_03 are identical except that case A07_02 sets ICHF=1, whereas case A07_03 sets ICHF=0.

The output of case A07_02 shows that initially at time t = 0, the heat transfer mode in all channels and all axial nodes is identified to be in the liquid regime. As power increases over time, phase change takes place, and it is initially reported in major edits in channel 4 at time t = 0.125 s, where heat transfer

changed from the liquid regime to the nucleate boiling regime. The transition boiling heat transfer regime starts to take place at t = 0.132 s in channel 4. To verify the code output and the selection of heat transfer regime, the output of channel 3 at time t = 0.135 s is selected. At the selected time in channel 3, all the three heat transfer regimes exist in the same channel, where it starts with liquid flow regime at the entrance (axial nodes 1 and 2), nucleate boiling (nodes 3 to 5), transition boiling (nodes 6 to 8), nucleate boiling (nodes 9 and 10), and then liquid phase for the rest of the channel (nodes 11 to 20).

The verification uses hand calculations performed in spreadsheets to verify the logic selection in different heat transfer regimes (liquid, nucleate boiling, and transition boiling), the calculations of the heat transfer coefficient used as a boundary condition for calculations of the cladding surface temperature, and the critical heat flux which is shown in PARET/ANL output as the burnout ratio defined as the ratio of the critical heat flux to the wall heat flux.

Water physical properties used in the hand calculations are obtained from the PARET/ANL output file at the given system pressure. Linear interpolation is used to obtain physical properties at the desired temperature at each axial node. Water properties are given as a function only of temperature because they are independent of the local pressure.

Table 2.26 summarizes the most relevant calculations results used in the comparisons between PARET/ANL and hand calculations.

The calculations consist of the following steps which are also illustrated in Figure 2.19:

- The enthalpy of liquid is compared against the enthalpy of vapor. For this case, the enthalpy of coolant is always less than the enthalpy of vapor. If the enthalpy of coolant exceeds the enthalpy of vapor, the code will proceed for single phase vapor calculations.
- The critical heat flux ($q_{DNB}$) is calculated from the Bernath DNB correlation (for ICHF = 1) or from the Tong DNB correlation (for ICHF = 0).
- The critical temperature ($T_{DNB}$) is calculated from the McAdams's correlation using $q_{DNB}$ obtained from the previous step.
- The nucleate boiling temperature ($T_{NB}$) is calculated from the McAdams' correlation using the wall heat flux.
- The heat transfer coefficient based on the Dittus-Boelter correlation (IONEP=0) is calculated, and the wall temperature based on forced convection ($T_{FC}$) is calculated.
- If the $T_{FC}$ is less than the saturation temperature ($T_{sat}$ = 313.44 °C) or the nucleate boiling temperature less than the saturation temperature, then liquid phase is applied at the corresponding axial node.
- If the above condition is false, the nucleate boiling heat flux is calculated (see Table 2.24) and compared against the forced convection heat flux. If the latter is higher, then the liquid regime is assumed.
- The burnout (BR) ratio is calculated as the DNB heat flux calculated from the Bernath or Tong correlations (at user option) divided by the wall heat flux.
- If the forced convection heat flux is less than the nucleate boiling heat flux, nucleate boiling prevails, otherwise the code will return to the liquid regime.
- If the nucleate boiling heat flux is higher than the DNB heat flux, it will move to film boiling regime calculations.

- If the above condition is false, the heat transfer coefficient is calculated by dividing the nucleate boiling heat flux by the temperature difference between the wall and bulk temperature.
- If $q_{NB} > q_{DNB}$, film boiling conditions are then checked. If the departure from transition boiling temperature $T_{DTB}$ is greater than the wall temperature, then film boiling prevails, otherwise transition boiling is assumed.
- The transition boiling heat flux $q_{TB}$ is calculated and compared against $q_{DNB}$. If $q_{TB}<q_{DNB}$, the heat transfer coefficient based on transition boiling heat flux is calculated.

The logic for heat transfer regime selection described above matches the output for this case and is consistent with the model description given in the User Guide [2]. Comparing the heat transfer coefficients from PARET/ANL output to hand calculations from a spreadsheet shows close agreements. The maximum difference is 1.27%, and the maximum difference for the burnout ratio is 1.6%. The small differences in the heat transfer coefficient between PARET/ANL and spreadsheet calculations are attributed to the difference in physical properties, i.e., in the spreadsheets, the physical properties are obtained from linear interpolation; however, PARET/ANL directly calculates them from refined models. Also, it should be noted that the correlations used to run these cases are selected for verification purposes only, and they are not necessarily the most appropriate choice to model the thermal hydraulics conditions, or they have the right range of operating conditions that is valid for this simulated case.

For ICHF=0, the same steps are applied except for $q_{DNB}$ which is calculated from Tong correlation. The verification made when ICHF=0, is also shown in Table 2.26 for axial node 4, where transition boiling is predicted. When the burnout ratio is less than one, it is not traced in PARET/ANL and it is set to -999 in the output. Comparing the critical heat flux from the spreadsheet ($q_{DNB}$=3980535.3 W/m$^2$) and from PARET/ANL output ($q_{DNB}$= 3980306.47 W/m$^2$) shows a tiny difference of 0.006%.

This exercise verifies that the process given in the User Guide [2] for selecting the correct boiling regime, heat flux, and heat transfer coefficient is executed correctly. The maximum difference in heat transfer coefficient is 1.3% and for burnout ratio is 1.6%, which are lower than the acceptance criteria defined in Table 1.2 for comparisons against hand calculations.

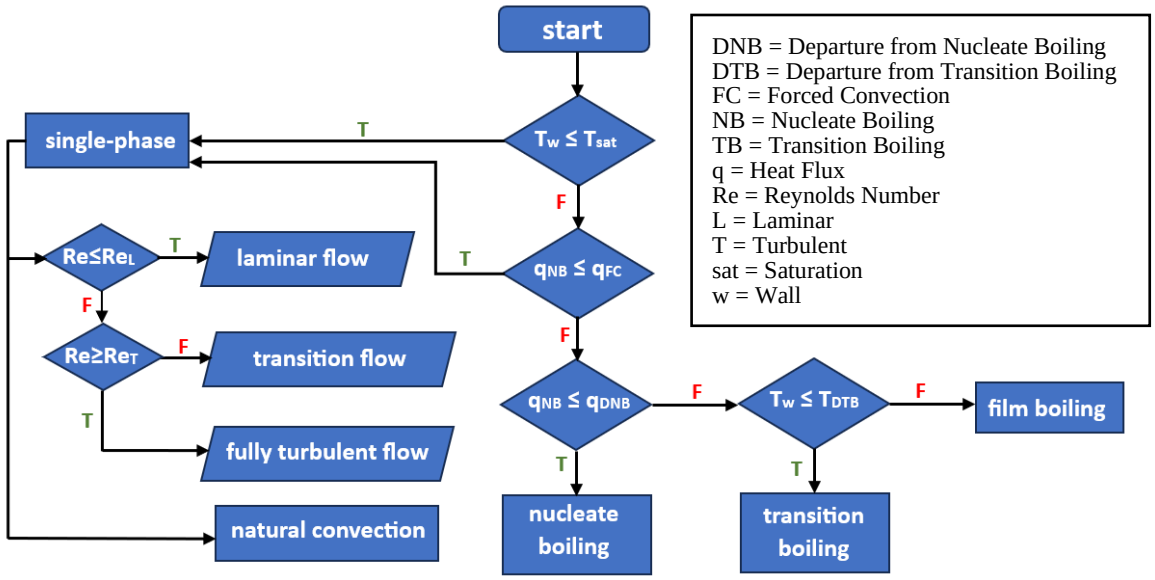


**Figure 2.19. Simplified Logic Description of Heat Transfer Modes in PARET/ANL**

**Table 2.26. Comparison of Heat transfer and Burnout Ratio in Channel 3 at t=0.135 s**

| Test Case | Node | PARET/ANL Output | | | | | | Spreadsheet Hand Calculations | | | | | | | | | | Diff. %, HTC | Diff. %, BR |
|---|---|---|---|---|---|---|---|---|---|---|---|---|---|---|---|---|---|---|---|
| | | q, W/m² | $T_b$, °C | $T_w$, °C | $T_{FC}$, °C | HTC, W/m².K | BR ratio | $q_{DNB}$, W/m² | $T_{DNB}$, °C | $T_{NB}$, °C | $q_{NB}$, W/m² | $q_{FC}$, W/m² | $T_{DTB}$, °C | $q_{TB}$, W/m² | HTC, W/m².K | BR Ratio | Phase | | |
| A07_02 | 1 | 1.65E6 | 262.49 | 313.81 | - | 32073.94 | 3.43 | 5.65E6 | 358.85 | 346.43 | -4.83E6 | 1.65E6 | - | - | 32023.08 | 3.43 | L | 0.2 | 0.0 |
| | 2 | 2.12E6 | 264.76 | 330.42 | - | 32229.97 | 2.61 | 5.53E6 | 358.60 | 348.65 | -2.21E6 | 2.12E6 | - | - | 32126.46 | 2.61 | L | 0.3 | 0.0 |
| | 3 | 2.96E6 | 266.86 | 351.86 | 351.86 | 34851.97 | 1.83 | 5.43E6 | 358.38 | 351.86 | 2.93E6 | 2.74E6 | - | - | 34416.42 | 1.86 | NB | 1.3 | 1.6 |
| | 4 | 4.30E6 | 268.86 | 355.76 | 355.76 | 49534.78 | 1.24 | 5.34E6 | 358.18 | 355.76 | 4.28E6 | 2.84E6 | - | - | 49233.36 | 1.25 | NB | 0.6 | 0.8 |
| | 5 | 5.25E6 | 270.67 | 357.99 | 357.99 | 60109.90 | 1.00 | 5.27E6 | 358.03 | 357.99 | 5.22E6 | 2.89E6 | - | - | 59762.08 | 1.01 | NB | 0.6 | 1.0 |
| | 6 | 5.17E6 | 272.12 | 364.96 | - | 55731.10 | -9999 | 5.22E6 | 357.93 | 357.83 | - | - | 1098.42 | 5.174E6 | 55727.63 | - | TB | 0.0 | - |
| | 7 | 5.13E6 | 273.03 | 368.48 | - | 53785.56 | -9999 | 5.20E6 | 357.89 | 357.74 | - | - | 1094.77 | 5.133E6 | 53780.69 | - | TB | 0.0 | - |
| | 8 | 5.18E6 | 273.41 | 364.04 | - | 57097.80 | -9999 | 5.21E6 | 357.92 | 357.83 | - | - | 1095.59 | 5.175E6 | 57091.43 | - | TB | 0.0 | - |
| | 9 | 5.17E6 | 273.14 | 357.81 | 357.81 | 61030.92 | 1.02 | 5.27E6 | 358.03 | 357.81 | 5.14E6 | 2.95E6 | - | - | 60686.05 | 1.02 | NB | 0.6 | 0.0 |
| | 10 | 4.21E6 | 272.20 | 355.53 | 355.53 | 50569.51 | 1.27 | 5.36E6 | 358.24 | 355.53 | 4.19E6 | 2.94E6 | - | - | 50257.29 | 1.28 | NB | 0.6 | 0.8 |
| | 11 | 2.84E6 | 270.91 | 350.36 | - | 35800.22 | 1.93 | 5.48E6 | 358.49 | 351.46 | 2.51E6 | 2.84E6 | - | - | 35792.21 | 1.93 | L | 0.0 | 0.0 |
| | 12 | 2.21E6 | 269.55 | 330.73 | - | 36053.89 | 2.53 | 5.58E6 | 358.71 | 349.03 | -2.32E6 | 2.21E6 | - | - | 36045.39 | 2.53 | L | 0.0 | 0.0 |
| | 13 | 1.65E6 | 268.20 | 313.79 | - | 36219.36 | 3.44 | 5.68E6 | 358.92 | 346.46 | -4.87E6 | 1.65E6 | - | - | 36250.59 | 3.44 | L | 0.1 | 0.0 |
| | 14 | 1.22E6 | 266.95 | 300.44 | - | 36366.17 | 4.74 | 5.77E6 | 359.10 | 343.96 | - | - | - | - | 36229.27 | 4.74 | L | 0.4 | 0.0 |
| | 15 | 8.90E5 | 265.88 | 290.31 | - | 36443.82 | 6.56 | 5.84E6 | 359.25 | 341.58 | - | - | - | - | 36339.79 | 6.56 | L | 0.3 | 0.0 |
| | 16 | 6.45E5 | 265.03 | 282.70 | - | 36529.24 | 9.15 | 5.90E6 | 359.37 | 339.33 | - | - | - | - | 36422.62 | 9.15 | L | 0.3 | 0.0 |
| | 17 | 4.60E5 | 264.36 | 276.93 | - | 36567.87 | 12.94 | 5.95E6 | 359.46 | 337.15 | - | - | - | - | 36484.06 | 12.94 | L | 0.2 | 0.0 |
| | 18 | 3.17E5 | 263.86 | 272.53 | - | 36604.98 | 18.86 | 5.98E6 | 359.53 | 334.98 | - | - | - | - | 36528.08 | 18.85 | L | 0.2 | 0.1 |
| | 19 | 2.19E5 | 263.43 | 269.40 | - | 36650.15 | 27.48 | 6.01E6 | 359.59 | 333.01 | - | - | - | - | 36561.03 | 27.48 | L | 0.2 | 0.0 |
| | 20 | 1.78E5 | 263.22 | 268.07 | - | 36656.42 | 33.94 | 6.03E6 | 359.62 | 331.98 | - | - | - | - | 36582.33 | 33.94 | L | 0.2 | 0.0 |
| A07_03 | 4 | 3.96E6 | 268.86 | 358.10 | - | 44376.12 | -9999 | 3.98E6 | 354.91 | 354.86 | - | - | - | - | 44378.31 | - | TB | 0.0 | - |

q=Heat Flux, T= Temperature, HTC=Heat Transfer Coefficient, BR ratio=Burnout Ratio, b=Bulk, w=Wall, FC=Forced Convection, DNB=Departure from Nucleate Boiling, NB=Nucleate Boiling, DTB=Departure from Transition Boiling, TB=Transition Boiling, L=Liquid

## 2.8 Capability A8 – Friction Factor Correlations

For an unheated channel, the friction factor is calculated for all Reynolds number ranges and geometry options as shown in Table 2.27. Verification of these correlations is performed by comparing results from PARET/ANL and hand calculations. For this comparison, test case A05_05 described in Section 2.5 is modified as follows:

- Set power to 1.0E-3 W to form a new test case A08_01;
- Set power to 1.0E-3 W and change IGEOM to 1 to form new test cases A08_02;
- Set power to 1.0E-3 W and increase mass flux to 2000 and 3000 kg/m$^2$s to form new test cases A08_03 and A8_04, respectively.

**Table 2.27. Friction Factor Correlation for Unheated Channel [2]**

| Re | Geometry Options | Friction Correlations | Test Case |
|---|---|---|---|
| Re ≤ 2000 | Rectangular channel (IGEOM = 0 or 2) | $f = 96/\mathrm{Re}$ | A08_01 |
| | Cylindrical channel (IGEOM = 1) | $f = 64/\mathrm{Re}$ | A08_02 |
| 2000 < Re ≤ 100,000 | All geometry options | $f = 0.210816 * \mathrm{Re}^{-0.213727}$ | A08_03 |
| Re > 100,000 | All geometry options | $f = 0.11437 * \mathrm{Re}^{-0.160608}$ | A08_04 |

As the verification for the calculation of Re has previously been performed under Section 2.5, the current hand calculation is simplified by using the Re calculated by the code. The comparison between PARET/ANL and hand calculations for all flow regimes presented in Table 2.28 confirms that the friction factor correlations for the unheated channel are implemented correctly.

**Table 2.28. Comparison of PARET/ANL and Hand Calculations**

| Test Case | Re (Calculated by PARET/ANL) | Friction Factor | | |
|---|---|---|---|---|
| | | PARET/ANL | Hand Calc. | Diff., % |
| A08_01 | 1576 | 0.0609 | 0.0609 | 0.0 |
| A08_02 | 1260 | 0.0508 | 0.0508 | 0.0 |
| A08_03 | 84027 | 0.0187 | 0.0187 | 0.0 |
| A08_04 | 126040 | 0.0173 | 0.0173 | 0.0 |

Given a heat source in fuel plates, the base friction factor calculated above is corrected using a multiplication factor (for Re < 2000) called "the heated wall effect" defined by

$$f_{hw} = 1.0 + \frac{p_{heat}}{p_{wet}} * \left[\left(\frac{\mu_w}{\mu_b}\right)^{0.54} - 1.0\right]$$

where $f_{hw}$ is the correction factor for the heated wall; $p_{heat}$ and $p_{wet}$ are heated and wetted perimeters ($p_{heat}/p_{wet}$ is set to 1.0 in the code); $\mu_w$ is coolant viscosity at temperature of the wall; and $\mu_b$ is the bulk coolant viscosity. The V&V of the friction factor involving the heated wall effect is included in the Section 2.4 in which very good agreement is obtained between the PARET/ANL and independent *Mathematica* calculations of test case. The results presented in Table 2.14 do not validate each friction factor at each axial node directly, but they do validate the total pressure drop, mass flow rate, and coolant exit temperature – all of which are extremely dependent on the friction factors involved. Agreement would be impossible if the friction factors were incorrect. The friction factor

comparison between PARET/ANL and *Mathematica* for test case A04-04 in the laminar flow range is presented in Figure 2.20.

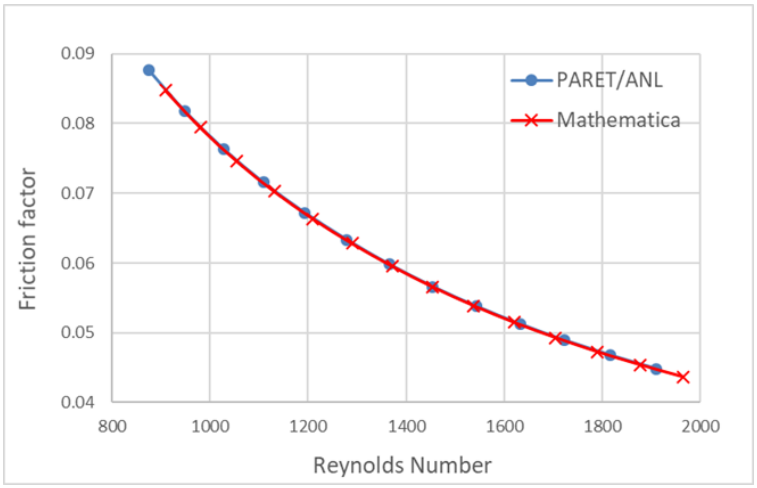


**Figure 2.20. Comparison of Friction Factor between PARET/ANL and Mathematica**

Overall, the comparisons between PARET/ANL calculations with auxiliary calculations for unheated channel cases and with the *Mathematica* calculation of test case A04_04 for a heated channel confirm that the friction factor correlations are implemented correctly. The identical results for all the reported values indicate also that the acceptance criteria defined in Table 1.2 are satisfied.

## 2.9 Capability A9 – Steady-State Initialization

PARET/ANL allows the user to control how steady-state initialization is performed through options on Input Card 22000. This capability is verified by comparing the initialization calculation and a null-transient run of a test case. In Section 2.5, the steady-state of test case A05_01 was constructed using the steady-state initialization option. This test case is modified by setting the initializing time to 0.0 s and running with constant power and mass flux for 10 s and for 300 s (null transient) to form a new test case A09_01. One can observe that the 10 s null transient is not fully converged to the steady-state result in column 3. The 300 s null transient agrees extremely closely with the steady-state result in column 3. Calculation results presented in Table 2.29 confirm that the steady-state initialization capability is implemented correctly in PARET/ANL. These tiny differences indicate that the acceptance criteria defined in Table 1.2 are satisfied with comparisons against hand calculations.

**Table 2.29. Comparison of PARET/ANL and Hand Calculations**

| Parameter | Axial Location | Transient time | | | [A] vs. [B] Diff., % |
|---|---|---|---|---|---|
| | | With Steady-State Initialization (A05_01) | Null Transient (A09_01) | | |
| | | 0.0 s [A] | 10.0 s | 300 s [B] | |
| Enthalpy, kJ/kg | Inlet | 83.66 | 83.66 | 83.66 | 0.000 |
| | Outlet | 125.32 | 126.16 | 125.33 | 0.003 |
| Coolant temperature, °C | Inlet | 19.98 | 19.98 | 19.98 | 0.000 |
| | Outlet | 29.98 | 30.18 | 29.98 | 0.003 |
| Cladding surface temp., °C | Inlet | 43.03 | 42.43 | 43.03 | 0.000 |
| | Outlet | 52.42 | 64.73 | 52.43 | 0.005 |
| Fuel centerline temp., °C | Inlet | 48.59 | 47.87 | 48.59 | 0.000 |
| | Outlet | 57.98 | 73.10 | 57.98 | 0.003 |
| Heat transfer coef., $W/m^2K$ | Inlet | 2409.86 | 2385.90 | 2409.86 | 0.000 |
| | Outlet | 2475.76 | 2914.73 | 2475.86 | 0.004 |

# 3 Verification of Transient Capabilities

## 3.1 Capability B1 - Point Kinetics Model

Several verification exercises have been carried out for the point kinetics algorithm used in PARET/ANL Version 7.6. PARET/ANL calculations are compared with semi-analytic solutions in the case of step reactivity changes or with a published benchmarking calculation for a positive ramp reactivity insertion. These cases demonstrate that the PARET/ANL point kinetics solution algorithm generates highly accurate solutions for the reactor power and for the delayed neutron concentrations as functions of time.

The verification of this capability considers both step and ramp reactivity changes using the test cases presented in Table 3.1. Note that the initial powers in PARET/ANL models are set to small values (1.0E-90 MW for cases B01_01 to B01_20 and 1.0E-30 MW for cases B01_21 to B01_28) to avoid any thermal hydraulics feedback reactivity effects. Hence, the corresponding output powers were multiplied by 1.0E+90 or 1.0E+30 to compare with the reference data.

**Table 3.1. Test Cases Used for the Verification of the Point Kinetics Model**

| Type | Reactivity Insertion | Maximum (input) Time Step Δt, s | Test Case |
|---|---|---|---|
| Step insertion | 1.0 $ | $10^{-4}$ | B01_01 |
| | | $10^{-3}$ | B01_02 |
| | | $10^{-2}$ | B01_03 |
| | | $10^{-1}$ | B01_04 |
| | 0.5 $ | $10^{-4}$ | B01_05 |
| | | $10^{-3}$ | B01_06 |
| | | $10^{-2}$ | B01_07 |
| | | $10^{-1}$ | B01_08 |
| | -0.5 $ | $10^{-4}$ | B01_09 |
| | | $10^{-3}$ | B01_10 |
| | | $10^{-2}$ | B01_11 |
| | | $10^{-1}$ | B01_12 |
| | -1.0 $ | $10^{-4}$ | B01_13 |
| | | $10^{-3}$ | B01_14 |
| | | $10^{-2}$ | B01_15 |
| | | $10^{-1}$ | B01_16 |
| | -10.0 $ | $10^{-4}$ | B01_17 |
| | | $10^{-3}$ | B01_18 |
| | | $10^{-2}$ | B01_19 |
| | | $10^{-1}$ | B01_20 |
| Ramp insertion | 0.1 $/s | $10^{-4}$ | B01_21 |
| | | $10^{-3}$ | B01_22 |
| | | $10^{-2}$ | B01_23 |
| | | $10^{-1}$ | B01_24 |
| | -0.1 $/s | $10^{-4}$ | B01_25 |
| | | $10^{-3}$ | B01_26 |
| | | $10^{-2}$ | B01_27 |
| | | $10^{-1}$ | B01_28 |
| Problem with feedback | | | B01_29 |

**Step Reactivity Changes**

Benchmarking solutions for step reactivity changes of 1.0 $, 0.5 $, -0.5 $ and -1.0 $ have been published by Ganapol [14]. The solutions for these cases were also obtained by using *Mathematica*. Comparisons with Ganapol's results, and to the *Mathematica* results, revealed that depending on the size of the time step, PARET/ANL was capable of greater precision than the ten significant figures published by Ganapol. To demonstrate this, the semi-analytic solution based on the Inhour equation [15] used in the Mathematica model was evaluated. For this purpose, the roots of the Inhour equation were calculated with an approximate precision of 11 to 12 significant figures. Comparison of PARET/ANL solutions for step reactivity changes of 1.0 $, 0.5 $, -0.5 $, -1.0 $, and -10 $ are shown in Table 3.2, with the percentage difference between PARET/ANL results and *Mathematica* results given for each case. Parameter $\Delta t$ in Table 3.1 and Table 3.2 is the maximum (input) time step size given to the integration process in PARET/ANL. That step size can be automatically reduced to maintain precision. It can also be automatically expanded up to that value. To demonstrate the stability of the PARET/ANL solution, the -0.5 $ and -10 $ cases were extended to a time interval of 2.8 hours (10,000 s). Even at the extreme time of 10,000 s, the PARET/ANL solution of the -10$ case with a time step of $10^{-1}$ s agrees very well (a difference of 2.6E-5 %) with the more accurate result shown for a time step size of $10^{-4}$ s. Ganapol did not publish results for the -10$ step reactivity case.

## Table 3.2. Comparison of Solutions Obtained for Step Reactivity Insertions

**Δt in this table is the maximum (input) time step size given to the integrator used by PARET/ANL**

| Time, s | Ganapol solution Power, MW | Mathematica Solution Power, MW | PARET/ANL Power, MW | | | | | | | |
|---|---|---|---|---|---|---|---|---|---|---|
| | | | $\Delta t = 10^{-1}$ s | Diff., % | $\Delta t = 10^{-2}$ s | Diff., % | $\Delta t = 10^{-3}$ s | Diff., % | $\Delta t = 10^{-4}$ s | Diff., % |
| **1.0 $** | | | | | | | | | | |
| | | | **Case B01_04** | | **Case B01_03** | | **Case B01_02** | | **Case B01_01** | |
| **0.1** | 2.515766141E+00 | 2.51576614140E+00 | 2.51576612593E+00 | -6.1E-7 | 2.51576611820E+00 | -9.2E-7 | 2.51576614132E+00 | -3.3E-9 | 2.51576614140E+00 | -4.9E-12 |
| **0.5** | 1.036253381E+01 | 1.03625338106E+01 | 1.03625164208E+01 | -1.7E-4 | 1.03625317858E+01 | -2.0E-5 | 1.03625338083E+01 | -2.3E-8 | 1.03625338106E+01 | -3.2E-11 |
| **1** | 3.218354095E+01 | 3.21835409455E+01 | 3.21806425169E+01 | -9.0E-3 | 3.21835271598E+01 | -4.3E-5 | 3.21835409306E+01 | -4.6E-8 | 3.21835409455E+01 | -6.4E-11 |
| **10** | 3.246978898E+09 | 3.24697889803E+09 | 3.23487551238E+09 | -3.7E-1 | 3.24696364864E+09 | -4.7E-4 | 3.24697888244E+09 | -4.8E-7 | 3.24697889801E+09 | -6.6E-10 |
| **100** | 2.596484646E+89 | 2.59648464655E+89 | 2.49410096469E+89 | -3.9E+0 | 2.59636137874E+89 | -4.7E-3 | 2.59648452118E+89 | -4.8E-6 | 2.59648464638E+89 | -6.6E-9 |
| **0.5 $** | | | | | | | | | | |
| | | | **Case B01_08** | | **Case B01_07** | | **Case B01_06** | | **Case B01_05** | |
| **0.1** | 1.533112646E+00 | 1.53311264595E+00 | 1.53311254579E+00 | -6.5E-6 | 1.53311256171E+00 | -5.5E-6 | 1.53311264580E+00 | -9.7E-9 | 1.53311264595E+00 | -1.2E-11 |
| **1** | 2.511494291E+00 | 2.51149429149E+00 | 2.51138523745E+00 | -4.3E-3 | 2.51149405604E+00 | -9.4E-6 | 2.51149429123E+00 | -1.0E-8 | 2.51149429149E+00 | -1.1E-11 |
| **10** | 1.421502524E+01 | 1.42150252424E+01 | 1.42123640817E+01 | -1.9E-2 | 1.42150214663E+01 | -2.7E-5 | 1.42150252385E+01 | -2.8E-8 | 1.42150252424E+01 | -4.1E-11 |
| **100** | 8.006143562E+07 | 8.00614356244E+07 | 7.99352367659E+07 | -1.6E-1 | 8.00612709794E+07 | -2.1E-4 | 8.00614354548E+07 | -2.1E-7 | 8.00614356242E+07 | -2.1E-10 |
| **-0.5 $** | | | | | | | | | | |
| | | | **Case B01_12** | | **Case B01_11** | | **Case B01_10** | | **Case B01_9** | |
| **0.1** | 6.989252256E-01 | 6.98925225571E-01 | 6.98925271554E-01 | 6.6E-6 | 6.98925264480E-01 | 5.6E-6 | 6.98925225666E-01 | 1.4E-8 | 6.98925225571E-01 | 1.4E-11 |
| **1** | 6.070535656E-01 | 6.07053565606E-01 | 6.07059473800E-01 | 9.7E-4 | 6.07053578449E-01 | 2.1E-6 | 6.07053565624E-01 | 2.9E-9 | 6.07053565606E-01 | -4.4E-12 |
| **10** | 3.960776907E-01 | 3.96077690715E-01 | 3.96081663828E-01 | 1.0E-3 | 3.96077698352E-01 | 1.9E-6 | 3.96077690725E-01 | 2.3E-9 | 3.96077690715E-01 | -1.3E-10 |
| **100** | 7.158285444E-02 | 7.15828544386E-02 | 7.15836080790E-02 | 1.1E-3 | 7.15828558259E-02 | 1.9E-6 | 7.15828544401E-02 | 2.1E-9 | 7.15828544385E-02 | -1.2E-10 |
| **1000** | - | 1.49213247261E-06 | 1.49215770511E-06 | 1.7E-3 | 1.49213251819E-06 | 3.1E-6 | 1.49213247265E-06 | 2.8E-9 | 1.49213247261E-06 | -1.0E-10 |
| **-1.0 $** | | | | | | | | | | |
| | | | **Case B01_16** | | **Case B01_15** | | **Case B01_14** | | **Case B0_13** | |
| **0.1** | 5.205642866E-01 | 5.20564286609E-01 | 5.20564302610E-01 | 3.1E-6 | 5.20564311673E-01 | 4.8E-6 | 5.20564286731E-01 | 2.4E-8 | 5.20564286609E-01 | 2.4E-11 |
| **1** | 4.333334453E-01 | 4.33333445301E-01 | 4.33338532849E-01 | 1.2E-3 | 4.33333456715E-01 | 2.6E-6 | 4.33333445319E-01 | 4.2E-9 | 4.33333445301E-01 | -5.2E-12 |
| **10** | 2.361106508E-01 | 2.36110650789E-01 | 2.36112922535E-01 | 9.6E-4 | 2.36110655566E-01 | 2.0E-6 | 2.36110650795E-01 | 2.7E-9 | 2.36110650788E-01 | -1.2E-10 |
| **100** | 2.866764245E-02 | 2.86676424545E-02 | 2.86678355664E-02 | 6.7E-4 | 2.86676428550E-02 | 1.4E-6 | 2.86676424550E-02 | 1.7E-9 | 2.86676424544E-02 | -1.1E-10 |
| **-10.0 $** | | | | | | | | | | |
| | | | **Case B01_20** | | **Case B01_19** | | **Case B01_18** | | **Case B01_17** | |
| **0.01** | - | 2.65423744138E-01 | - | - | 2.65423745175E-01 | 3.9E-7 | 2.65423745433E-01 | 4.9E-7 | 2.65423744140E-01 | 8.1E-10 |
| **0.1** | - | 8.79467364532E-02 | 8.79467599256E-02 | 2.7E-5 | 8.79467396575E-02 | 3.6E-6 | 8.79467364848E-02 | 3.6E-8 | 8.79467364532E-02 | 1.6E-11 |
| **0.5** | - | 7.78700077417E-02 | 7.78700925973E-02 | 1.1E-4 | 7.78700101857E-02 | 3.1E-6 | 7.78700077627E-02 | 2.7E-8 | 7.78700077418E-02 | 9.4E-12 |
| **1** | - | 6.94112428147E-02 | 6.94113725364E-02 | 1.9E-4 | 6.94112446998E-02 | 2.7E-6 | 6.94112428297E-02 | 2.2E-8 | 6.94112428147E-02 | 3.2E-12 |
| **10** | - | 2.65443026189E-02 | 2.65443324285E-02 | 1.1E-4 | 2.65443029122E-02 | 1.1E-6 | 2.65443026208E-02 | 7.2E-9 | 2.65443026189E-02 | -7.2E-11 |
| **100** | - | 2.05500634866E-03 | 2.05500719307E-03 | 4.1E-5 | 2.05500635638E-03 | 3.8E-7 | 2.05500634870E-03 | 2.2E-9 | 2.05500634866E-03 | -5.0E-11 |
| **1000** | - | 1.25870180432E-08 | 1.25870213689E-08 | 2.6E-5 | 1.25870180726E-08 | 2.3E-7 | 1.25870180433E-08 | 1.3E-9 | 1.25870180432E-08 | -4.7E-11 |

Examination of the results in Table 3.2 shows that for the larger time steps of $10^{-1}$ s and $10^{-2}$ s, the differences are smaller over the first few tenths of a second than at greater times. For these larger time steps, the PARET/ANL point kinetics algorithm iteratively subdivides the time step until a more accurate solution is obtained. In the 1 $ step insertion problem such iterations continue throughout nearly the first second of the transient. A few such iterations occur during the first time step even with the time step size of $10^{-3}$ s. For the other cases in Table 3.2, the iterations cease by a transient time of 0.5 s or less. While the high accuracy indicated in the table for time step sizes of $10^{-3}$ s and $10^{-4}$ s is of academic interest, such accuracy is not required in practical calculations. The results in the table show that very accurate solutions can be expected even for the larger time step size of $10^{-2}$ s. These tiny differences indicate that the acceptance criteria defined in Table 1.2 are satisfied for comparisons against analytical solutions.

**Ramp Reactivity Insertions**

Table 3.1 includes eight test cases for ramp reactivity insertions, Cases B01_21 through B01_28. In addition to the step reactivity insertions referenced above, Ganapol [14] also published a benchmark solution (to 10 significant figures) of the point kinetics equations for a ramp reactivity insertion of 0.1 $/s. The PARET/ANL solution to this case is compared with Ganapol's result and to the result from *Mathematica* in Table 3.3. The Mathematica solution is identical to the Ganapol solution for 10 significant figures. The results shown indicate that PARET/ANL provides an accurate solution for this case with a time step size (maximum) of $10^{-2}$ s. Also included in Table 3.3 are results for a ramp reactivity insertion of -0.1 $/s. A benchmark solution was not available for this case, but the GEAR solution method [16] has been used at Argonne for many years for point kinetics problems as well as for other problems. It was applied to the step problems in Table 3.2 and to the 0.1 $/s ramp problem in Table 3.3 using functional iteration and very tight convergence, the GEAR solutions were found to be very accurate for the published step and ramp benchmarks. The PARET/ANL results are compared with the GEAR solution for the -0.1 $/s case in Table 3.3. As indicated in the table, excellent agreement was found between the GEAR and PARET/ANL solutions, and these differences are much smaller than the acceptance criteria defined in Table 1.2 for comparisons against analytical solutions.

## Table 3.3. Comparison of Solutions Obtained for Ramp Reactivity Insertions

| Time, s | Reference | | PARET/ANL | | | | | | | |
|---|---|---|---|---|---|---|---|---|---|---|
| | | | $\Delta t = 10^{-1}$ s | Diff., % | $\Delta t = 10^{-2}$ s | Diff., % | $\Delta t = 10^{-3}$ s | Diff., % | $\Delta t = 10^{-4}$ s | Diff., % |
| **0.1 $/s** | **Ganapol** | **Mathematica** | | | | | | | | |
| 2.0 | 1.338200050E+00 | 1.338200050 | 1.33811150E+00 | -6.6E-3 | 1.33819924E+00 | -6.1E-5 | 1.33820005E+0 | 0.0E+0 | 1.33820005E+0 | 0.0E+0 |
| 4.0 | 2.228441897E+00 | 2.228441897 | 2.22793320E+00 | -2.3E-2 | 2.22843841E+00 | -1.6E-4 | 2.22844189E+0 | -3.1E-7 | 2.22844190E+0 | 1.3E-7 |
| 6.0 | 5.582052449E+00 | 5.582052449 | 5.57727954E+00 | -8.6E-2 | 5.58202830E+00 | -4.3E-4 | 5.58205241E+0 | -7.0E-7 | 5.58205245E+0 | 1.8E-8 |
| 8.0 | 4.278629573E+01 | 42.786295730 | 4.25655601E+01 | -5.2E-1 | 4.27855585E+01 | -1.7E-3 | 4.27862948E+1 | -2.2E-6 | 4.27862957E+1 | -7.0E-8 |
| 10.0 | 4.511636239E+05 | 4.511636239E+05 | 4.48163388E+05 | -6.6E-1 | 4.51074537E+05 | -2.0E-2 | 4.51163526E+05 | -2.2E-5 | 4.51163624E+05 | 2.2E-8 |
| 11.0 | 1.792213607E+16 | 1.792213607E+16 | 1.78003939E+16 | -6.8E-1 | 1.79178130E+16 | -2.4E-2 | 1.79221320E+16 | -2.3E-5 | 1.79221361E+16 | 1.7E-7 |
| **- 0.1 $/s** | **GEAR** | | | | | | | | | |
| 2.0 | 7.920047774E-01 | - | 7.92016185E-01 | 1.4E-3 | 7.92004998E-01 | 2.8E-5 | 7.92004778E-01 | 8.0E-8 | 7.92004777E-01 | -4.6E-8 |
| 4.0 | 6.130158504E-01 | - | 6.13026669E-01 | 1.8E-3 | 6.13016044E-01 | 3.2E-5 | 6.13015851E-01 | 1.0E-7 | 6.13015850E-01 | -6.0E-8 |
| 6.0 | 4.740567389E-01 | - | 4.74065598E-01 | 1.9E-3 | 4.74056891E-01 | 3.2E-5 | 4.74056739E-01 | 1.4E-8 | 4.74056739E-01 | 1.4E-8 |
| 8.0 | 3.691679393E-01 | - | 3.69174796E-01 | 1.9E-3 | 3.69168053E-01 | 3.1E-5 | 3.69167940E-01 | 1.8E-7 | 3.69167939E-01 | -9.2E-8 |
| 10.0 | 2.906533723E-01 | - | 2.90658552E-01 | 1.8E-3 | 2.90653456E-01 | 2.9E-5 | 2.90653373E-01 | 2.3E-7 | 2.90653372E-01 | -1.1E-7 |
| 12.0 | 2.317971695E-01 | - | 2.31801051E-01 | 1.7E-3 | 2.31797231E-01 | 2.7E-5 | 2.31797170E-01 | 2.0E-7 | 2.31797170E-01 | 2.0E-7 |
| 100.0 | 2.547385731E-03 | - | 2.54739834E-03 | 4.9E-4 | 2.54738589E-03 | 6.3E-6 | 2.54738573E-03 | -2.4E-8 | 2.54738573E-03 | -2.4E-8 |
| 1000.0 | 1.342156214E-09 | - | 1.34216004E-09 | 2.9E-4 | 1.34215626E-09 | 3.5E-6 | 1.34215621E-09 | -2.6E-7 | 1.34215621E-09 | -2.6E-7 |

**Problem with reactivity insertion and reactivity feedback**

The PARET/ANL model for reactivity insertion accident analysis, described in test case B01_29, served as the basis for a verification problem involving reactivity feedback. The external reactivity shown in Figure 3.1 was imposed in the PARET/ANL model. The imposed reactivity inserts 0.1 $/s over the first second of the transient. At 1.0 s, a step reactivity insertion occurs, taking the imposed reactivity from 0.1 $ to 0.784 $. For the next half second, the imposed reactivity is held constant at 0.784 $. Then the imposed reactivity steps down to 0 $, and from 1.5 s to 2.0 s the imposed reactivity decreases linearly from 0 to -10 $. Rather than trying to use GEAR to reconstruct the reactivity feedback from associated from the effects of the imposed reactivity, the imposed reactivity was subtracted from the net reactivity calculated by PARET/ANL. The feedback reactivity so obtained is shown in Figure 3.2. A GEAR solution to the problem was run using the imposed reactivity shown in Figure 3.1 and feedback reactivity interpolated from the table of values used to construct the curve shown in Figure 3.2. The resulting reactor power, including 0.76806 MW of decay heat, is shown as a function of time in Figure 3.3. The legend in the figure indicates that both the PARET/ANL and GEAR solutions are shown, but as is apparent from the plot, the two solutions are indistinguishable from each other. By requiring the GEAR solution to produce the power at the same times for which PARET/ANL reported the power, it was possible to make a time-point by time-point comparison between the two calculations. The largest percent difference between the two calculations is 0.13%, which is smaller than the acceptance criteria defined in Table 1.2 for comparisons of PARET/ANL results against analytical solutions. This difference occurs near 1.5 s where the power is decreasing very rapidly.

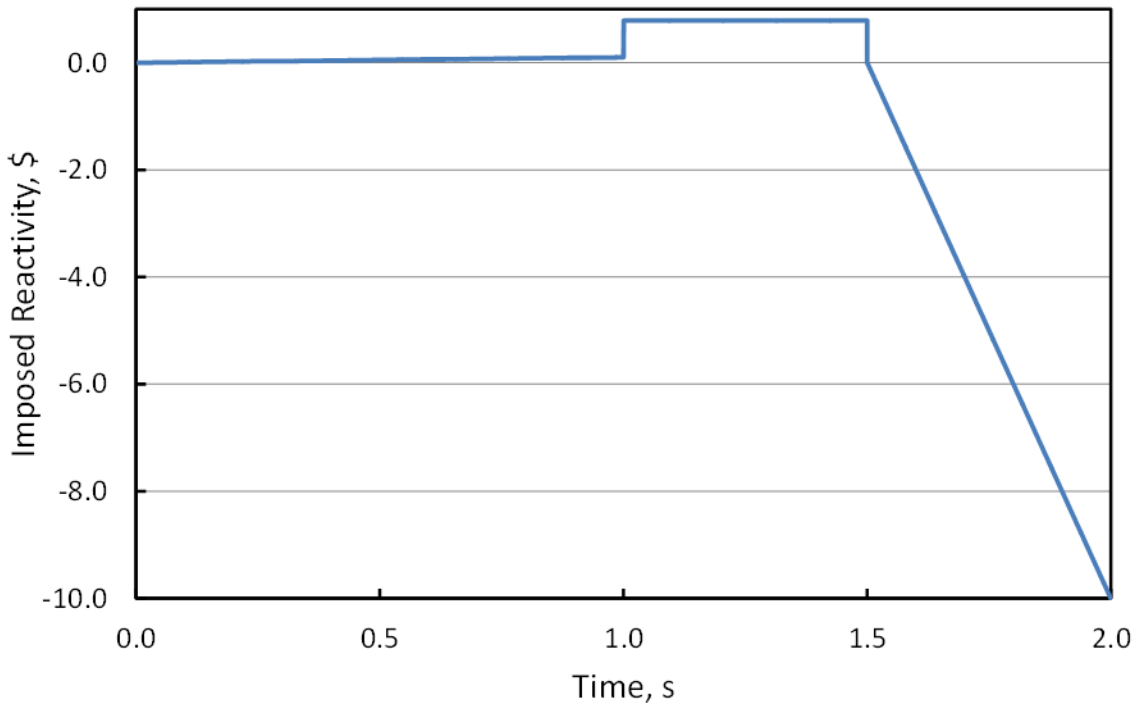


**Figure 3.1. Imposed Reactivity for The Verification Problem with Feedback.**

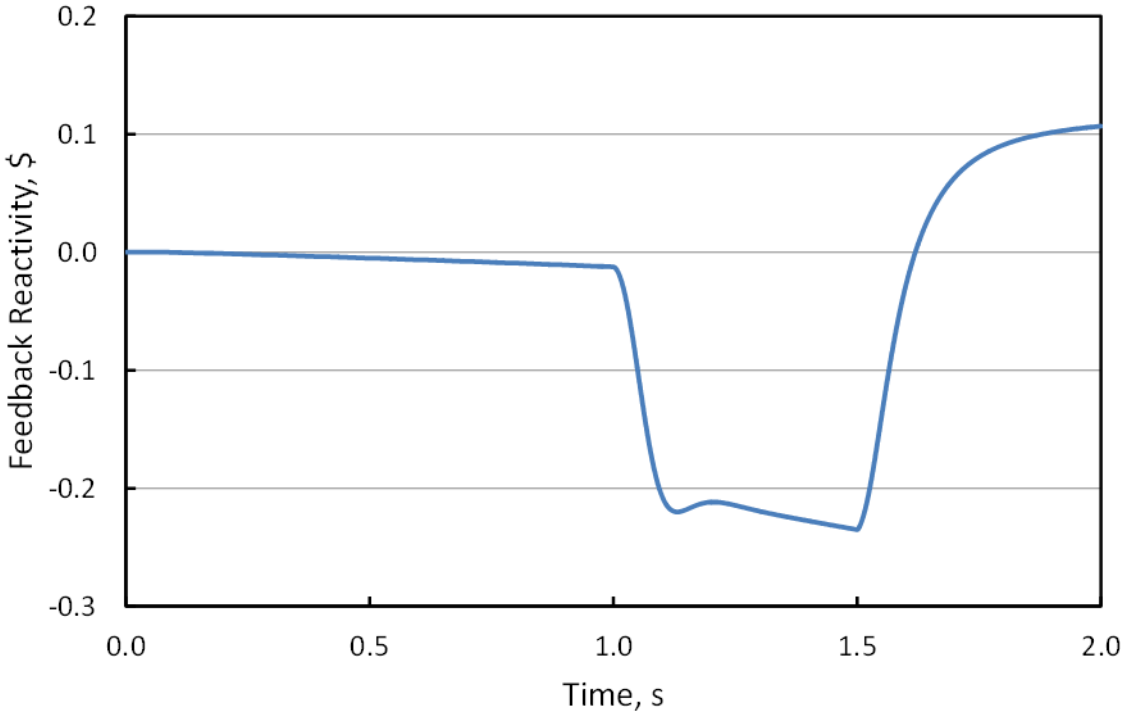


**Figure 3.2. Feedback Reactivity for the Verification Problem with Feedback.**

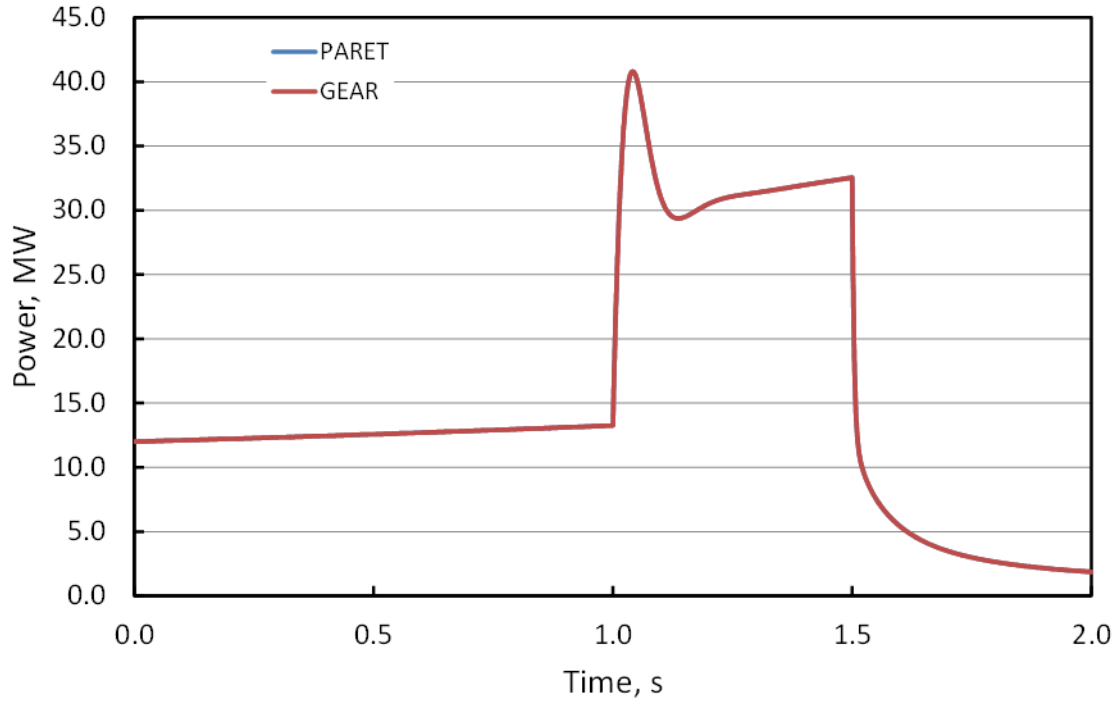


**Figure 3.3. Reactor Power for the Verification Problem with Feedback.**

## 3.2 Capability B2 – Reactivity Feedback

PARET/ANL is capable of handling reactivity feedback including the impact of the axial dependence of the power density. This section documents a series of test problems that enable checking the functionality of the reactivity feedback profiles given in variables VOIDVC and TEMPC. Reactivity feedback from coolant void is computed and scaled by the value of VOIDVC in each fluid axial mesh interval. The profile TEMPC scales the reactivity feedback from coolant temperature changes in each fluid axial mesh interval. Likewise, the profile from DOPPLR scales the fuel temperature Doppler effect from each fuel meat mesh interval.

Additionally, the verification of reactivity feedback due to the thermal expansion of fuel plates is also included. PARET/ANL input cards 11xxx are used in the calculation of linear thermal expansion of fuel plate cladding. The fuel plates in typical plate-type fuel assemblies can expand radially from near-instantaneous heat-up during a reactivity transient. When this occurs, there is a loss of coolant channel cross section area which amounts to causing a loss of moderation. The edges of the fuel plates may be confined in side plates that do not heat up as quickly as do the heated plate sections. The PARET/ANL model for thermal expansion of cladding assumes that there is essentially no heat transfer from the heated meat section to the side plates during a short transient. The same assumption applies to grid plates that define the spacing of the fuel assemblies. Therefore, the side plate dimensions, and fuel assembly pitch remain fixed over a rapid transient. PARET/ANL input cards 11xxx contains the linear thermal expansion of the cladding material in percent as a function of temperature. The table is piecewise linear. It is supplied as % linear thermal expansion at a series of temperatures which must span the temperature range expected. The expansion is computed at every time step using the radial average temperature of the cladding in every axial node in every channel.

As will be discussed in the following subsections, PARET/ANL processes correctly the reactivity feedback due to the change of moderator density, fuel temperature, and thermal expansion.

### 3.2.1 Testing of Moderator Reactivity Feedback

**Test Plan**

The reference case for testing moderator reactivity feedback is a model comprised of two channels of flat-plate fuel geometry. The transient is a reactivity insertion accident scenario with a linear ramp insertion of 1.50 $ over 0.5 s, beginning from an initial power of 10 MW. There are four variations of the reference case with modifications to the user input for reactivity feedback. By design, the reactivity feedback is very small in these test cases compared to the 1.50 $ insertion. This minimizes the nonlinear inter-dependency of the reactivity feedback mechanisms in the transient response. This allows for the effect of modifying a particular input variable to be isolated.

All five test cases include reactivity feedback derived from coolant void (density) changes or coolant temperature changes. From input cards 5xxx, DVOID is the overall density/void coefficient. VOIDVC is the dimensionless coolant density feedback weighting factor at each axial node. DTMP is the feedback reactivity coefficient. TEMPC is the dimensionless coolant temperature feedback weighting factor at each axial node.

Each case is defined as follows and summarized in Table 3.4.

- Case B02_01: The reference case is derived from a standard test case which has an axial profile defined for each of VOIDVC and TEMPC. A flat axial profile is assumed for DOPPLR (all values = 1.0).

- Case B02_02: Change the axial profiles for VOIDVC, DOPPLR, and TEMPC to a flat profile (all values = 1.0), to eliminate the weighting factor effect.

- Case B02_03: Scale the axial profiles used in Case B02_02 by a factor of 2 for VOIDVC, DOPPLR, and TEMPC.

- Case B02_04: Isolate the reactivity change to that from TEMPC and DOPPLR: i.e., scaling the axial profiles used in Case B02_02 by a factor of 2 for DOPPLR, and TEMPC (all values = 2.0), while keeping the scale factor (all values = 1.0) for VOIDVC.

- Case B02_05: Isolate the reactivity change due to using the axial profile from Case B02_01 only on the VOIDVC input and keeping the scale factor (all values = 1.0) for DOPPLR and TEMPC.

**Table 3.4. Summary of Cases for Testing Moderator Reactivity Feedback**

| Case | VOIDVC | DOPPLR | TEMPC |
|---|---|---|---|
| **B02_01** | varying axial profile | All values = 1.0 | varying axial profile |
| **B02_02** | All values = 1.0 | All values = 1.0 | All values = 1.0 |
| **B02_03** | All values = 2.0 | All values = 2.0 | All values = 2.0 |
| **B02_04** | All values = 1.0 | All values = 2.0 | All values = 2.0 |
| **B02_05** | Like B02_01 | All values = 1.0 | All values = 1.0 |

The expected results of interest are:

1. The moderator reactivity effect from expansion and void changes should be the same (within a small numerical tolerance) for Case B02_01 and Case B02_05.

2. The moderator reactivity effect from coolant expansion and void changes for Case B02_03 should be double (within a small numerical tolerance) that of Case B02_02.

3. The moderator reactivity effect from coolant temperature changes for Case B02_03 should be double (within a small numerical tolerance) that of Case B02_02, because the axial weighting factor is doubled.

4. The effect of the perturbation weighting (which enhances core axial mid-plane worths over top or bottom worths) of Case B02_01 vs. Case B02_02 should show slightly lower peak power, peak fuel centerline temperature, and peak cladding temperature.

5. The moderator reactivity effect from coolant expansion should be the same for Case B02_04 and B02_02 and the effect of coolant temperature for Case B02_04 should be double that of Case B02_02 because the axial weighting factor is doubled.

6. Case B02_03 should have the lowest peak power, because it has the most reactivity feedback from temperature, void, and Doppler Effects. It should also have the lowest peak fuel centerline temperature, and peak cladding temperature.

Note: The comparisons are made at a time of 10.135 s into the transient. This time was found by observing that this is the time of the major edit near to the scram time where the three feedback effects are at their maxima. At later times, the control rods have begun insertion, and the power is quickly reduced. Reactivity feedback terms are also quickly reduced. One must keep in mind that PARET/ANL initializes the feedback terms to zero at time zero. This physically corresponds to the assumption that the reactor is critical and in steady-state at time zero. If the reactor at time zero is at significant power, then there will be a reactivity offset computed at time zero that will automatically be compensated for. As the reactor first heats up and then cools down, one may observe in the major edit how the various feedback terms change.

Acceptance of these tests requires that the output from all cases be consistent and in agreement at time t=0.0 s. The coolant exit temperature in channel 1 at 0.0 s should agree within 0.02 °C, in order to ensure that the same coolant average density is attained in steady-state. The reactivity feedback at 0.0 s should be zero. The steady-state initialization process sets it to zero.

**Results and Discussion**

Results from varying the input axial profile data for variables affecting the computation of the reactivity feedback are presented in Table 3.5. The primary output file results show that the coolant exit temperature in channel 1 at time t=0 is the same for all cases. The value is 53.94 °C. As expected, the feedback reactivity was shown to be 0.0 $.

**Table 3.5. Calculation Results**

| Test Case | B02_01 | B02_02 | B02_03 | B02_04 | B02_05 |
|---|---|---|---|---|---|
| Peak Power, MW | 13.17 | 13.18 | 13.14 | 13.16 | 13.18 |
| Time of Power Peak, s | 10.090 | 10.090 | 10.090 | 10.090 | 10.090 |
| Energy Release to time of Peak, MW·s | 101.09 | 101.08 | 101.12 | 101.11 | 101.08 |
| Fuel Max. T, °C | 81.221 | 81.225 | 81.209 | 81.216 | 81.224 |
| Cladding Max T, °C | 79.234 | 79.237 | 79.222 | 79.229 | 79.221 |
| Trip Time, s | 10.0636 | 10.0636 | 10.0637 | 10.0636 | 10.0636 |
| Reactivity changes from Moderator Expansion & Void, $ at t=10.135 s | 0.00428 | 0.00376 | 0.00751 | 0.00376 | 0.00428 |
| Reactivity Change from Moderator Temperature, $ at t=10.135 s | 0.00529 | 0.00455 | 0.00909 | 0.00910 | 0.00455 |

The checking of expected results from this series of tests is as follows:

1. The moderator reactivity effect from expansion and void changes should be the same (within a small numerical tolerance) for Case B02_01 and Case B02_05.

   Yes, the same moderator reactivity of 0.00428 $ for both Cases B02_01 and B02_05.

2. The moderator reactivity effect from expansion and void changes for Case B02_03 should be double (within a small numerical tolerance) that of Case B02_02. The reactivity change is tiny and accordingly the power changes will vary slightly over time.

   Yes, the predicted ratio is 0.00751/0.00376=1.99734, a difference of 0.13%. The difference of 0.13% is due to a slight change in power versus time. However, the expected result of the ratio of reactivity effects is extremely close to 2.0, confirming the reactivity effect is accounted correctly.

3. The moderator reactivity effect from temperature changes for Case B02_03 should be double (within a small numerical tolerance) that of Case B02_02, because the axial weighting factor is doubled.

   Yes, the predicted ratio is 0.00909/0.00455 = 1.99780, a difference of 0.11%.

4. The effect of the perturbation weighting (which enhances core axial mid-plane worths over top or bottom worths) of Case B02_01 vs. Case B02_02 shows slightly lower peak power, peak fuel centerline temperature, and peak cladding temperature.

   Yes, a very small effect is noticed.

5. The moderator reactivity effect from coolant expansion should be the same for Case B02_04 and B02_02 and the effect of coolant temperature for Case B02_04 should be double that of Case B02_02 because the axial weighting factor is doubled.

   Yes, the same moderator reactivity of 0.00376 $ for both Cases B02_04 and B02_02. Also, the reactivity changes from moderator temperature for Case B04_02 is 0.0091 $ which double that of Case B02_02 which is given as 0.00455 $.

6. Expect that Case B02_03 should have the lowest peak power, because it has the most reactivity feedback from temperature and void effects. It should also have the lowest peak fuel centerline temperature, and peak cladding temperature.

   Yes, 13.14 MW is the lowest. The peak fuel and cladding temperatures from Case B02_03 are very slightly lower than from all other cases, as expected.

**Conclusion**

These tests confirm that the code computes two reactivity feedback effects (coolant density/void, coolant temperature) consistent with expectations when scaled by an axial worth shape factor. The Doppler feedback also approximately doubles but has too few significant digits to be obvious (0.00002 vs 0.00005). The differences calculated above are smaller than the acceptance criteria defined in Table 1.2.

## 3.2.2 Testing of Doppler Feedback

**Test Plan**

In research reactors fueled by uranium, the presence of resonance neutron absorbers such as U-238 may have a significant effect on reactor core excess reactivity. Neutron absorption by resonances for neutron energies above thermal (approximately the eV-keV range) depends on the fuel meat temperature. The neutron absorption increases with fuel meat temperature. The reactivity effect caused by resonance capture is called the Doppler effect.

The description and analysis of the SPERT-III tests are described in Refs. [17], [18], [19], and [20]. This set of calculations shall be performed for three scenarios. In all cases, reactivity feedback derived from input cards 5xxx, DVOID, VOIDVC, DOPPLR, and the Doppler feedback equation given in Section 5.8 of the PARET/ANL User Guide [2] shall be computed. That equation uses variables GAMMA0, GAMMA1, GAMMA2, GAMMA3, GAMMA4, and DOPPNK. This present work shall qualify the Doppler effect equation for a linear variation of feedback reactivity with temperature, using GAMMA1 only. The GAMMA0 term can be used to set the feedback at t=0. It has no effect on any results and is therefore recommended to be set to zero. The terms GAMMA2, GAMMA3, GAMMA4, and DOPPNK shall be set to 0.

As the code prints out the average composition temperatures at the end of the last major edit, just before the problem terminates, a reference test case is run with different transient times as follows:
Case B02_06: Define a reference case from a standard SPERT-III test case (use Test T-82) which uses fuel rods modeled using IGEOM=1. It has an axial profile defined for each of VOIDVC, DOPPLR, and TEMPC. This case will be a reactivity insertion transient to take the core average fuel temperature well above initial hot, full power conditions in steady-state. The linear term of the Doppler Feedback equation was input as 0.002552 $/°C, obtained from an MCNP model analysis. Higher-order terms were all input as zero coefficients.

Case B02_07: Change the transient time to the time from Case B02_06 where the power peak occurs.

Case B02_08: Change the transient time to 0.001 s, near enough to the initial conditions.

**Results and Discussion**

Case B02_06 was run to 0.2501 s . The power peak was 1558.93 MW at 0.1243 s . At this time step, the Doppler feedback reactivity was 0.17768 $.

Case B02_07 was run to 0.12430 s, which is the time the power peak of 1558.93 MW was reached in Case B02_06. The edit just before the end of the standard output showed:

```
TIME=    0.1243
     SYSTEM AVG. TEMPERATURES(C) FOR EACH COMPOSITION
     340.69      307.30
```

Note that the “340.69” temperature listed above is for the first composition, which is always the fuel meat.

Case B02_08 was run to 0.001 s in order to obtain system temperatures at the beginning of the transient. The edit just before the end of the standard output showed:

```
SYSTEM AVG. TEMPERATURES(C) FOR EACH COMPOSITION
271.07      263.97
```

Using the reported average fuel temperatures at 0.001 s (Case B02_08) and 0.1243 s (Case B02_07), and the linear term input of the Doppler feedback equation, a simple hand calculation of expected reactivity change from Doppler effect alone:

Reactivity change ($) = 0.002552*(340.69-271.07) = 0.002552*69.62 = 0.17767 $.

The results obtained agree extremely well with the Doppler effect reactivity reported by the code as 0.17768 $. The percentage difference is very tiny, and the acceptance criteria defined in Table 1.2 are satisfied.

It is important to realize that this result is from a five-channel model with 20 axial fuel zones by five radial fuel zones. It has five complex axial power shapes with a peak/average ratio up to 2.87 in the most-peaked channel. All five channels have a different axial power profile. In order to match the hand calculation of reactivity feedback, the code must consistently compute the contributions to that feedback for five channels, times 20 axial nodes, times five radial nodes in the fuel meat.

**Conclusion**

These cases verify that the Doppler Effect equation in PARET/ANL is correct for the linear term based on GAMMA1. That is the form used in standard core analysis.

### 3.2.3 Testing of Feedback due to Thermal Expansion

**Test plan**

Note that the methodology for computing the thermal expansion feedback is essentially the same for the IGEOM=2 option as it is for the IGEOM=0 option. The geometry variable IGEOM is 0 for slab geometry for the fuel plate and channel. It is 1 for cylindrical geometry. It is 2 for slab geometry where the channel dimensions can be changed by channel. Precise definitions for the IGEOM options are given in Section 5.6 of the User Guide [2]. For IGEOM=1, the “effective coolant channel thickness” is obtained in the same way as for slabs by dividing the channel volume by the cladding surface area. Calculations were performed in slab geometry (IGEOM=0) with the radial dimension across the fuel plate thickness specified by Table 3.6.

**Table 3.6. Radial Dimensions**

| Input Parameter | Description | Value, m |
|---|---|---|
| RF | Radial distance to outer surface of the fuel meat | 2.55E-4 |
| RC | Radial distance to inner surface of the cladding | 2.55E-4 |
| RS | Radial distance to outer surface of the cladding | 6.35E-4 |
| RN | The radial distance from the center of the rod to the center of the water channel | 1.75E-3 |

Doppler and temperature feedback were zeroed, leaving only expansion feedback derived from PARET/ANL input cards 11xxx, the overall density or void coefficient (DVOID) specified by input card 5xxx, and other geometric factors. It was not possible to turn off the usual void coefficient calculation by simply setting DVOID and VOIDVC to zero because the reactivity effect of expansion needs those quantities. Instead, in order to isolate the feedback from rod expansion, it was necessary to introduce a positive reactivity effect that would compensate for the negative feedback for moderator expansion and void alone. The remaining feedback would then be just from rod expansion. The test cases are as follows:

Case B02_09: A standard IAEA test case for 1.50 $ insertion, was run to 0.64 s. There is an edit of core-average meat and cladding temperatures at the very end of the standard output. Those temperatures are needed to check the thermal expansion. The input card 5xxx gave the moderator expansion and void coefficient of 0.2357 $/% void. The input cards 11xxx gave a thermal expansion linearly with temperature of 4.0701E-3 % per degree K. Since input cards 11xxx include a zero value at 273.15 K (0 °C), the expansion is computed from 0 °C to any desired average temperature.

Case B02_10: Modify case B02_09 by introducing a positive reactivity to compensate for the feedback of moderator expansion and void. It was necessary to iterate several times, changing PARET/ANL input cards 11xxx, in order to force the expansion case B02_10 to match the case B02_09 reactivity decrement at time 0.64 s. Physically, the expansion effect of cladding when it is heated up is isolated in this case.

Case B02_11: Modify case B02_09 by zeroing the thermal expansion coefficient at the input cards 11xxx. This case involves only moderator expansion and void.

**Results and Discussion**

The key results are presented in Table 3.7. It is clear that an excellent match is achieved. From the Case B02_10 data, using the input void coefficient value for DVOID of 0.3257 $/% void, the reactivity loss of -0.01379 $ is due to a void change of 0.01399/0.3257 or 0.042954% void.

Using a cladding average temperature of 56.76 °C (329.91 K), the core average cladding expansion is 0.23102%. Scaling by DVOID yields 0.07524%. For this case, the cladding surface radius (input parameter RS) is 6.35E-4 m, and the coolant channel half-thickness (the difference of input parameters RN and RS) is 11.15E-4 m. Therefore, the effect of cladding expansion as a percentage is reduced for the coolant channel by the ratio of the radius RS to (RN-RS), or 0.56951. Scaling 0.07524% by 0.56951 yields 0.042851% effective void. This can be compared to the previous paragraph value of 0.042954%. The difference is only 0.24%.

Table 3.7 also shows that the results of Cases B02_10 and B02_11 agree extremely well with each other. It means that the reactivity feedback due to the rod expansion is equivalent to that due to the moderator expansion and void as expected. These percentage differences are tiny and the acceptance criteria defined in Table 1.2 are satisfied.

**Table 3.7. Calculation Results at 0.64 s**

| Parameter | Case B02_09 | Case B02_10 (Increase reactivity insertion to compensate for moderator expansion and void. Physically, only feedback from Rod expansion) | Case B02_11 (Turn off the rod expansion feedback, moderator expansion and void remain) |
|---|---|---|---|
| Hot channel power, MW | 0.2877 | 0.2955 | 0.2969 |
| Rod expansion Δ reactivity, $ | -0.01379 | -0.01399 | 0.00000 |
| Moderator expansion & void, Δ reactivity, $ | -0.01383 | -0.01396 | -0.01406 |
| Average cladding temperature, °C | 56.50 | 56.76 | 56.77 |
| Average fuel meat temp., °C | 58.30 | 58.60 | 58.61 |
| Net reactivity, $ | 1.34088 | 1.3535 | 1.3515 |
| Channel 1 outlet temperature, °C | 38.9249 | 38.9307 | 38.9373 |

**Conclusion**

It is concluded that the PARET/ANL code uses the cladding surface outer dimension RS as the basis for fuel plate expansion for the plate option IGEOM=0. It is handled the same way for IGEOM=2. This is reasonable for plate-type fuels such as the aluminum-based types used in the MIT reactor, and in various SPERT-type test reactors. In those systems, the fuel meat also expands. However, the meat is typically just a few degrees hotter than the cladding. This is because it has the fission source, and because it has a high thermal conductivity close to but less than that of pure aluminum cladding.

## 3.3 Capability B3 – Reactor Trips and Delay Time

Trips can be specified to occur when the power exceeds a specified value (over-power trip), when the reactor period is smaller than a specified value (period trip), and/or when the coolant flow falls below a specified value (low-flow trip). In the paragraphs that follow, examples for each of these types of reactor trip are described to demonstrate that PARET/ANL correctly reports when the trip occurs and when the associated scram is initiated. Cases are also included to show that the shutdown reactivity is correctly inserted when the scram occurs.

### 3.3.1 Over-Power Trip

In order to verify the over-power trip capability a transient is considered for a reactor operating at an initial power of 32 MW (Case B03_01). Reactivity feedback was disabled by using very small reactivity feedback coefficients. During the transient, the reactivity was held at its initial value of zero for 1 s. Then 0.5 $ of reactivity was inserted instantaneously at 1 s. In this case, an over-power trip was set to occur when the power level reached 38.4 MW, and there was an assumed 10 ms delay between the time of the trip and the time of scram. PARET/ANL determines the trip time by performing a linear interpolation using the results for the last time step before reaching the over-power trip and the first time step after. Thus, if $P_t$ is the power level at which the trip is to occur, $P_1$ is the power on the last time step before reaching the trip power, and $P_2$ is the power on the first time step after the trip, the time of the trip can be estimated using the linear interpolation formula (assuming that the logarithm

of the power is a constant function of time, which it is over a short time interval when the reactor is on a period)

$$T = t_1 + (t_2 - t_1) \frac{\ln(P_t / P_1)}{\ln (P_2 / P_1)}$$

where $t_1$ and $t_2$ are the times corresponding, respectively, to the powers $P_1$ and $P_2$. The time of the scram is then given by

$$t_s = T + t_d.$$

Here $t_d$ is the delay time between the time of the trip and the time of the scram.

In the decay heat verification problem (Section 3.5) using the 2005 ANS standard [21] the decay heat, 10 days of irradiation prior to the start of the transient, and an energy per fission of 200 MeV/fission, the conditions just before and just after reaching the trip power of 38.4 MW were found to be

$t_1 = 1.052$ s and $P_1 = 38.3998781$ MW

$t_2 = 1.053$ s and $P_2 = 38.5086337$ MW

Inserting these values into the formula for the trip time, one finds T= 1.052001 s. Adding the delay time of 10 ms yields a scram time of $t_s = 1.062001$ s. PARET/ANL reports $T = 1.052001$ s and $t_s = 1.062001$ s. The agreement between the calculation described above and the PARET/ANL results is exact for the seven significant figures reported by PARET/ANL and accordingly the acceptance criteria defined in Table 1.2 are satisfied.

### 3.3.2 Period Trip

PARET/ANL does not use interpolation to determine the time for a trip on the reactor period. Instead, the time of the trip is set to the time of the time step for which the period is first found to be less than the value set for the period trip. Using the same model as used above for verification of the over-power trip, the input was modified to set a trip to occur when the period dropped below 0.221 s and for the scram to occur 30 ms later (Case B03_02). When the case was run with these input values, PARET/ANL reported that the trip occurred at 1.002000 s when the period had the value 0.1879772 s. These values were reported just before the time step 1002, the first time step when the period had a value less than the input period trip value. PARET/ANL then reported a scram at 1.032000 s into the transient, between time steps 1032 and 1033, 30 ms after the trip. This is the expected behavior. This verification of the code behavior confirms that the acceptance criteria described in Table 1.2 are satisfied for comparisons against hand calculations.

### 3.3.3 Low-Flow Trip

The model described above for verifying the over-power trip can be used also to verify the low-flow trip for the case when the coolant flow is determined by PARET/ANL input cards 10xxx with IFLOW =1. In this case (Case B03_03), the time of the trip is determined by interpolation directly in the input cards. To verify this, the flow on the input card 10001 was set to decrease linearly over a time period of 2.0 s from an initial value of -8175 kg $m^{-2}$ $s^{-1}$ to zero. In addition, the low-flow trip was set to occur when the flow reached 60% of the initial flow with the scram to occur 10 ms after the trip. The

time of the trip can be calculated just as described above for the over-power trip with the values for $t_1$, $t_2$, $M_1$, and $M_2$ set to the values listed in the following table.

$t_1$= 0.0 s and $M_1$ = -8175.0 kg m$^{-2}$ s$^{-1}$

$t_2$= 2.0 s and $M_2$ = 0.0 kg m$^{-2}$ s$^{-1}$

The linear equation to solve for t is

$$M(t) = M(0) + b*t$$

Slope b is 8175./2. or 4087.5

M(0) is M1 = -8175.0

Solving the above linear equation for M(t) = 0.60*(-8175) yields the trip time of

$$t = (8175.-4905.)/4087.5 = 0.80000.$$

After adding a delay time of 10 ms, the scram time is $t_s = 0.81000$ s. These are the values reported by PARET/ANL.

For other ways to specify the flow, PARET/ANL determines the time of the trip in subroutine flowp.f. To test the reported trip and scram times, use was made of a two-channel case (Case B03_04) in which IFLOW=4 and a flow coastdown is determined by PARET/ANL input cards 17xxx. The low-flow trip was set to occur when the flow reached 85% of the initial flow. A scram was to occur 200 ms after the trip. A low-flow trip at 4.0939 s and a scram at 4.293941 s were reported by PARET/ANL. This indicates that the scram was occurring at the correct time relative to the reported time of the trip. Edits for channel 1 and channel 2 provide the value of the flow in each channel to five significant figures. Flow results are the same for each channel on the time step just before the reported low-flow trip and the time step just after the trip. The code interpolates using flow values on these time steps in the same manner as described above for the over-power trip. Results used for this interpolation, to the number of significant figures reported by PARET/ANL, are listed in the following table.

$t_1$= 4.09300 s and $\ln(P_1) = -2321.0$ kg m$^{-2}$ s$^{-1}$

$t_2$= 4.09400 s and $\ln(P_2) = -2320.9$ kg m$^{-2}$ s$^{-1}$

The initial flow is $-2730.5$ kg m$^{-2}$ s$^{-1}$ and the value for the trip flow is $\ln(P_t) = 0.85 \times (-2730.5) = -2320.925$ kg m$^{-2}$ s$^{-1}$. Inserting these values into the interpolation formula, one finds $T = 4.09375$ s and $t_s = 4.29375$ s. Given the number of significant figures available in the foregoing table, these results are in good agreement with the values reported in the PARET/ANL output, and accordingly the acceptance criteria defined in Table 1.2 are satisfied.

Case B03_04 is provided here to qualitatively show the transient behavior during a loss-of-flow-event. The Loss-of-Flow event shown in Figure 3.4 (a), (b), and (c), is one in which the reactor is running in steady-state when the coolant pump suffers a loss of electrical power. The pump slows down exponentially at a rate determined mostly by its rotational inertia. The pump is assumed to slow to zero flow 25 s after it loses power. PARET/ANL does not model a pump. It models the mass flux

produced by the pump as an input table. The reactor control system is set to trip on low-flow when the mass flux is reduced to 85% of its initial steady-state value. There is a small control system time delay between trip and scram. Figure 3.4 (a) shows the time evolution of the reactor power. Figure 3.4 (b) shows the time evolution of the flow coastdown. Figure 3.4 (c) shows the time evolution of the peak cladding surface temperature.

The trip time is 4.094 s, and the trip is 0.200 s later at 4.294 s. The mass flux is initially in downflow. After the trip and the pump stops, buoyancy forces cause the mass flux to reverse and become upflow. The time of flow reversal is approximately 64.8 s. With close inspection of part (b), one can see a small peak in the upflow at about 70.7 s, after which the power drops and the buoyancy forces diminish, causing the mass flux to slowly diminish.

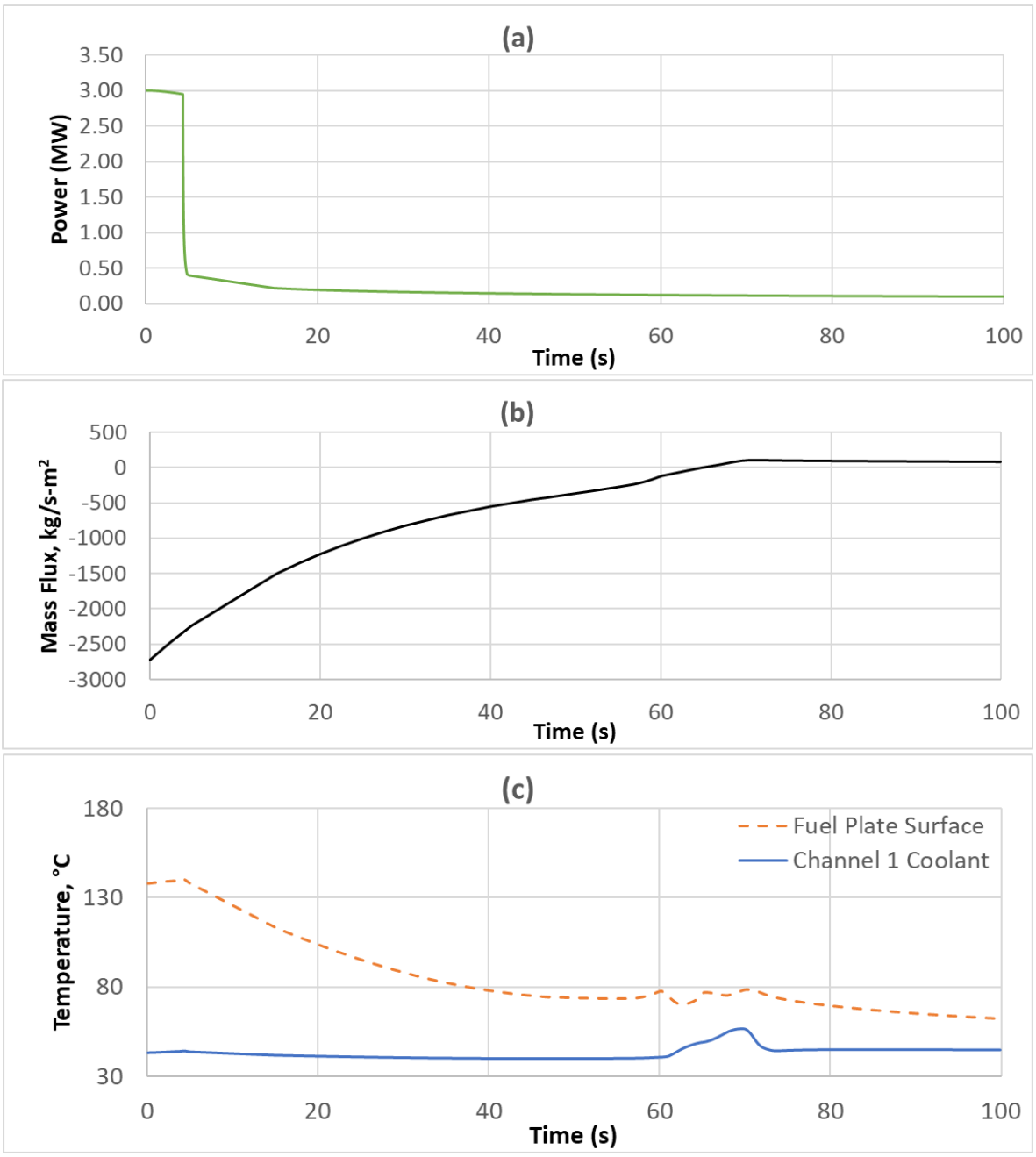


**Figure 3.4. Loss-Of-Flow Case B03_04, Showing Time History of (a) Power, (b) Mass Flux, and (c) Peak Cladding Surface Temperature**

## 3.4 Capability B4 – Control Rod Reactivity

PARET/ANL uses input cards 18xxx to represent the control rod reactivity worth vs. insertion. It is piecewise-linearly interpolated. The use of this input data is controlled by variable RDRATE supplied on input card 1113. Given input cards 18xxx, and a reactor model that begins a transient event such as a step insertion, the power will exponentially increase until a trip occurs. After the reactor trip is initiated by the reactor control system, there is a reactor scram after a prescribed delay. The control rods are inserted and the shutdown reactivity insertion proceeds. It must be shown that the reactivity expected at full insertion occurs at the time expected according to the time of trip plus the time since trip plus the time for full insertion.

To verify this capability, a new test case B04_01 is created by modifying the test case B03_01 mentioned in Section 3.3. All reactivity feedbacks are removed and the step reactivity insertion is set at 0.5 $. The input cards 18xxx describe the control rods which insert -15.04 $ within 0.5 s. The PARET/ANL calculation results (Figure 3.5) show that the power trip and reactor scram occur at 1.052 and 1.062 s, respectively. The total reactivity reported at 1.062 + 0.5 = 1.562 s is -14.04 $ which exactly equals the sum of step reactivity insertion (0.5 $) and reactivity introduced by the control rods (-15.04 $) as expected, and accordingly the acceptance criteria summarized in Table 1.2 are satisfied.

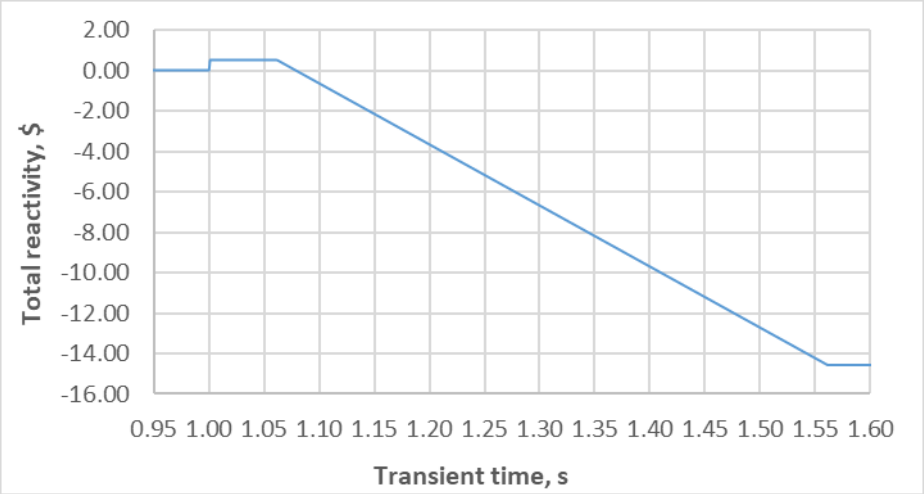


**Figure 3.5. Total Reactivity Calculated by PARET/ANL**

## 3.5 Capability B5 – Decay Heat

The PARET/ANL computer code contains an approximate treatment of decay heat resulting from the irradiation of the fuel both prior to the start of a transient and during the transient. For the decay heat calculation, PARET/ANL uses a constant fission power, specified by the user, for the entire time period from the beginning of the irradiation prior to the start of a transient up until the time of a scram that results from a reactor trip during the transient. In addition, a time delay between the time of the trip and the time of the scram can be specified by the user. At the beginning of the transient the fission power calculated by PARET/ANL is initialized to the total reactor power minus whatever decay heat power has built up as a result of the prior irradiation. Following the scram, there is no further irradiation of the fuel for the purpose of decay heat production even though the actual fission power may be significant for some period of time following the scram. At the user's choice, the code will use the ANS 2005 Standard [21] (the recommended default option) or the ANS 1973 Standard [22] (a

legacy option) for the calculation of decay heat. Whichever standard is chosen, the code assumes that the fuel contains $^{235}U$ as primary fissile isotope. However, the user can change the MeV/fission input to match that of some other mixture of fissile isotopes.

To verify the PARET/ANL model, the model was independently recreated in a spreadsheet using macro capabilities. Mathematically, the model can be described as follows. Let f(t) be the decay power at time t resulting from a single fission at time zero. Then if $t \geq 0$, the decay heat at time t due to a constant fission rate of 1 fission/s for all times prior to time zero can be expressed as

$$F(t)= \int_{-\infty}^{0} dt' f(t-t').$$

If a reactor is operated at a fission power $P_0$ for a time T prior to the start of a transient and continues to operate at the same power level for a time t after the transient starts, this function can be used to evaluate the decay heat as

$$P_d(t)= \frac{P_0}{Q} [F(0)- F(t+T)]$$

when the scram has not occurred. If a scram occurs at time $t_S$ after the start of the transient the decay heat at time t after the start of the transient can be evaluated as

$$P_d(t)= \frac{P_0}{Q} [F(t-t_S)- F(t+T)] .$$

In these expressions, Q is the energy released per fission. In PARET/ANL, Q=200 MeV/fission is the default value (but is an input). When the 2005 ANS Standard is used, the function f(t) is expressed as a sum of 23 exponentials and the expressions involving the function F(t) can be expressed as the sum of 23 terms using the parameters from the 23 exponentials. When the 1973 ANS Standard is used, the decay power is evaluated by linear interpolation in a table of the logarithm of F(t) as a function of the logarithm of t.

To verify the PARET/ANL calculation, the code was run for two irradiation times, 3 days and 10 days, prior to the start of the transient. For purposes of the decay heat calculation, the fission power was assumed to be 32 MW. During the transient, the initial total power of the reactor was assumed to be 32 MW and reactivity feedback was disabled by using very small reactivity feedback coefficients. At 1.0 s into the transient, 0.5 $ of reactivity was inserted over a time period of 0.00001 s. A trip was set to occur when the power reached a user determined trip-power. To estimate the time when the trip occurred, PARET/ANL interpolates a time between the time of the last time step before the trip-power is reached and the time of the first time step when the power exceeds the trip-power (as described in Section 3.3.1). Different aspects of the decay heat calculation are verified by comparing the PARET/ANL and hand calculations of the test cases presented in Table 3.8.

**Table 3.8. Test Cases Used for Verification of Decay Heat Calculation**

| Test Case | ANS Standard | # Day Prior Irradiation | Trip Power, MW | Delay Time, ms | MeV/fission |
|---|---|---|---|---|---|
| B05_01 | 2005 | 3 | 32.001 | 0.0 | 200 |
| B05_02 | 2005 | 10 | 32.001 | 0.0 | 200 |
| B05_03 | 1973 | 3 | 32.001 | 0.0 | 200 |
| B05_04 | 1973 | 10 | 32.001 | 0.0 | 200 |
| B05_05 | 2005 | 10 | 38.400 | 10.0 | 200 |
| B05_06 | 1973 | 10 | 38.400 | 10.0 | 200 |
| B05_07 | 2005 | 3 | 32.001 | 0.0 | 210 |
| B05_08 | 1973 | 3 | 32.001 | 0.0 | 210 |
| B05_09 | 2005 | 45 | 32 | 0.0 | 200 |
| B05_10 | 2005 | 60 | 24 | 0.0 | 200 |

An initial set of calculations for 3-day prior irradiation (Case B05_01) and for 10-day prior irradiation (Case B05_02) were run with the trip-power set to 32.001 MW and a time delay between the estimated trip time and the scram time of zero. This choice of trip-power and time delay had the consequence that the calculated decay heat power on the first time step after the power reached 32.001 MW retained the value it would have had if the trip and corresponding scram had not occurred. At all the following time steps the decay heat power is calculated as if the irradiation of the fuel stopped at the estimated scram time. The PARET/ANL results for this case are compared with spreadsheet calculations in Table 3.9 for the case when the 2005 ANS Standard is selected.

**Table 3.9. Comparison of Calculations Using 2005 ANS Standard**

| Times, s | Decay Heat Power, MW | | | |
|---|---|---|---|---|
| | 3 Day Prior Irradiation | | 10 Day Prior Irradiation | |
| | PARET/ANL | Hand Calc. | PARET/ANL | Hand Calc. |
| 0.00100 | 2.028175 | 2.028175 | 2.059238 | 2.059238 |
| 1.00000 | 2.028175 | 2.028175 | 2.059238 | 2.059238 |
| 1.00100 | 2.028175 | 2.027936 | 2.059238 | 2.059016 |
| 1.00200 | 2.027712 | 2.027712 | 2.058792 | 2.058792 |
| 40.00000 | 1.076172 | 1.076172 | 1.107249 | 1.107249 |

For both the 3-day and 10-day prior irradiations the estimated scram time was 1.000009 s. If the delay time had been set to a value larger than the size of the time step used in the PARET/ANL calculation, the decay power calculated on the first time step after the scram would have agreed with the spreadsheet calculation. As can be seen in Table 3.9, for all times except the time step immediately following the scram, the PARET/ANL and spreadsheet calculations are identical for the number of significant figures reported by the PARET/ANL code.

Table 3.10 shows the results from a repetition of the foregoing calculations using the 1973 ANS Standard instead of the 2005 ANS Standard. For these cases for 3-day prior irradiation (Case B05_03) and for 10-day prior irradiation (Case B05_04), the estimated scram time for the 3-day and 10-day prior irradiations is 1.000011 s. The small difference compared to the case of 2005 ANS Standard is due to the numerical solution which interpolates the trip time between the time steps and it has negligible effect on the results. The fact that the PARET/ANL and spreadsheet calculations agree for the first time step following the scram time is caused by the fact that the tabulated values for the function F(t) in the 1973 Standard do not include a value for t=0. The function F(t+T) changes very slowly during the transient. The function $F(t-t_S)$ is assigned the value F(0.1) until $t>t_S+0.1$. As can be

seen in Table 3.10, PARET/ANL and hand calculations agree for all of the significant figures reported by PARET/ANL.

**Table 3.10. Comparison of Calculations Using 1973 ANS Standard**

| Times, s | Decay Heat Power, MW | | | |
|---|---|---|---|---|
| | 3 Day Prior Irradiation | | 10 Day Prior Irradiation | |
| | PARET/ANL | Hand Calc. | PARET/ANL | Hand Calc. |
| 0.00100 | 2.039682 | 2.039682 | 2.071445 | 2.071445 |
| 1.00000 | 2.039682 | 2.039682 | 2.071445 | 2.071445 |
| 1.00100 | 2.039682 | 2.039682 | 2.071445 | 2.071445 |
| 1.00200 | 2.039682 | 2.039682 | 2.071445 | 2.071445 |
| 40.00000 | 1.152817 | 1.152817 | 1.184577 | 1.184577 |

Table 3.11 shows the results of two additional calculations using the 2005 ANS Standard (Case B05_05) and using the 1973 ANS Standard (Case B05_06), carried out for a 10-day prior irradiation and the more realistic values of 38.4 MW for the trip-power and a delay time of 10 ms between the trip time and the scram time. Scram times for these calculations were 1.062001 s and 1.062025 s, respectively, for the 2005 and 1973 ANS Standards. Because of the 10 ms delay between the trip time and the scram time, several time steps occurred during the delay time period. The PARET/ANL and the spreadsheet calculations agree at all times for the number of significant figures reported by PARET/ANL.

**Table 3.11. Comparison for a Trip Power of 38.4 MW and Delay Time of 10 ms**

| Times, s | Decay Heat Power, MW | | | |
|---|---|---|---|---|
| | 2005 ANS Standard | | 1973 ANS Standard | |
| | PARET/ANL | Hand Calc. | PARET/ANL | Hand Calc. |
| 0.00100 | 2.059238 | 2.059238 | 2.071445 | 2.071445 |
| 1.06200 | 2.059238 | 2.059238 | 2.071445 | 2.071445 |
| 1.06300 | 2.059014 | 2.059014 | 2.071445 | 2.071445 |
| 40.00000 | 1.107610 | 1.107610 | 1.184951 | 1.184951 |

As noted earlier, the default value for the energy release per fission is 200 MeV/fission. However, the input card 1700 allows the user to assign a different value to Q. To verify that the user assigned value is correctly implemented, the input card 1700 was used to assign the value Q=210 MeV/fission for the cases listed in Table 3.9 and Table 3.10 for prior irradiation of 3 days. PARET/ANL calculations using the 2005 ANS Standard (Case B05_07) and using the 1973 ANS Standard (Case B05_08) with this new value for Q are compared with corresponding spreadsheet calculation in Table 3.12.

**Table 3.12. Comparison for a Prior Irradiation of 3 Days with Q = 210 MeV/fission**

| Times, s | Decay Heat Power, MW | | | |
|---|---|---|---|---|
| | 2005 ANS Standard | | 1973 ANS Standard | |
| | PARET/ANL | Hand Calc. | PARET/ANL | Hand Calc. |
| 0.00100 | 1.931578 | 1.931578 | 1.942555 | 1.942555 |
| 1.00000 | 1.931579 | 1.931579 | 1.942555 | 1.942555 |
| 1.00100 | 1.931579 | 1.931367 | 1.942555 | 1.942555 |
| 1.00200 | 1.931154 | 1.931154 | 1.942555 | 1.942555 |
| 40.00000 | 1.024925 | 1.024925 | 1.097921 | 1.097921 |

As in the previous cases, the PARET/ANL and spreadsheet calculations agree for all of the significant figures reported by PARET/ANL. In addition, the decay heat values listed in Table 3.9 and Table 3.10 are scaled by a factor of 200/210 in Table 3.12, as expected. These comparisons show that the acceptance criteria defined in Table 1.2 are satisfied.

## 3.6 Capability B6 – Power-Driven Mode

The PARET/ANL option which allows the user to specify the reactor power as a function of time can be verified by first running a problem in which the imposed reactivity as a function of time is specified. The input cards 9xxx can then be used to specify the power that results from the reactivity transient. Thermal hydraulics results that are calculated during a transient driven by the power as a function of time can then be compared with the corresponding results obtained in the original reactivity driven transient. The specification using input cards 9xxx is limited to no more than 100 power/time pairs. Because linear interpolation is used in PARET/ANL, the accuracy obtained in the comparisons will be somewhat limited. Nevertheless, the results to be described in the following paragraphs, using three sets of time points for input cards 9xxx, demonstrate that very good agreement can be obtained between the power and reactivity driven transients.

Test case B01_29 mentioned in Section 3.1 provides a suitable test problem for verification of the PARET/ANL power as a function of time option. For the first set of time points (Case B06_01), PARET/ANL input cards 9xxx included 51 time points starting with time t=0 and ending at 2.0 s separated by time intervals of 0.04 s. Figure 3.6 shows the power interpolated from input cards 9xxx as well as the power from the reactivity-driven case. As shown in Figure 3.6, the interpolated power falls below the power of the reactivity-driven case from slightly after 1.0 s, especially near the time of peak power and near 1.5 s. The power at the time 1.5 s is not included in the Table 10 input (the comparison would have been more accurate if it was included).

The second set of time points (Case B06_02) includes 100 time points in Table 10 from time=0 to time=2 s. All time points are separated by time intervals of length (2/99) s except for one time point adjusted to match the time of the peak power shown in the reactivity-driven case, 1.0412 s. The power interpolated from input cards 9xxx is compared with the power from of reactivity-driven case in Figure 3.7. It can be seen that the agreement between these data is better than in the case with 51 time points. For the third set of time points (Case B06_03), 25 equal-length time intervals were placed between 0 and 1.0 s, 50 time intervals between 1.0 s and 1.5 s, five time intervals between 1.5 s and 1.55 s, and nine time intervals between 1.55 s and 2.0 s. This gives a total of 90 time points in the 9xxx input cards.

Some key results from the three power vs. time cases are compared with the original reactivity vs. time case in Table 3.13. While the reactor model used for this verification exercise includes four channels,

the comparisons in Table 3.13 include only the first two channels. For the most part, the results from the 100-point and 90-point of input cards 9xxx are very similar. The temperatures at 1.5 s for the 90-point results agree more closely with the reactivity-driven case because more points were included in the time interval between 1.0 s and 1.5 s. Also, the powers at 1.0 s and 1.5 s are included in the input cards 9xxx. The time interval from 1.0 s to 1.5 s includes the highest power and contributes the largest fraction of the energy release.

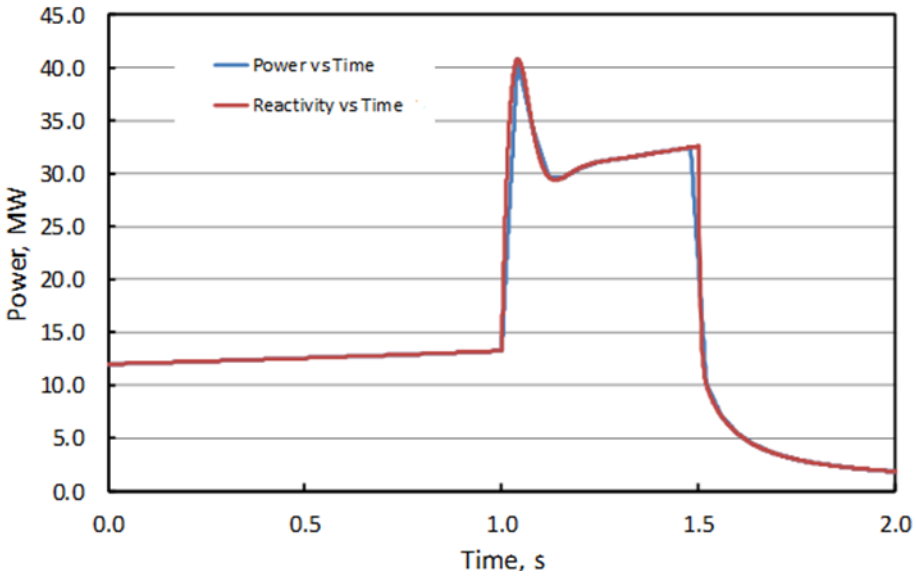


**Figure 3.6. Comparison of Power Table of 51 Time Points with Reactivity Driven Case.**

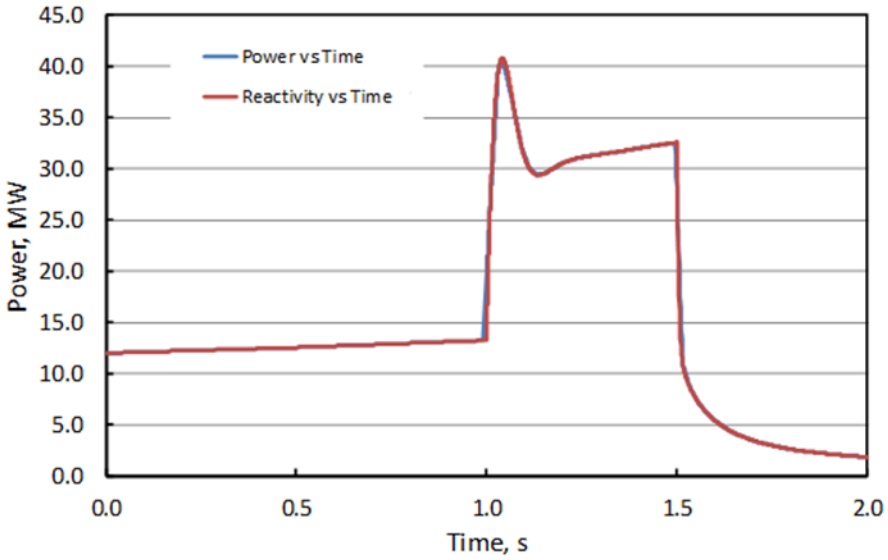


**Figure 3.7. Comparison of Power Table of 100 Time Points with Reactivity Driven Case.**

**Table 3.13. Comparison of Key Results**

| Chanel | Parameter | Time | Reactivity-Driven Mode | Power-Driven Mode | | | | | |
|---|---|---|---|---|---|---|---|---|---|
| | | | | 51 Points | Diff., % | 100 Points | Diff., % | 90 Points | Diff., % |
| 1&2 | Energy, MJ | 1 s, Prior to Reactivity Step | 12.5876 | 12.5743 | -0.106 | 12.6053 | 0.141 | 12.5743 | -0.106 |
| | | Time of Peak Power, s | 1.0413 | 1.0400 | -0.125 | 1.0413 | 0.000 | 1.0400 | -0.125 |
| | | At Time of Peak Power | 13.9402 | 13.6679 | -1.953 | 13.9736 | 0.240 | 13.8692 | -0.509 |
| | | 1.5 s, Prior to Reactivity Step | 28.5454 | 28.2177 | -1.148 | 28.5613 | 0.056 | 28.5311 | -0.050 |
| | | 2.0 s | 30.5975 | 30.2946 | -0.990 | 30.6543 | 0.186 | 30.6313 | 0.110 |
| 1 | Fuel Temp., °C | 1 s, Prior to Reactivity Step | 113.38 | 113.38 | 0.000 | 117.15 | 3.325 | 113.38 | 0.000 |
| | | Time of Peak, s | 1.5000 | 1.4800 | -1.333 | 1.4950 | -0.333 | 1.5000 | 0.000 |
| | | Peak | 190.71 | 190.25 | -0.241 | 190.6 | -0.058 | 190.71 | 0.000 |
| | | 1.5 s, Prior to Reactivity Step | 190.71 | 181.27 | -4.950 | 189.03 | -0.881 | 190.71 | 0.000 |
| | | 2.0 s | 64.059 | 64.067 | 0.012 | 64.062 | 0.005 | 64.075 | 0.025 |
| | Cladding Temp., °C | 1 s, Prior to Reactivity Step | 93.025 | 93.024 | -0.001 | 93.942 | 0.986 | 93.024 | -0.001 |
| | | Time of Peak, s | 1.5011 | 1.4820 | -1.270 | 1.4950 | -0.404 | 1.501 | -0.005 |
| | | Peak | 143.2 | 142.92 | -0.196 | 143.13 | -0.049 | 143.21 | 0.007 |
| | | 1.5 s, Prior to Reactivity Step | 143.2 | 139.74 | -2.416 | 142.94 | -0.182 | 143.2 | 0.000 |
| | | 2.0 s | 60.908 | 60.914 | 0.010 | 60.911 | 0.005 | 60.922 | 0.023 |
| | Coolant Temp., °C | 1 s, Prior to Reactivity Step | 68.735 | 68.733 | -0.003 | 68.714 | -0.031 | 68.733 | -0.003 |
| | | Time of Peak, s | 1.5051 | 1.491 | -0.935 | 1.504 | -0.071 | 1.508 | 0.195 |
| | | Peak | 89.283 | 89.19 | -0.104 | 89.282 | -0.001 | 89.314 | 0.035 |
| | | 1.5 s, Prior to Reactivity Step | 89.269 | 89.135 | -0.150 | 89.267 | -0.002 | 89.269 | 0.000 |
| | | 2.0 s | 56.841 | 56.843 | 0.004 | 56.842 | 0.002 | 56.846 | 0.009 |
| | Critical Heat Flux Ratio | 1 s, Prior to Reactivity Step | 8.436 | 8.433 | -0.036 | 8.175 | -3.094 | 8.433 | -0.036 |
| | | Time of Minimum, s | 1.5000 | 1.4800 | -1.333 | 1.4950 | -0.333 | 1.5 | 0.000 |
| | | Minimum | 3.279 | 3.292 | 0.396 | 3.282 | 0.091 | 3.279 | 0.000 |
| | | 1.5 s, Prior to Reactivity Step | 3.279 | 3.455 | 5.367 | 3.292 | 0.396 | 3.279 | 0.000 |
| | | 2.0 s | 54.85 | 54.8 | -0.091 | 54.82 | -0.055 | 54.76 | -0.164 |
| 2 | Fuel Temp., °C | 1 s, Prior to Reactivity Step | 156.43 | 156.43 | 0.000 | 164.13 | 4.922 | 156.43 | 0.000 |
| | | Time of Peak, s | 1.0555 | 1.0614 | 0.559 | 1.0538 | -0.161 | 1.0555 | 0.000 |
| | | Peak | 255.45 | 251.1 | -1.703 | 254.28 | -0.458 | 255.13 | -0.125 |
| | | 1.5 s, Prior to Reactivity Step | 241.99 | 225.69 | -6.736 | 238.39 | -1.488 | 241.99 | 0.000 |
| | | 2.0 s | 71.326 | 71.34 | 0.020 | 71.33 | 0.006 | 71.349 | 0.032 |
| | Cladding Temp., °C | 1 s, Prior to Reactivity Step | 133.53 | 133.53 | 0.000 | 135.88 | 1.760 | 133.53 | 0.000 |
| | | Time of Peak, s | 1.0582 | 1.0653 | 0.671 | 1.0578 | -0.038 | 1.0591 | 0.085 |
| | | Peak | 193.05 | 191.98 | -0.554 | 192.78 | -0.140 | 192.98 | -0.036 |
| | | 1.5 s, Prior to Reactivity Step | 189.67 | 185.52 | -2.188 | 189.23 | -0.232 | 189.67 | 0.000 |
| | | 2.0 s | 67.698 | 67.711 | 0.019 | 67.702 | 0.006 | 67.719 | 0.031 |
| | Coolant Temp., °C | 1 s, Prior to Reactivity Step | 81.684 | 81.682 | -0.002 | 81.644 | -0.049 | 81.682 | -0.002 |
| | | Time of Peak, s | 1.1013 | 1.1120 | 0.972 | 1.1020 | 0.064 | 1.1019 | 0.054 |
| | | Peak | 123.61 | 120.93 | -2.168 | 123.38 | -0.186 | 123.43 | -0.146 |
| | | 1.5 s, Prior to Reactivity Step | 120.97 | 120.04 | -0.769 | 120.95 | -0.017 | 120.97 | 0.000 |
| | | 2.0 s | 58.925 | 58.93 | 0.008 | 58.927 | 0.003 | 58.934 | 0.015 |
| | Critical Heat Flux Ratio | 1 s, Prior to Reactivity Step | 3.639 | 3.638 | -0.027 | 3.509 | -3.572 | 3.638 | -0.027 |
| | | Time of Minimum, s | 1.0598 | 1.0663 | 0.613 | 1.0589 | -0.085 | 1.0604 | 0.057 |
| | | Minimum | 1.1260 | 1.202 | 6.750 | 1.1450 | 1.687 | 1.1310 | 0.444 |
| | | 1.5 s, Prior to Reactivity Step | 1.349 | 1.638 | 21.423 | 1.38 | 2.298 | 1.349 | 0.000 |
| | | 2.0 s | 24.63 | 24.61 | -0.081 | 24.63 | 0.000 | 24.6 | -0.122 |

The energy release as a function of time obtained using the 90-point of input cards 9xxx is compared with the corresponding energy release from the PARET/ANL calculation with the reactivity specified as a function of time in Figure 3.8. As can be seen, the two results are indistinguishable from one

another. In Figure 3.9, Figure 3.10, and Figure 3.11, the corresponding peak fuel temperatures, peak coolant temperatures, and minimum critical heat flux ratios are compared for the power vs. time case (also using the 90-point of input cards 9xxx) and the reactivity vs. time case. The comparisons are for channel 1, the channel representing the average behavior in the core. Not shown are similar plots for channels 2, 3, and 4 that exhibit equally good agreement. Channels 2, 3, and 4 are higher powered channels. Nucleate boiling occurs in each of the channels, starting near the time of peak power and ending a short time after 1.5 s. Agreement between the power vs. time calculation and the reactivity vs. time calculation is as good for these channels as for channel 1 with exception that at most of the input cards 9xxx time points where nucleate boiling is in progress in the power vs. time case, the minimum critical heat flux ratio exhibits an oscillation. Between the time points, the critical heat flux ratio plots agree very closely with no oscillations in either of the calculations.

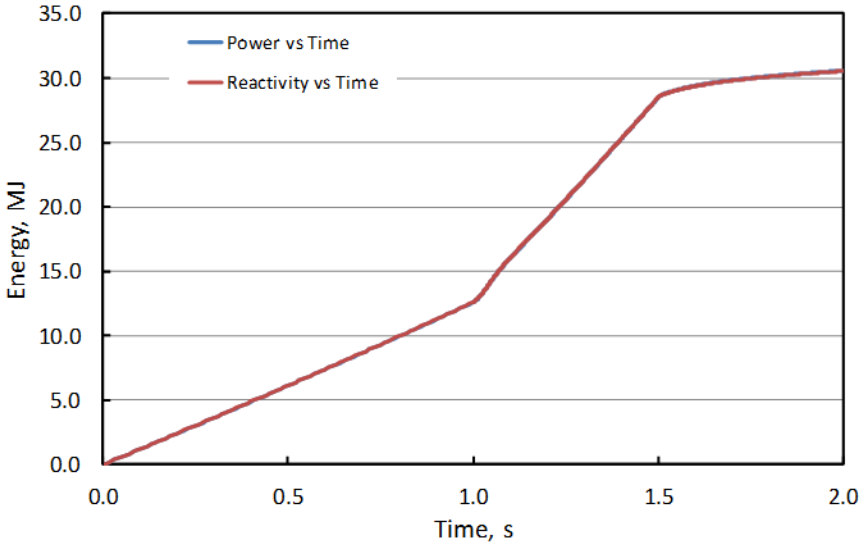


**Figure 3.8. Energy Release.**

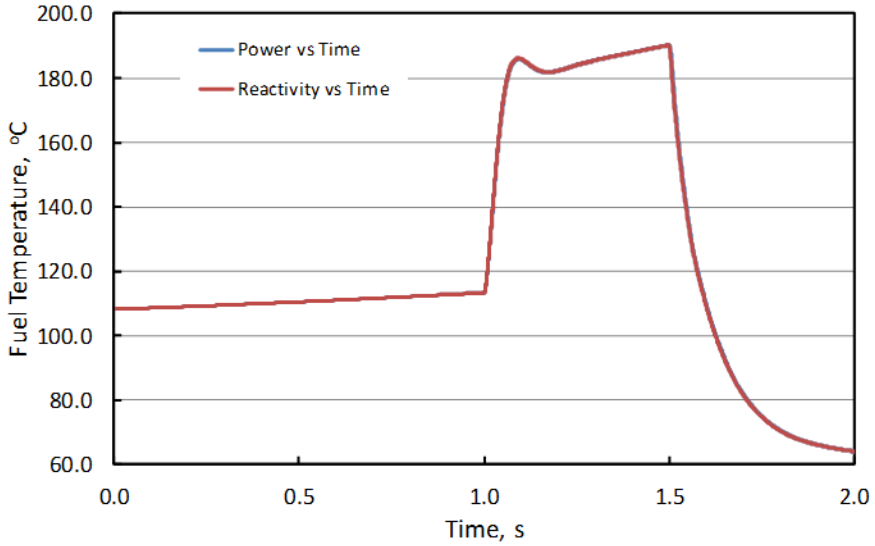


**Figure 3.9. Peak Fuel Temperature in Channel 1.**

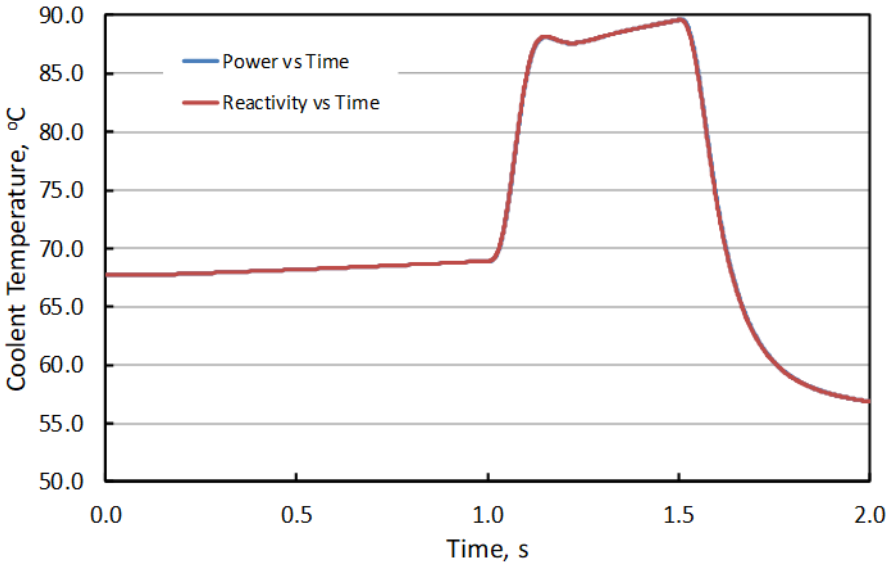


**Figure 3.10. Peak Coolant Temperature in Channel 1.**

Figure 3.12, Figure 3.13, and Figure 3.14 show comparisons of the axial distributions, respectively, of the coolant temperature, cladding surface temperature, and maximum fuel temperature from the power vs. time calculation with the corresponding results from the reactivity vs. time calculation. The comparisons are made at 1.06 s, a time just after the time of peak power. In the power vs. time option, input cards 9xxx contained 90 time points. The results shown indicate very good agreement between the two calculations. The maximum percent differences between the two calculations are 0.61%, 0.34%, and 0.32%, respectively for the coolant, cladding, and fuel temperatures, which are lower than the acceptance criteria defined in Table 1.2. It should be noted that for the power vs. time calculation, PARET/ANL reports nucleate boiling in axial nodes 1 through 14. It should also be noted that for the reactivity vs. time calculation, PARET/ANL also reports nucleate boiling in axial nodes 1 through 14. Similar results were observed for channels 3 and 4.

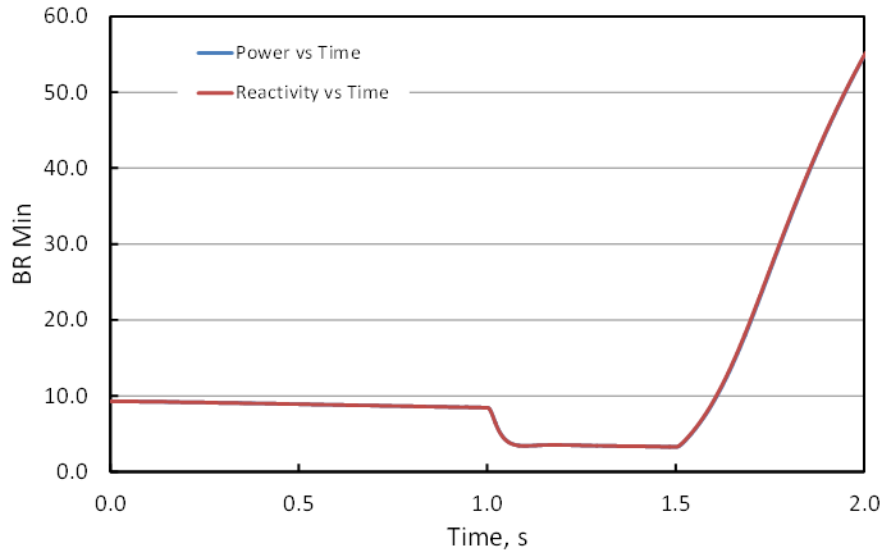


**Figure 3.11. Minimum CHF Ratio in Channel 1.**

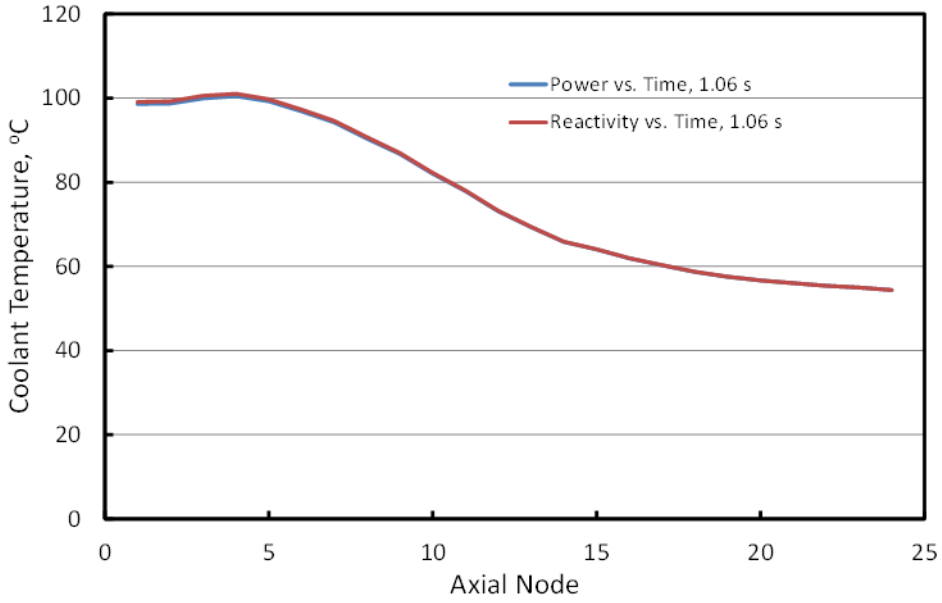


**Figure 3.12. Coolant Temperatures in Channel 2.**

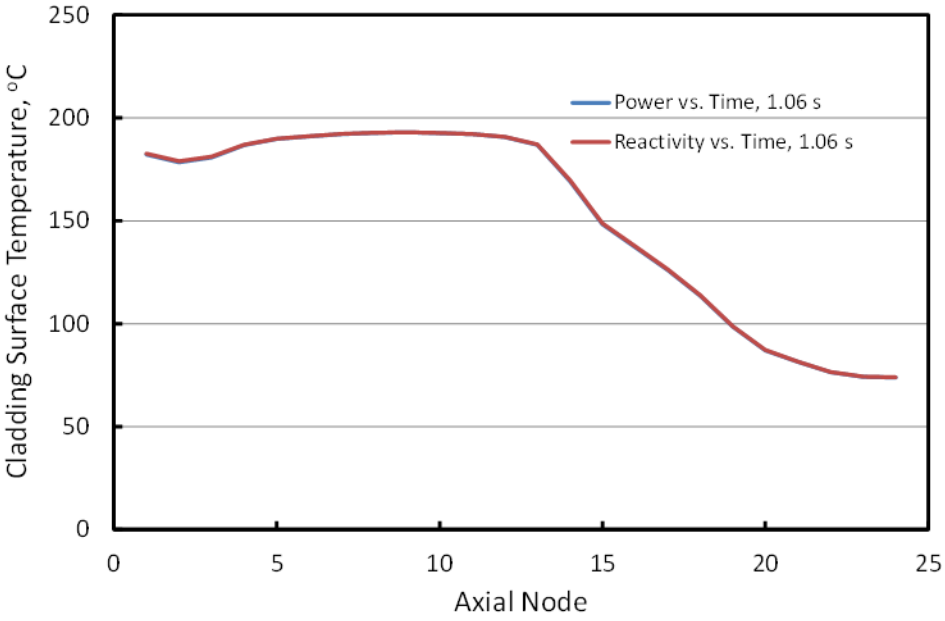


**Figure 3.13. Cladding Surface Temperatures in Channel 2.**

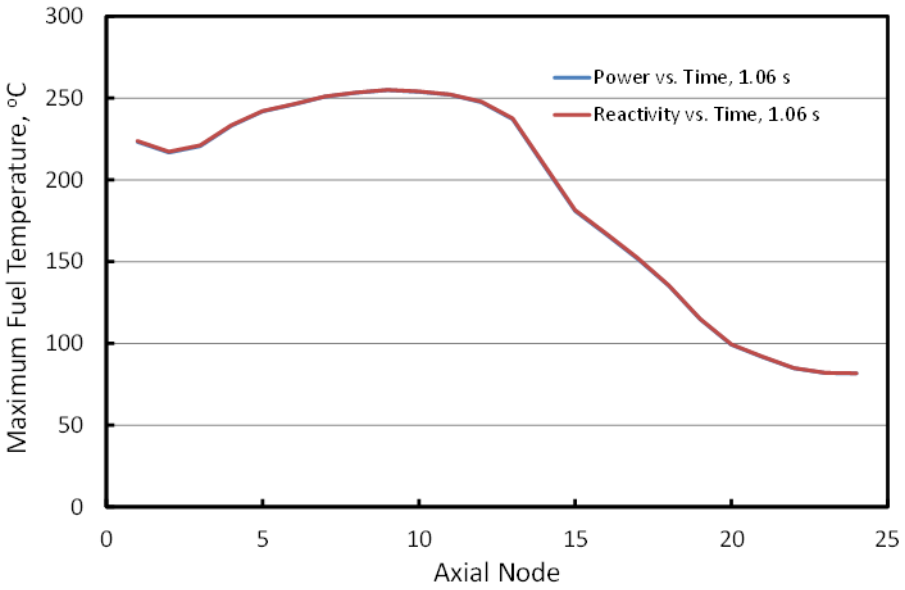


**Figure 3.14. Maximum Fuel Temperatures in Channel 2.**

# 4 Integral V&V Exercises

In the previous chapters, PARET/ANL was validated for each of the selected capabilities that reflect the most commonly used features of the code for applications to research and test reactors analyses. Each capability was verified separately by comparing code results against analytical solutions, hand calculations, or other code calculations. In this chapter, a PARET/ANL integral reactor code model is validated by comparison of code results against experimental data measured in SPERT-I and SPERT-IV reactors' experiments. In the following sections, the SPERT-I [23] and SPERT-IV [24] experiments are initially described, and then the PARET/ANL model is presented along with the comparison results.

## 4.1 SPERT-I and SPERT-IV Experiments Description

The SPERT experimental program was created to investigate the self-limiting power excursion behavior of reactors under reactivity runaway conditions. In particular, extensive data for power, temperature and pressure were obtained from many series of transient tests performed on several water-moderated reactors with highly enriched uranium (HEU) fuel. These tests encompassed wide variations in core parameters and in reactor safety system conditions. These test series were carried out over a range of reactor periods varying in severity of consequences, up to the point where minor fuel plate damage first occurred. Self-limiting power excursion experiments were performed to characterize the reactor response to step reactivity insertions [23].

The SPERT-I and SPERT-IV tests used HEU fuel plates with aluminum alloy cladding. SPERT-I had no pump, and the coolant was initially a static pool. SPERT-IV improved on SPERT-I by adding a coolant pump for forced flow, enabling parametric studies at various mass flow rates, covering a wide range of operating conditions and accident severities. SPERT-IV was also able to replicate selected tests in SPERT-I by shutting the pump off. The SPERT-I and SPERT-IV D-12/25 cores are the focus of the current integral code verification exercise. The first number in the label of the core is the number of fuel plates in the fuel assembly and the second number is the total number of assemblies in the reactor core, including fuel and control assemblies. This reactor core is composed of 20 fuel assemblies, four control rod assemblies and one transient rod assembly in a 5×5 array as shown in Figure 4.1. The SPERT-I and SPERT-IV D-12/25 are identical except for the positions of the control rods within the core. Each fuel assembly has 12 HEU fuel plates connected to two grooved side plates. Control of the reactor is achieved using the four control rods, each of which contains two neutron absorbing plates. The transient rod is used to initiate the step reactivity insertion and is similar to the control rod. However, its poison section is positioned below the active core region, and it is located partially within the core prior to the transient initiation. The transient rod is raised to decrease the reactivity and is dropped to increase the core reactivity.

The experimental procedure starts with the reactor being subcritical. Then, the transient rod is withdrawn to the height that corresponds to the desired nominal reactivity to be inserted. In this state, the reactor is still subcritical because all control rods are fully inserted. Next, the reactor is brought to critical by withdrawing the control rods while monitoring the neutron flux detectors (flux level and reactor period). Finally, the reactor reaches the critical state (with a very long period) and is at a nominal power of 5 W. The power was not measured, but estimated by the experimentalists as 5 W. The bulk coolant temperature was 20 °C at the initiation of each test. The test was initiated by rapid ejection of the transient rod (average duration of 70 ms), making the reactor supercritical. This fast insertion of reactivity creates an exponential evolution of the neutron flux and power. The fuel,

cladding, and coolant temperatures also increase rapidly. In extreme cases of large reactivity insertion, damage to fuel plates can result in melting or bursting of the cladding.

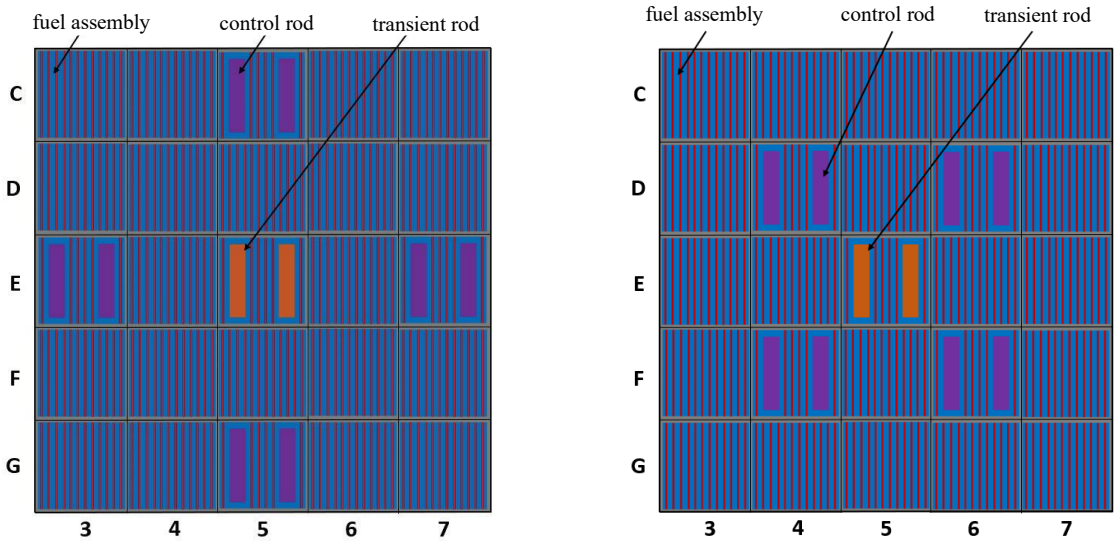


**SPERT-I core** **SPERT-IV core**

**Figure 4.1. SPERT-I (left) and SPERT-IV (right) D-12/25 Core Layouts.**

The SPERT-IV reactor conducted experiments with no pump in operation (i.e., the reactor was cooled by natural convection), as well as many experiments with forced flow provided by a coolant pump operating at various mass fluxes. The forced-flow rate in the core ranged between 0 and 5000 GPM, corresponding to channel inlet velocities between 0 and 3.66 m/s (12 ft/s). The nominal water level water above the core was 4.5 ft above the core in most experimental tests, resulting in a total inlet pressure at the bottom of the fuel assemblies of 143,900 Pa. The exception is SPERT-IV Test Cases B-17 to B-19, which have 2 ft water head above the fuel meat. The SPERT-IV D-12/25 experimental tests flow rate and range of reactivity insertions conditions are summarized in Table 4.1.

**Table 4.1. Flow Conditions and Reactivity Insertion for SPERT-IV D-12/25 Test Cases**

| SPERT -IV Test Case | Pump Flow Rate, (GPM) | Water Level Above Core (ft) | Reactivity Insertion Range ($) |
|---|---|---|---|
| B-1 to B-16 | 0 (no pump operating) | 4.5 | 0.80 – 1.91 |
| B-17 to B-19 | 0 (no pump operating) | 2.0 | 0.80 – 1.91 |
| B-20 to B-23 | 500 | 4.5 | 0.88 – 1.80 |
| B-24 to B-29 | 1000 | 4.5 | 0.88 – 1.80 |
| B-30 to B-33 | 2500 | 4.5 | 0.88 – 1.80 |
| B-34 to B-39 | 5000 | 4.5 | 0.88 – 1.80 |

The neutron flux was determined by measurements from several ion chambers. One was located in the core where the highest fission density was expected to be reached. Others were in the reflector. The knowledge of neutron flux was used to determine the reported power in the core. By integration of power versus time, the energy released at any time was found.

The temperatures of several fuel plate locations were measured by buried or attached surface thermocouples. Thermocouples were placed at carefully selected locations in the reactor core in order to determine the spatial shape of the temperature distribution. Pressure during the transient was measured in the reflector at several positions by strain gauges and transducers.

## 4.2 PARET/ANL Model and Comparisons of Results against SPERT-I and SPERT-IV D-12/25 Core

The PARET/ANL model for the SPERT-I core is very similar to that for the SPERT-IV D-12/25 core. It is composed of two channels: one hot channel used to predict the thermal hydraulics conditions in the hottest fuel plate of the core, and one average channel used to determine reactivity feedback of the core. The channels are subdivided into 20 axial nodes. The fuel plate has five interfaces (four sub-volumes) in the fuel meat and two sub-volumes in the cladding in order to track internal temperatures at seven interfaces. The code option IGEOM=0 for plate-type geometry was used. The inlet and outlet pressure loss coefficients in these experiments were set at 0.55 and 0.65, respectively. These factors account for the effect on pressure due to cross-section area changes between the end fittings and the heated channels.

All SPERT experiments were assumed to be started with a power level of 5 W, an inlet temperature of 20 °C, and with an unpressurized open pool. As indicated earlier, the 5 W value of power is an estimate rather than a measurement. Because the initial power is so small, the transient behavior is not sensitive to it. Small variations in this initial power only affect the time of a later power peak, and not the magnitude of the peak. It has no impact on the reactor period that is held during most of the time when power is rising exponentially, before any reactivity feedback effects become significant.

All reactivity insertion events were initiated by rapidly ejecting the transient rod from the core. In principle, the rod reactivity worth versus position is non-linear, and difficult to define precisely. The reactivity insertion was modeled as a ramp insertion with a duration of 70 ms. This ramp introduces the desired additional reactivity and puts the neutron flux amplitude on a period that depends upon the total reactivity inserted at the end of the ramp. A linear ramp is found to be adequate as shown by comparison to experiments. The reactivity insertion (in $) is derived at any time from interpolation within the linear ramp which extends over 70 ms. Table 9 input in PARET/ANL defines the height and duration of this ramp. After 70 ms, the reactivity insertion remains constant over the duration of the transient event.

Experiment tests B-1 to B-19 were conducted with initially static coolant where there was no pump in operation, and the reactor was cooled by natural convection. However, the thermal hydraulics model within the PARET/ANL code required a tiny nominal non-zero mass flow at steady-state. So, for modeling purposes, the input coolant mass flux is set as 3 kg/s/m$^2$ (0.1% of the full flow at 3.66 m/s, or 12 ft/s, in SPERT-IV). The input for the mass flux for different sets of test cases is described in Table 4.2.

**Table 4.2. Initial Mass Flux in PARET/ANL Model for SPERT-IV D-12/25 Test Cases**

| SPERT -IV Test Case | Mass Flux (kg/s/m$^2$) |
|---|---|
| B-1 to B-19 | 3. |
| B-20 to B-23 | 365. |
| B-24 to B-29 | 730. |
| B-30 to B-33 | 1825. |
| B-34 to B-39 | 3650. |

The IONEP=1 option is used to select the Sieder-Tate correlation for single phase heat transfer, and the McAdams correlation (ITWOP=1) is used for two-phase heat transfer. IMODE=1 is selected for the single-phase to two-phase transition model, and ICHF=0 is selected for the original DNB Tong correlation [2]. The IHT=0 option is selected for the SPERT-I and SPERT-IV B-1 to B-19 experimental campaigns where the reactor core is cooled by natural convection. This choice of the IHT option activates natural convection heat transfer correlation when Reynolds number is less than the user defined limit for laminar flow, REL_T. In this analysis, REL_T was set to 2300. For other SPERT-IV tests with forced flow, IHT=2 is used. The heat transfer coefficient for single phase flow will be calculated from the Rosenthal & Miller (R&M) correlation if it predicts higher heat transfer coefficients than those predicted by the natural convection heat transfer correlation or by the forced convection Sieder-Tate correlation.

Neutronics simulations for SPERT cores were not performed in the current analyses to obtain the power distributions or reactivity feedback coefficients. Instead, the power profile is assumed to have a cosine axial distribution throughout the event. The ratio of the peak local power density to the average core power density (PFQ) is set to 2.4 in the hot channel (as in Reference [23]) and 1.311 for the average channel (as in Reference [25]). The cosine shape of power distribution is modeled using 21 axial mesh nodes, as was historically modeled [25][26].

Following Ref. [25], the simulations in the current analyses have been run with temperature feedback coefficient DTMP=0.028008, and void feedback coefficient DVOID=0.4214, while the effect of Doppler reactivity feedback is ignored (i.e., GAMMA values are set to 0.0). This is because the fuel is HEU and therefore the U-238 content is very small at less than 7 wt.%. The Doppler effect from the U-235 is negligible. This is a reasonable (and conservative) approximation that could be improved by a detailed neutronics analysis in the future.

An automation script was created to run each experimental series for a given inlet flow rate, while varying the reactivity insertion with a uniform interval of 0.05 $ to obtain trends of various output variables. The peak power, energy release at peak power, and cladding surface temperature at peak power versus inverse reactor periods are plotted in Figure 4.2 for SPERT-I. The PARET/ANL results obtained using the current version of the code are consistent with the results obtained with a previous version in [25][26]. The trends for the peak power, energy release, and maximum cladding temperature are well captured by the code. The maximum cladding surface temperature at the peak power shows good agreement with the experimental data up to an inverse reactor period of 18.55 $s^{-1}$ (corresponding to a reactivity insertion of 1.13 $), and it is overestimated for higher reactivity insertions. Below this limit, the flow remains in single phase until the peak power is reached. For higher reactivity insertions, subcooled nucleate boiling and subcooled transition boiling regimes start to occur at several axial nodes before the peak power is reached.

Similar trends are observed for the SPERT-IV D-12/25 cases with the reactor core cooled by natural convection as show in Figure 4.3. These results are similar to the results obtained by a previous version of PARET/ANL in [26]. In that study, both PARET/ANL and RELAP5/MOD3.2 codes were used to simulate SPERT-IV D-12/25 with natural convection cooling conditions. The RELAP5/MOD3.2 code was modified to include the R&M correlation. The results showed that both PARET/ANL and the modified RELAP5/MOD3.2 code with the R&M correlation were in good agreement with each other and with the experimental results in the low reactivity range (<1.1 $). For higher reactivity insertions, PARET/ANL overestimated the maximum cladding surface temperature, but RELAP5/MOD3.2 predictions showed much deviated results from the experimental data. This was attributed to the inadequacy of boiling heat transfer correlations in RELAP5/MOD3.2 for low pressure applications.

Figure 4.4 to Figure 4.7 show the comparisons of SPERT-IV D-12/25 simulation results with experimental data for the peak power, energy at peak power, and maximum cladding surface temperature for the sets of test cases with 500 GPM, 1000 GPM, 2500 GPM, and 5000 GPM, respectively. Few experimental data points are available for comparisons with these test cases with forced flow compared to test cases with the reactor core cooled by natural convection. The first experimental data point is available at 1.14 $ reactivity insertion. The results reproduce the trends of the experimental data well; however, the prediction of the maximum cladding surface temperature is overestimated, which is a conservative prediction for the safety limit. These test cases with high reactivity insertions are characterized by violent and very rapid steam generation which are challenging to predict as heat transfer correlations for subcooled transition and film boiling regimes have high uncertainties.

Literature review shows that other experts in the research reactor safety community have been similarly challenged by the complexity of modeling the high reactivity insertion SPERT-IV D12/25 cases. Particularly, literature about SPERT-IV D12/25 simulations showed large discrepancies in the predictions compared to the experimental data. For instance, in the work reported in [27], the cladding surface temperature showed large variations in predictions depending on the selected DNB correlation. In [28], SPERT-IV D12/25 experiments were simulated using a coupled neutronics thermal hydraulics analysis and the results showed that the neutron fluxes compared well with the experimental data, but significant discrepancies were found for the cladding surface temperature predictions even for lower reactivity insertions of 0.88 $. The EUREKA-2/RR code was used in [29] to simulate SPERT-IV D12/25 experiments. Although the cladding surface temperature agreed with the experimental data, the peak power was greatly underestimated.

The time evolution of the power and maximum cladding surface temperature for SPERT-IV D-12/25 for the test case with a reactivity insertion of 1.15 $ and natural convection cooling are shown in Figure 4.8 and Figure 4.9, respectively. The time evolution of power takes a bell-shaped trend due to the initial increase of power following the reactivity insertion, and the quick decrease afterwards is caused by negative reactivity feedback effects. The event is terminated by control rod insertion at a predetermined time.

For test series characterized by higher inlet flow rate as in the series with inlet flow rate of 5000 GPM, power and temperature oscillations occurred due to cycles of steam bubble generation and collapse, leading to large fluctuations in reactivity feedback time and consequently power oscillations. This behavior is well reproduced in the PARET/ANL simulations as shown in Figure 4.10 and Figure 4.11 for the reactivity insertion of 1.14 $ and inlet flow rate of 5000 GPM.

For the high reactivity insertion cases, the overestimation of the cladding surface temperature in these cases is likely attributed to the high uncertainty in DNB correlations for subcooled transition and film

boiling regimes. The overestimation of the peak power may be partially attributed to coolant temperature and void feedback coefficients in the model, which were determined from prior work (i.e., [23], [25], [26]) based on limited information about the core and critical control rod positions. Also, it is noted that the predicted peak power is very sensitive to the reactivity insertion, and therefore to the experimental error in the measured (reported) value of the reactivity insertion. Additionally, the axial power distribution adopted in these simulations was assumed to be a cosine shape, which is an assumption expected to impact the predicted results for the axial temperature distribution. Nevertheless, the analysis showed that the code produced conservative results for safety limits with respect to the cladding surface temperature.

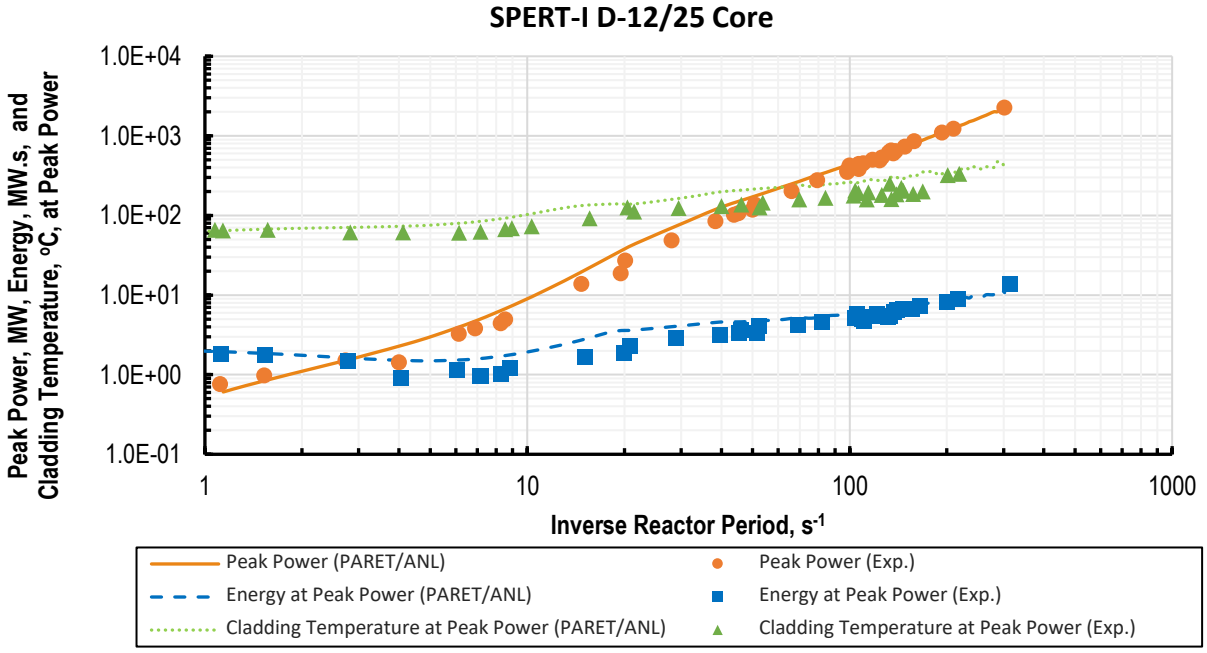


**Figure 4.2. Peak Power, Energy at Peak Power, and Cladding Surface Temperature at peak Power for SPERT-I.**

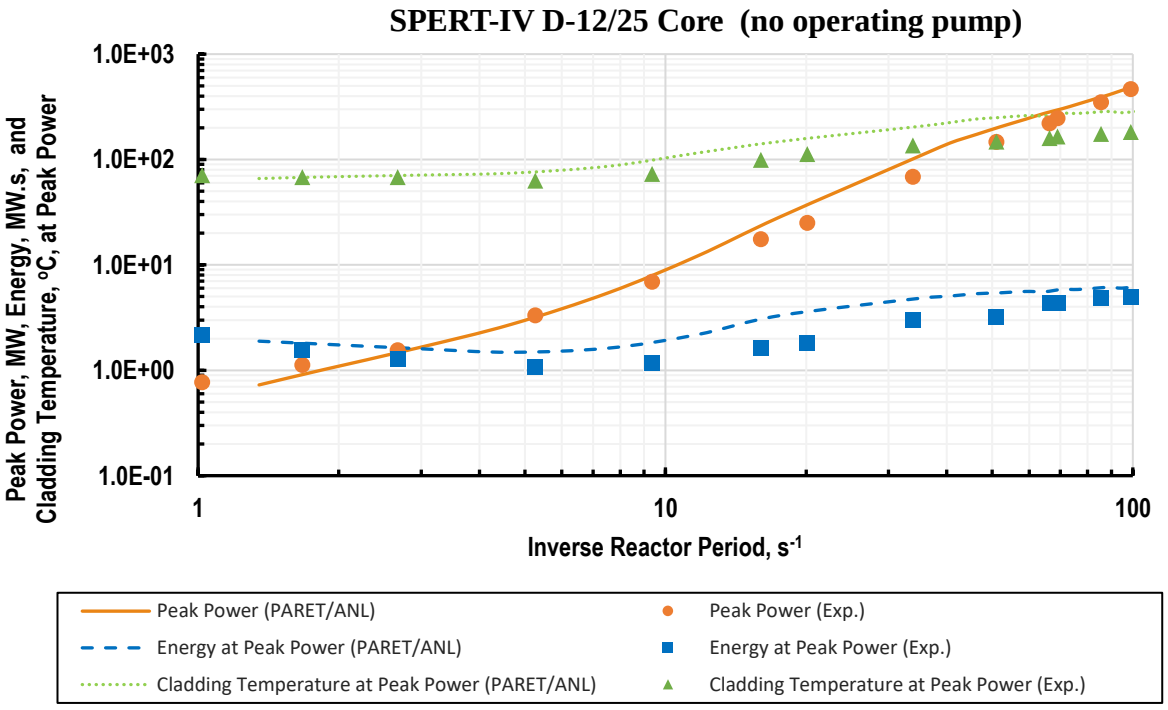


**Figure 4.3. Peak Power, Energy at Peak Power, and Cladding Surface Temperature at peak Power for SPERT-IV D-12/25 Core with no Operating Pump.**

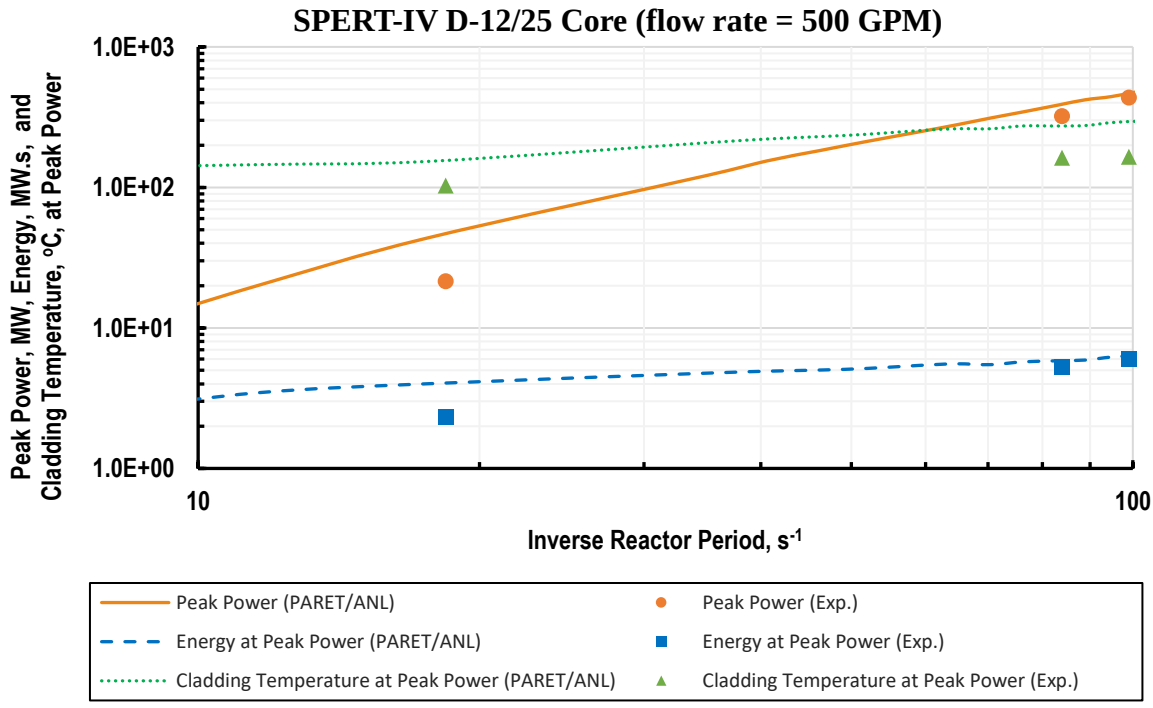


**Figure 4.4. Peak Power, Energy at Peak Power, and Cladding Surface Temperature at peak Power for SPERT-IV D-12/25 Core with 500 GPM Flow.**

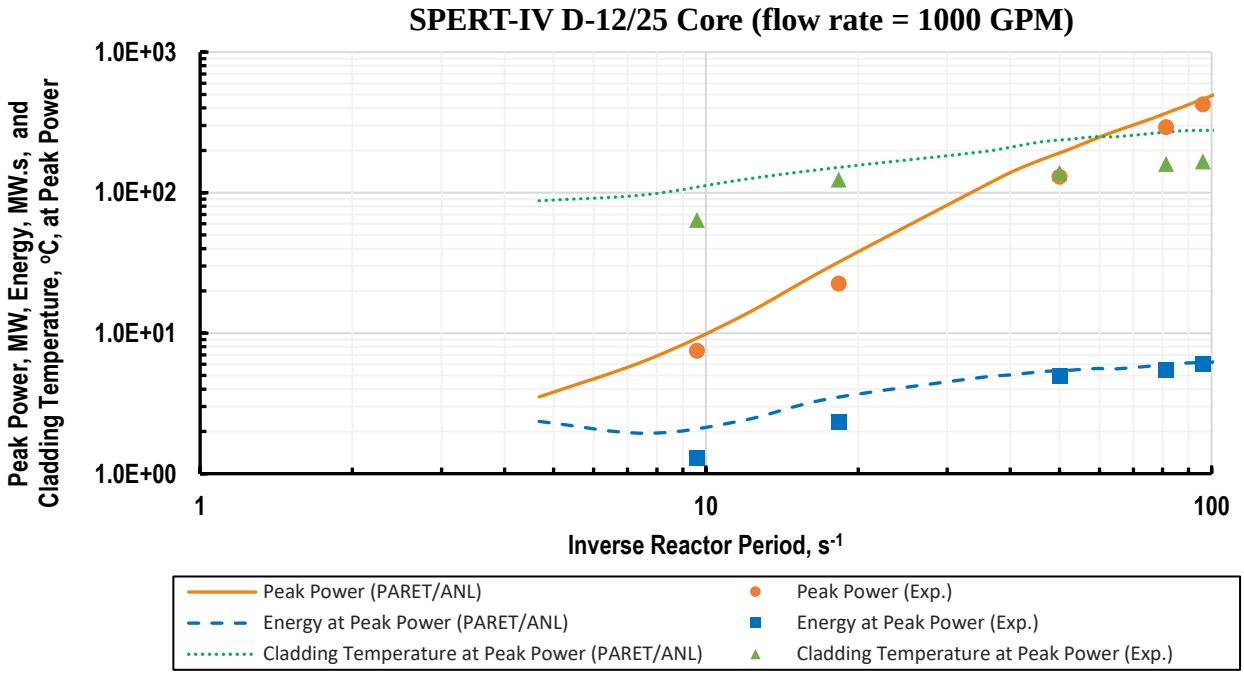


**Figure 4.5. Peak Power, Energy at Peak Power, and Cladding Surface Temperature at peak Power for SPERT-IV D-12/25 Core with 1000 GPM Flow.**

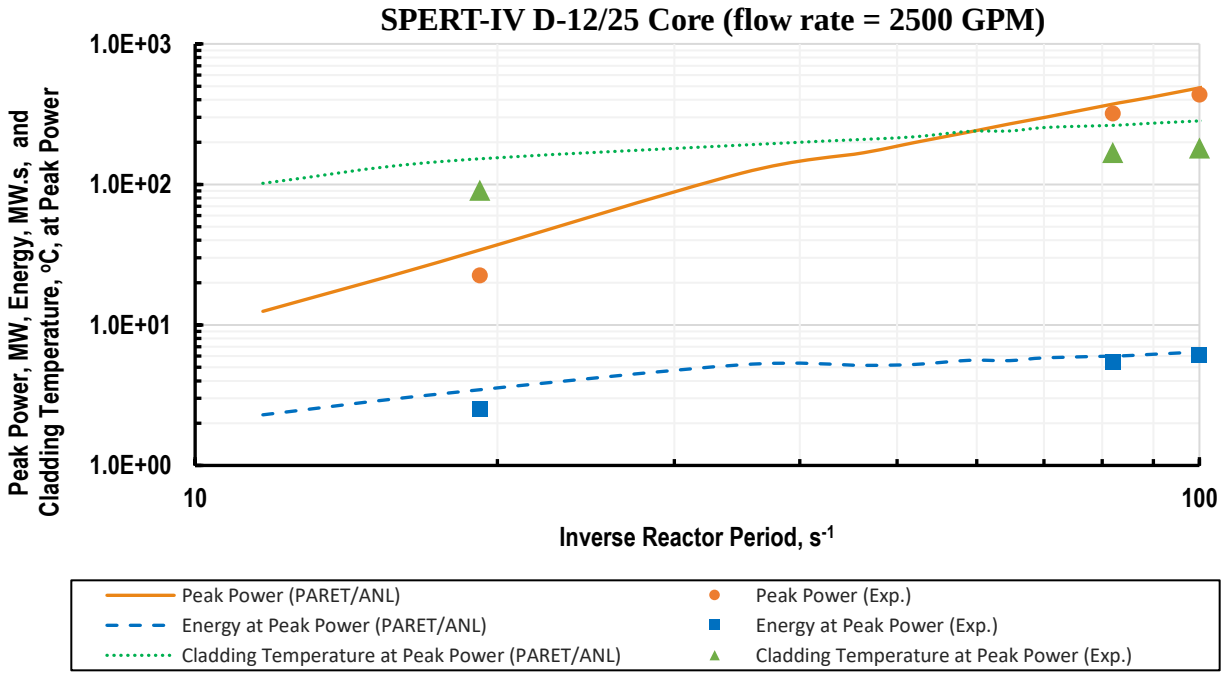


**Figure 4.6. Peak Power, Energy at Peak Power, and Cladding Surface Temperature at peak Power for SPERT-IV D-12/25 Core with 2500 GPM Flow.**

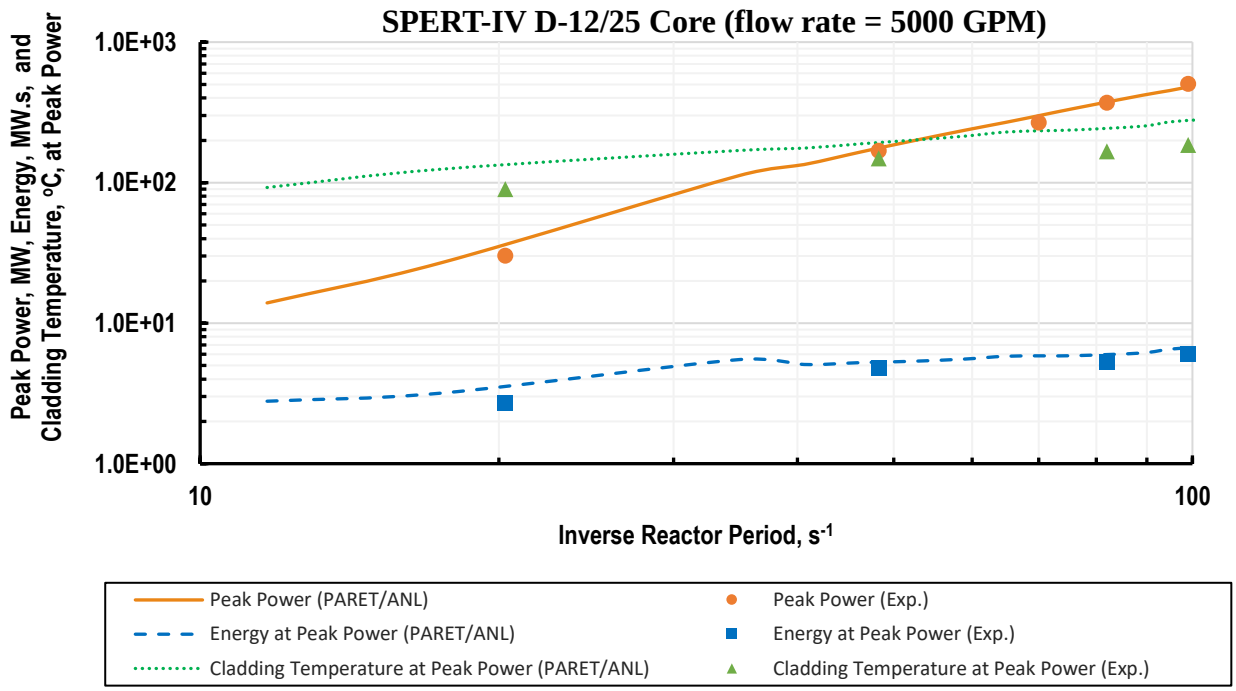


**Figure 4.7. Peak Power, Energy at Peak Power, and Cladding Surface Temperature at peak Power for SPERT-IV D-12/25 Core with 5000 GPM Flow.**

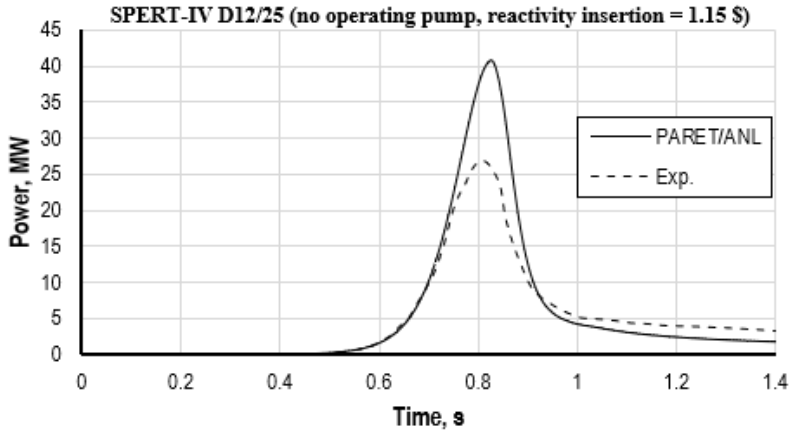


**Figure 4.8. Power versus Time (no operating pump, reactivity insertion = 1.15 $)**

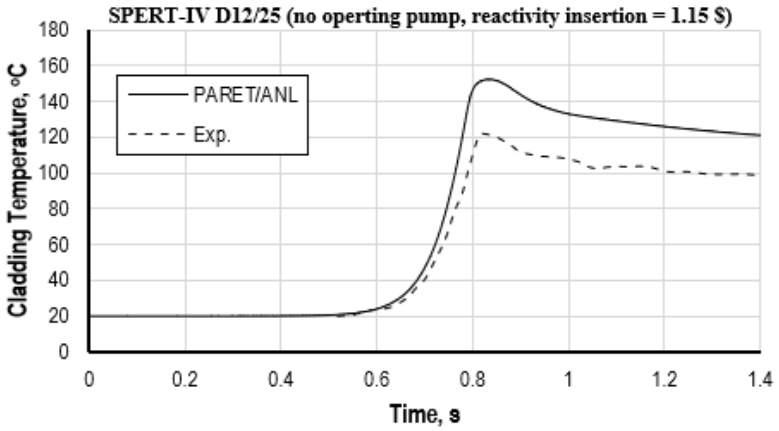


**Figure 4.9. Cladding Surface Temperature versus Time (no operating pump, reactivity insertion = 1.15 $)**

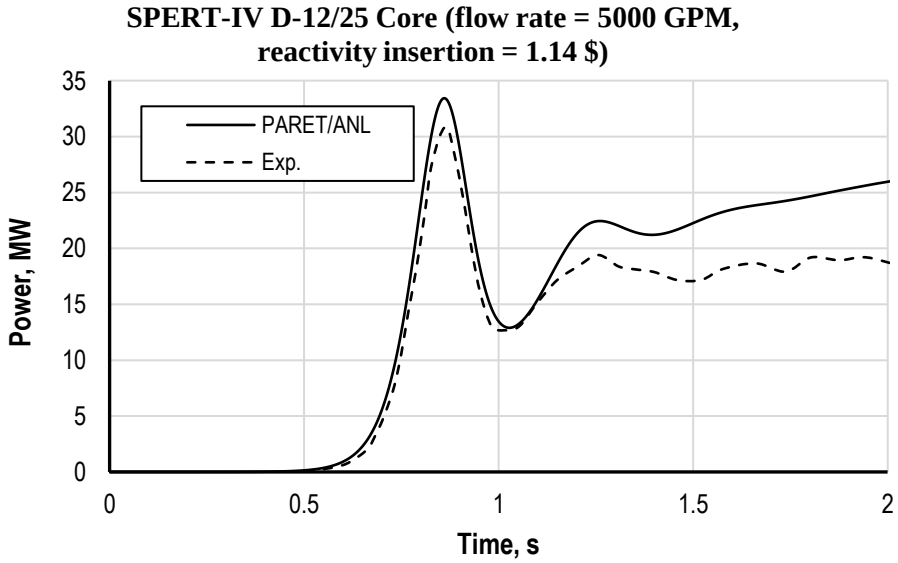


**Figure 4.10. Power versus Time (flow rate = 5000 GPM, reactivity insertion = 1.14 $).**

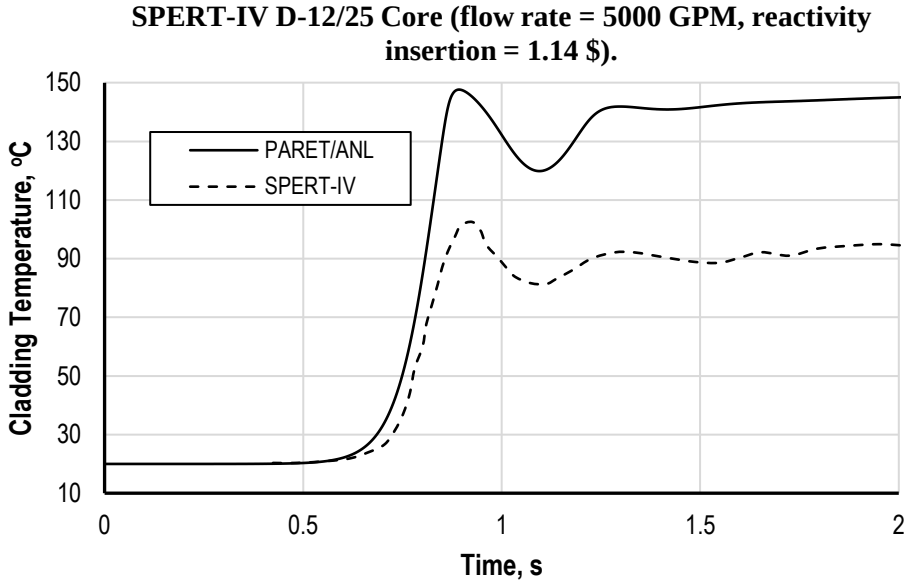


**Figure 4.11. Cladding Surface Temperature versus Time (flow rate = 5000 GPM, reactivity insertion = 1.14 $)**

# 5 Conclusions

The data and discussion presented in this report confirm that nine steady-state and six transient capabilities of PARET/ANL are implemented correctly. Furthermore, the code-to-code comparison between PARET/ANL and RELAP5 performed for scenarios involving nucleate boiling shows good agreement. These results provide strong evidence that the capabilities also work together correctly. Agreement of reference results with measured data for each case is consistent with the acceptance criteria identified in Table 1.2.

An integral reactor PARET/ANL model for SPERT-I and SPERT-IV experiments is validated by comparison of code results against experimental data. Good agreement is obtained for peak power for a wide range of experimental conditions. Cladding surface temperature predictions agree well for low reactivity insertion cases. For higher reactivity insertions, the discrepancy in cladding surface temperature increases but remains conservative. The discrepancy is mostly attributed to the uncertainty in modeling transition boiling encountered at these conditions.

# Acknowledgement

The authors greatly acknowledge contributions to PARET/ANL over its long history of development, including recent efforts for the detailed review and valuable suggestions provided by John Stillman (ANL) and Lap-Yan Cheng (BNL) during the NQA-1 compliant software dedication.

This work was sponsored by the U.S. Department of Energy, Office of Material Management and Minimization in the U.S. National Nuclear Security Administration Office of Defense Nuclear Nonproliferation under Contract DE-AC02-06CH11357.

# References


[1] C. F. Obenchain, *PARET - A program for the analysis of reactor transients*, Phillips Petroleum Company, AEC Research and Development Report, Reactor Technology, Idaho Falls, Idaho, IDO-17282, January 1969.

[2] A. P. Olson, M. Kalimullah, M. Sharabi, S. R. Yang, J. R. Licht, and J. W. Thomas, *PARET/ANL v7.7 User Guide*, ANL/RTR/TM-24/12, Argonne National Laboratory, Lemont, USA, March 2025.

[3] W. L. Woodruff and R. S. Smith*, A User Guide for the ANL Version of the PARET Code, PARET/ANL (2001 Rev.)*, ANL/RERTR/TM-16, Argonne National Laboratory, Lemont, IL, USA, March 2001.

[4] E. R. Cohen, "Some Topics in Reactor Kinetics," in Proc. 2nd. U.N. Intl. Conf. on the Peaceful Uses of Atomic Energy, Vol. 11, p. 302, Geneva, 1958.

[5] The RELAP5-3D Code Development Team, *RELAP5-3D Code Manual Volume I: Code Structure, System, Models, and Solutions Methods*, Idaho National Laboratory, INEEL-EXT-98-00834, Revision 2.4, Idaho Falls, Idaho 83415, June 2005.

[6] *Quality Assurance Requirements for Nuclear Facility Applications,* ASME NQA-1-2008/NQA-1a-2009, American Society of Mechanical Engineers, 2009.

[7] A. P. Olson, M. Kalimullah, S. H. Pham, *Verification and Validation of PARET/ANL V7.6*, ANL/RTR/TM-16/6-Rev. 1, Argonne National Laboratory, Lemont, USA, December 2020.

[8] H. J. White, International Association for the Properties of Steam (IAPS), Secretary, National Bureau of Standards, Washington, D.C., 1977, revised 1983.

[9] webbook.nist.gov/chemistry/, National Institute of Standards and Technology (NIST), 100 Bureau Drive, Gaithersburg, Maryland 20899, USA, 2011.

[10] E. W. Lemmon, I. H. Bell, M. L. Huber, M. O. McLinden, *NIST Standard Reference Database 10: Reference Fluid Thermodynamic and Transport Properties-REFPROP, Version 3.0*, National Institute of Standards and Technology, Standard Reference Data Program, Gaithersburg, 2013.

[11] R. E. Heffner, E. L. Morris, D. T. Jones, D. R. Seaman, and M. K. Shane, *SPERT IV Facility*, AEC Research and Development Report, Reactor Technology, Phillips Petroleum Company, Idaho Falls, Idaho, IDO-16745, February 1962.

[12] The RELAP5 Development Team*, RELAP5/MOD3.3 Code Manual*, *U.S. Nuclear Regulatory Commission,* Washington, DC 20555, March 2006.

[13] DUGONE, J. (Ed.), *SPERT III Reactor Facility: E-Core Revision*, AEC Research and Development Report IDO-17036, Phillips Petroleum Company, 1965.

[14] B. D. Ganapol, "A highly accurate algorithm for the solution of the point kinetics equations," *Annals of Nuclear Energy,* vol. 62, pp. 564-571, (2013).

[15] G. I. Bell and S. Glasstone, *Nuclear Reactor Theory*, New York: Van Nostrand Reinhold Company, 1970.

[16] A. C. Hindmarsh, *GEAR: Ordinary Differential Equation System Solver,* Lawrence Livermore Laboratory, Report UCID-30001, Rev. 3, 1974.

[17] IAEA, *Research Reactor Benchmarking Database: Facility Specification and Experimental Data*, IAEA, Technical Report Series No. 480, Vienna, 2015.

[18] A. P. Olson, *SPERT III E core: Facility specification*, IAEA Research Reactor Benchmarking Database: Facility Specification and Experimental Data, 2015.

[19] A. P. Olson, *Neutronics Calculations for SPERT-III, E-core*, ANL/GTRI/TM-13/10, Argonne National Laboratory, Lemont, IL, USA, May 30, 2013.

[20] A. P. Olson, *Consolidator's Report for the SPERT-III-Benchmark*, ANL/GTRI-TM-13/9, Argonne National Laboratory, Lemont, IL, USA, May, 2013.

[21] American Nuclear Society, *American National Standard Decay Heat Power in Light Water Reactors*, ANSI/ANS-5.1-2005, Approved April 1, 2005.

[22] American Nuclear Society, *Decay Energy Release Rates Following Shutdown of Uranium-Fueled Thermal Reactors*, Proposed ANS Standard, Approved by Subcommittee ANS-5, American Nuclear Society Standards Committee, October, 1971, Revised, October, 1973.

[23] R. W. Miller, A. Sola, R. K. McCardell, *Report of the SPERT I Destructive Test Program on an Aluminum, Plate-Type, Water-Moderated Reactor*, Phillips Petroleum Company, June 1964.

[24] J. G. Crocker, L. A. Stephan, *Reactor Power Excursion Tests in the SPERT IV Facility*, Report IDO-17000, Phillips Petroleum Company, August 1964.

[25] W. L. Woodruff, "A Kinetic and Thermal-Hydraulics Capability for the Analysis of Research Reactors," *Nuclear Technology*, vol. 64 (1984).

[26] W. L. Woodruff, N. A. Hanan, J. E. Matos, "A Comparison of the RELAP5/MOD3 and PARET/ANL Codes with the Experimental Data from SPERT-IV D-12/25 Series," RERTR meeting, Jackson Hole, WM, Oct. 5-10, 1997.

[27] S. Chatzidakis, A. Ikonomopoulos, S. E. Day, "PARET/ANL Modeling of a SPERT-IV Experiment under Different Departure from Nucleate Boiling Correlation," *Nuclear Technology*, vol. 177 (2012).

[28] M. Margulis, E. Gilad, "Simulations of SPERT-IV D12/15 Transient Experiments Using the System Code THERMO-T," *Progress in Nuclear Energy*, vol. 109 (2018).

[29] N. H. Bardun, M. H. Altaf, M. A. Motalab, M. S. Mahmood, M. J. H. Khan, "Modeling SPERT-IV reactivity initiated transient test in EUREKA-2/RR code," *Int. J. of Nuclear Energy* (2014).

# Appendix A Acceptance Criteria for Modification, Release, and Acceptance Testing

Development of PARET/ANL is controlled by a Software Quality Assurance Plan (SQAP), which complies with ASME NQA-1 2008 with the 2009 addenda [6]. There was an extensive effort to formalize the V&V case for PARET/ANL v7.6 and qualify it for use under the SQAP. Most of the test cases in Table 1.1, including their corresponding acceptance criteria, were established and documented in the PARET/ANL v7.6 V&V Report [7]. As part of the development process under the NQA-1 compliant SQAP, testing is regularly performed to ensure that the modified software produces results that satisfy the acceptance criteria established for PARET/ANL v7.6. By corollary, this process ensures that PARET/ANL v7.7 and future versions maintain agreement with the original comparisons to analytical solutions, hand calculations, other code calculations, and experimental measurements performed for the V&V testing of PARET/ANL v7.6. For each test case included in the test suite, key output parameters were selected for comparison. These output parameters, along with their anticipated output values and tolerances, for each test case, as provided in the tables following this Appendix. The names of output parameters in these tables are intended to be consistent with the text in the output file. The acceptance criterion for each test case is that the value of the output parameter produced by modified software must match the anticipated output value with a discrepancy less than the specified tolerance.

This testing is performed for each software modification, for version release, and for acceptance testing in a particular computing environment. For such code modifications and changes in computing environment, changes in the code predictions are anticipated to be small. Thus, the tolerances in the tables in this appendix are significantly smaller (i.e., tighter) than those for the V&V testing, which compared code predictions to analytical solutions, hand calculations, other code calculations, and experimental measurements. These tolerances allow for accepting insignificant differences caused by the compiler and/or host operation system changes. During the software development process, the anticipated output values and tolerances may be updated given a documented justification, should the need arise, e.g., if a bug in PARET/ANL is fixed.

The data provided by the main output file (*.out) is used to check most of the steady-state capabilities and data provided by the channel output files (*.out.ch*) are used for the transient capabilities. The reference time points of transient results are selected in order to confirm the data at important events such as initiating the reactor trip, starting of scram, peak power, etc.

In the following tables, the anticipated output values are the same as parameters edited in the output files. The tolerances are decided based on the number of meaningful digits after the decimal point that are edited in the output file or essential for the safety analysis.

**Table A.1. Test Cases A01_01 to A01_11 – Light Water Properties**

| Test Case | Reference Temp., °C | Output Parameter | Anticipated Output Value | Tolerance |
|---|---|---|---|---|
| A01_01 | 40.0 | Enthalpy, J/kg | 1.66959E+05 | 1.0E+01 |
| | | Thermal Conductivity, W/m.K | 6.34891E-01 | 1.0E-05 |
| | | Specific heat capacity, J/kg.K | 4.17606E+03 | 1.0E-01 |
| | | Density, kg/m$^3$ | 9.92497E+02 | 1.0E-02 |
| | | Viscosity, Pa.s | 6.52399E-04 | 1.0E-08 |
| | Saturation | Saturation temperature, °C | 9.96320E+01 | 1.0E-03 |
| | 139.0 | Enthalpy, J/kg | 2.75031E+06 | 1.0E+02 |
| | | Thermal Conductivity, W/m.K | 2.77929E-02 | 1.0E-06 |
| | | Specific heat capacity, J/kg.K | 2.04849E+03 | 1.0E-01 |
| | | Density, kg/m$^3$ | 5.28966E-01 | 1.0E-05 |
| | | Viscosity, Pa.s | 1.36424E-05 | 1.0E-09 |
| A01_02 | 56.0 | Enthalpy, J/kg | 2.33957E+05 | 1.0E+01 |
| | | Thermal Conductivity, W/m.K | 6.53131E-01 | 1.0E-05 |
| | | Specific heat capacity, J/kg.K | 4.18648E+03 | 1.0E-01 |
| | | Density, kg/m$^3$ | 9.85890E+02 | 1.0E-02 |
| | | Viscosity, Pa.s | 4.91984E-04 | 1.0E-08 |
| | Saturation | Saturation temperature, °C | 1.20231E+02 | 1.0E-02 |
| | 157.0 | Enthalpy, J/kg | 2.78138E+06 | 1.0E+02 |
| | | Thermal Conductivity, W/m.K | 2.95106E-02 | 1.0E-06 |
| | | Specific heat capacity, J/kg.K | 2.10285E+03 | 1.0E-01 |
| | | Density, kg/m$^3$ | 1.01957E+00 | 1.0E-04 |
| | | Viscosity, Pa.s | 1.43349E-05 | 1.0E-09 |
| A01_03 | 64.0 | Enthalpy, J/kg | 2.67740E+05 | 1.0E+01 |
| | | Thermal Conductivity, W/m.K | 6.61024E-01 | 1.0E-05 |
| | | Specific heat capacity, J/kg.K | 4.19342E+03 | 1.0E-01 |
| | | Density, kg/m$^3$ | 9.81945E+02 | 1.0E-02 |
| | | Viscosity, Pa.s | 4.36851E-04 | 1.0E-08 |
| | Saturation | Saturation temperature, °C | 1.51849E+02 | 1.0E-02 |
| | 185.0 | Enthalpy, J/kg | 2.82069E+06 | 1.0E+02 |
| | | Thermal Conductivity, W/m.K | 3.25566E-02 | 1.0E-06 |
| | | Specific heat capacity, J/kg.K | 2.27737E+03 | 1.0E-01 |
| | | Density, kg/m$^3$ | 2.43822E+00 | 1.0E-04 |
| | | Viscosity, Pa.s | 1.53826E-05 | 1.0E-09 |
| A01_04 | 72.0 | Enthalpy, J/kg | 3.01732E+05 | 1.0E+01 |
| | | Thermal Conductivity, W/m.K | 6.68106E-01 | 1.0E-05 |
| | | Specific heat capacity, J/kg.K | 4.19689E+03 | 1.0E-01 |
| | | Density, kg/m$^3$ | 9.77622E+02 | 1.0E-02 |
| | | Viscosity, Pa.s | 3.91277E-04 | 1.0E-08 |
| | Saturation | Saturation temperature, °C | 1.79883E+02 | 1.0E-02 |
| | 207.0 | Enthalpy, J/kg | 2.81862E+06 | 1.0E+02 |
| | | Thermal Conductivity, W/m.K | 3.56977E-02 | 1.0E-06 |
| | | Specific heat capacity, J/kg.K | 2.72942E+03 | 1.0E-01 |
| | | Density, kg/m$^3$ | 4.89382E+00 | 1.0E-04 |
| | | Viscosity, Pa.s | 1.61533E-05 | 1.0E-09 |
| A01_05 | 88.0 | Enthalpy, J/kg | 3.69840E+05 | 1.0E+01 |
| | | Thermal Conductivity, W/m.K | 6.79764E-01 | 1.0E-05 |
| | | Specific heat capacity, J/kg.K | 4.21425E+03 | 1.0E-01 |
| | | Density, kg/m$^3$ | 9.67718E+02 | 1.0E-02 |
| | | Viscosity, Pa.s | 3.26431E-04 | 1.0E-08 |
| | Saturation | Saturation temperature, °C | 2.12369E+02 | 1.0E-02 |

| | | | | |
|---|---|---|---|---|
| | 237.0 | Enthalpy, J/kg | 2.85878E+06 | 1.0E+02 |
| | | Thermal Conductivity, W/m.K | 4.06529E-02 | 1.0E-06 |
| | | Specific heat capacity, J/kg.K | 2.79808E+03 | 1.0E-01 |
| | | Density, kg/m$^3$ | 9.38521E+00 | 1.0E-04 |
| | | Viscosity, Pa.s | 1.72545E-05 | 1.0E-09 |
| A01_06 | 96.0 | Enthalpy, J/kg | 4.04346E+05 | 1.0E+01 |
| | | Thermal Conductivity, W/m.K | 6.84416E-01 | 1.0E-05 |
| | | Specific heat capacity, J/kg.K | 4.22119E+03 | 1.0E-01 |
| | | Density, kg/m$^3$ | 9.62441E+02 | 1.0E-02 |
| | | Viscosity, Pa.s | 3.00556E-04 | 1.0E-08 |
| | Saturation | Saturation temperature, °C | 2.33838E+02 | 1.0E-02 |
| | 255.0 | Enthalpy, J/kg | 2.86928E+06 | 1.0E+02 |
| | | Thermal Conductivity, W/m.K | 4.47594E-02 | 1.0E-06 |
| | | Specific heat capacity, J/kg.K | 2.93541E+03 | 1.0E-01 |
| | | Density, kg/m$^3$ | 1.39499E+01 | 1.0E-03 |
| | | Viscosity, Pa.s | 1.79254E-05 | 1.0E-09 |
| A01_07 | 104.0 | Enthalpy, J/kg | 4.38879E+05 | 1.0E+01 |
| | | Thermal Conductivity, W/m.K | 6.88250E-01 | 1.0E-05 |
| | | Specific heat capacity, J/kg.K | 4.22813E+03 | 1.0E-01 |
| | | Density, kg/m$^3$ | 9.56868E+02 | 1.0E-02 |
| | | Viscosity, Pa.s | 2.77417E-04 | 1.0E-08 |
| | Saturation | Saturation temperature, °C | 2.50333E+02 | 1.0E-02 |
| | 269.0 | Enthalpy, J/kg | 2.87040E+06 | 1.0E+02 |
| | | Thermal Conductivity, W/m.K | 4.86732E-02 | 1.0E-06 |
| | | Specific heat capacity, J/kg.K | 3.11279E+03 | 1.0E-01 |
| | | Density, kg/m$^3$ | 1.86152E+01 | 1.0E-03 |
| | | Viscosity, Pa.s | 1.84840E-05 | 1.0E-09 |
| A01_08 | 112.0 | Enthalpy, J/kg | 4.73454E+05 | 1.0E+01 |
| | | Thermal Conductivity, W/m.K | 6.91283E-01 | 1.0E-05 |
| | | Specific heat capacity, J/kg.K | 4.23508E+03 | 1.0E-01 |
| | | Density, kg/m$^3$ | 9.51047E+02 | 1.0E-02 |
| | | Viscosity, Pa.s | 2.56736E-04 | 1.0E-08 |
| | Saturation | Saturation temperature, °C | 2.63914E+02 | 1.0E-02 |
| | 279.0 | Enthalpy, J/kg | 2.86033E+06 | 1.0E+02 |
| | | Thermal Conductivity, W/m.K | 5.26262E-02 | 1.0E-06 |
| | | Specific heat capacity, J/kg.K | 3.34167E+03 | 1.0E-01 |
| | | Density, kg/m$^3$ | 2.35661E+01 | 1.0E-03 |
| | | Viscosity, Pa.s | 1.88959E-05 | 1.0E-09 |
| A01_09 | 120.0 | Enthalpy, J/kg | 5.09126E+05 | 1.0E+01 |
| | | Thermal Conductivity, W/m.K | 6.93585E-01 | 1.0E-05 |
| | | Specific heat capacity, J/kg.K | 4.23508E+03 | 1.0E-01 |
| | | Density, kg/m$^3$ | 9.45765E+02 | 1.0E-02 |
| | | Viscosity, Pa.s | 2.37768E-04 | 1.0E-08 |
| | Saturation | Saturation temperature, °C | 2.90512E+02 | 1.0E-02 |
| | 303.0 | Enthalpy, J/kg | 2.83529E+06 | 1.0E+02 |
| | | Thermal Conductivity, W/m.K | 6.28187E-02 | 1.0E-06 |
| | | Specific heat capacity, J/kg.K | 3.98254E+03 | 1.0E-01 |
| | | Density, kg/m$^3$ | 3.64777E+01 | 1.0E-03 |
| | | Viscosity, Pa.s | 2.01218E-05 | 1.0E-09 |
| A01_10 | 128.0 | Enthalpy, J/kg | 5.44784E+05 | 1.0E+01 |
| | | Thermal Conductivity, W/m.K | 6.95067E-01 | 1.0E-05 |
| | | Specific heat capacity, J/kg.K | 4.24202E+03 | 1.0E-01 |
| | | Density, kg/m$^3$ | 9.40394E+02 | 1.0E-02 |
| | | Viscosity, Pa.s | 2.20984E-04 | 1.0E-08 |
| | Saturation | Saturation temperature, °C | 3.10960E+02 | 1.0E-02 |

| | | | | |
|---|---|---|---|---|
| | 320.0 | Enthalpy, J/kg | 2.78545E+06 | 1.0E+02 |
| | | Thermal Conductivity, W/m.K | 7.49071E-02 | 1.0E-06 |
| | | Specific heat capacity, J/kg.K | 4.98390E+03 | 1.0E-01 |
| | | Density, kg/m$^3$ | 5.16182E+01 | 1.0E-03 |
| | | Viscosity, Pa.s | 2.15421E-05 | 1.0E-09 |
| A01_11 | 136.0 | Enthalpy, J/kg | 5.80428E+05 | 1.0E+01 |
| | | Thermal Conductivity, W/m.K | 6.95747E-01 | 1.0E-05 |
| | | Specific heat capacity, J/kg.K | 4.24896E+03 | 1.0E-01 |
| | | Density, kg/m$^3$ | 9.35000E+02 | 1.0E-02 |
| | | Viscosity, Pa.s | 2.06161E-04 | 1.0E-08 |
| | Saturation | Saturation temperature, °C | 3.27780E+02 | 1.0E-02 |
| | 334.0 | Enthalpy, J/kg | 2.71984E+06 | 1.0E+02 |
| | | Thermal Conductivity, W/m.K | 9.03523E-02 | 1.0E-06 |
| | | Specific heat capacity, J/kg.K | 6.58035E+03 | 1.0E-01 |
| | | Density, kg/m$^3$ | 6.99239E+01 | 1.0E-03 |
| | | Viscosity, Pa.s | 2.34782E-05 | 1.0E-09 |

**Table A.2. Test Cases A01_12 to A01_22 – Heavy Water Properties**

| Test Case | Reference Temp., °C | Output Parameter | Anticipated Output Value | Tolerance |
|---|---|---|---|---|
| A1_12 | 48.0 | Enthalpy, J/kg | 1.82168E+05 | 1.0E+01 |
| | | Thermal Conductivity, W/m.K | 6.16619E-01 | 1.0E-05 |
| | | Specific heat capacity, J/kg.K | 4.11059E+03 | 1.0E-01 |
| | | Density, kg/m$^3$ | 1.09784E+03 | 1.0E-01 |
| | | Viscosity, Pa.s | 6.78066E-04 | 1.0E-08 |
| | Saturation | Saturation temperature, °C | 1.01065E+02 | 1.0E-02 |
| | 141.0 | Enthalpy, J/kg | 2.54846E+06 | 1.0E+02 |
| | | Thermal Conductivity, W/m.K | 2.73183E-02 | 1.0E-06 |
| | | Specific heat capacity, J/kg.K | 1.86335E+03 | 1.0E-01 |
| | | Density, kg/m$^3$ | 5.87188E-01 | 1.0E-05 |
| | | Viscosity, Pa.s | 1.43659E-05 | 1.0E-09 |
| A1_13 | 56.0 | Enthalpy, J/kg | 2.15108E+05 | 1.0E+01 |
| | | Thermal Conductivity, W/m.K | 6.21460E-01 | 1.0E-05 |
| | | Specific heat capacity, J/kg.K | 4.10579E+03 | 1.0E-01 |
| | | Density, kg/m$^3$ | 1.09359E+03 | 1.0E-01 |
| | | Viscosity, Pa.s | 5.89049E-04 | 1.0E-08 |
| | Saturation | Saturation temperature, °C | 1.21408E+02 | 1.0E-02 |
| | 158.0 | Enthalpy, J/kg | 2.57370E+06 | 1.0E+02 |
| | | Thermal Conductivity, W/m.K | 2.92819E-02 | 1.0E-06 |
| | | Specific heat capacity, J/kg.K | 1.92634E+03 | 1.0E-01 |
| | | Density, kg/m$^3$ | 1.13547E+00 | 1.0E-04 |
| | | Viscosity, Pa.s | 1.50044E-05 | 1.0E-09 |
| A1_14 | 64.0 | Enthalpy, J/kg | 2.48173E+05 | 1.0E+01 |
| | | Thermal Conductivity, W/m.K | 6.25686E-01 | 1.0E-05 |
| | | Specific heat capacity, J/kg.K | 4.10486E+03 | 1.0E-01 |
| | | Density, kg/m$^3$ | 1.08901E+03 | 1.0E-01 |
| | | Viscosity, Pa.s | 5.18284E-04 | 1.0E-08 |
| | Saturation | Saturation temperature, °C | 1.52642E+02 | 1.0E-02 |
| | 186.0 | Enthalpy, J/kg | 2.61175E+06 | 1.0E+02 |
| | | Thermal Conductivity, W/m.K | 3.27972E-02 | 1.0E-06 |
| | | Specific heat capacity, J/kg.K | 2.06283E+03 | 1.0E-01 |
| | | Density, kg/m$^3$ | 2.70692E+00 | 1.0E-04 |
| | | Viscosity, Pa.s | 1.60176E-05 | 1.0E-09 |
| A1_15 | 80.0 | Enthalpy, J/kg | 3.14263E+05 | 1.0E+01 |
| | | Thermal Conductivity, W/m.K | 6.31983E-01 | 1.0E-05 |
| | | Specific heat capacity, J/kg.K | 4.11257E+03 | 1.0E-01 |
| | | Density, kg/m$^3$ | 1.07860E+03 | 1.0E-01 |
| | | Viscosity, Pa.s | 4.15251E-04 | 1.0E-08 |
| | Saturation | Saturation temperature, °C | 1.80367E+02 | 1.0E-02 |
| | 217.0 | Enthalpy, J/kg | 2.65332E+06 | 1.0E+02 |
| | | Thermal Conductivity, W/m.K | 3.67443E-02 | 1.0E-06 |
| | | Specific heat capacity, J/kg.K | 2.21204E+03 | 1.0E-01 |
| | | Density, kg/m$^3$ | 5.16336E+00 | 1.0E-04 |
| | | Viscosity, Pa.s | 1.71179E-05 | 1.0E-09 |
| A1_16 | 88.0 | Enthalpy, J/kg | 3.47885E+05 | 1.0E+01 |
| | | Thermal Conductivity, W/m.K | 6.34480E-01 | 1.0E-05 |
| | | Specific heat capacity, J/kg.K | 4.11724E+03 | 1.0E-01 |
| | | Density, kg/m$^3$ | 1.07326E+03 | 1.0E-01 |
| | | Viscosity, Pa.s | 3.77100E-04 | 1.0E-08 |
| | Saturation | Saturation temperature, °C | 2.12516E+02 | 1.0E-02 |

| | | | | |
|---|---|---|---|---|
| | 237.0 | Enthalpy, J/kg | 2.65571E+06 | 1.0E+02 |
| | | Thermal Conductivity, W/m.K | 4.12465E-02 | 1.0E-06 |
| | | Specific heat capacity, J/kg.K | 2.54819E+03 | 1.0E-01 |
| | | Density, kg/m$^3$ | 1.03393E+01 | 1.0E-03 |
| | | Viscosity, Pa.s | 1.76912E-05 | 1.0E-09 |
| A1_17 | 96.0 | Enthalpy, J/kg | 3.81530E+05 | 1.0E+01 |
| | | Thermal Conductivity, W/m.K | 6.36303E-01 | 1.0E-05 |
| | | Specific heat capacity, J/kg.K | 4.12203E+03 | 1.0E-01 |
| | | Density, kg/m$^3$ | 1.06761E+03 | 1.0E-01 |
| | | Viscosity, Pa.s | 3.44966E-04 | 1.0E-08 |
| | Saturation | Saturation temperature, °C | 2.33769E+02 | 1.0E-02 |
| | 255.0 | Enthalpy, J/kg | 2.65994E+06 | 1.0E+02 |
| | | Thermal Conductivity, W/m.K | 4.53687E-02 | 1.0E-06 |
| | | Specific heat capacity, J/kg.K | 2.82881E+03 | 1.0E-01 |
| | | Density, kg/m$^3$ | 1.55015E+01 | 1.0E-03 |
| | | Viscosity, Pa.s | 1.82441E-05 | 1.0E-09 |
| A1_18 | 104.0 | Enthalpy, J/kg | 4.15196E+05 | 1.0E+01 |
| | | Thermal Conductivity, W/m.K | 6.37462E-01 | 1.0E-05 |
| | | Specific heat capacity, J/kg.K | 4.12635E+03 | 1.0E-01 |
| | | Density, kg/m$^3$ | 1.06166E+03 | 1.0E-01 |
| | | Viscosity, Pa.s | 3.17492E-04 | 1.0E-08 |
| | Saturation | Saturation temperature, °C | 2.50098E+02 | 1.0E-02 |
| | 269.0 | Enthalpy, J/kg | 2.65834E+06 | 1.0E+02 |
| | | Thermal Conductivity, W/m.K | 4.92643E-02 | 1.0E-06 |
| | | Specific heat capacity, J/kg.K | 3.10175E+03 | 1.0E-01 |
| | | Density, kg/m$^3$ | 2.07960E+01 | 1.0E-03 |
| | | Viscosity, Pa.s | 1.86767E-05 | 1.0E-09 |
| A1_19 | 112.0 | Enthalpy, J/kg | 4.48878E+05 | 1.0E+01 |
| | | Thermal Conductivity, W/m.K | 6.37966E-01 | 1.0E-05 |
| | | Specific heat capacity, J/kg.K | 4.13002E+03 | 1.0E-01 |
| | | Density, kg/m$^3$ | 1.05543E+03 | 1.0E-01 |
| | | Viscosity, Pa.s | 2.93698E-04 | 1.0E-08 |
| | Saturation | Saturation temperature, °C | 2.63542E+02 | 1.0E-02 |
| | 279.0 | Enthalpy, J/kg | 2.64772E+06 | 1.0E+02 |
| | | Thermal Conductivity, W/m.K | 5.32649E-02 | 1.0E-06 |
| | | Specific heat capacity, J/kg.K | 3.41681E+03 | 1.0E-01 |
| | | Density, kg/m$^3$ | 2.64227E+01 | 1.0E-03 |
| | | Viscosity, Pa.s | 1.89634E-05 | 1.0E-09 |
| A1_20 | 120.0 | Enthalpy, J/kg | 4.83517E+05 | 1.0E+01 |
| | | Thermal Conductivity, W/m.K | 6.38656E-01 | 1.0E-05 |
| | | Specific heat capacity, J/kg.K | 4.12996E+03 | 1.0E-01 |
| | | Density, kg/m$^3$ | 1.04979E+03 | 1.0E-01 |
| | | Viscosity, Pa.s | 2.73356E-04 | 1.0E-08 |
| | Saturation | Saturation temperature, °C | 2.89846E+02 | 1.0E-02 |
| | 302.0 | Enthalpy, J/kg | 2.62410E+06 | 1.0E+02 |
| | | Thermal Conductivity, W/m.K | 6.36229E-02 | 1.0E-06 |
| | | Specific heat capacity, J/kg.K | 4.21823E+03 | 1.0E-01 |
| | | Density, kg/m$^3$ | 4.11533E+01 | 1.0E-03 |
| | | Viscosity, Pa.s | 1.97554E-05 | 1.0E-09 |
| A1_21 | 128.0 | Enthalpy, J/kg | 5.18116E+05 | 1.0E+01 |
| | | Thermal Conductivity, W/m.K | 6.38747E-01 | 1.0E-05 |
| | | Specific heat capacity, J/kg.K | 4.12972E+03 | 1.0E-01 |
| | | Density, kg/m$^3$ | 1.04392E+03 | 1.0E-01 |
| | | Viscosity, Pa.s | 2.55448E-04 | 1.0E-08 |
| | Saturation | Saturation temperature, °C | 3.10074E+02 | 1.0E-02 |

| | | | | |
|---|---|---|---|---|
| | 320.0 | Enthalpy, J/kg | 2.59109E+06 | 1.0E+02 |
| | | Thermal Conductivity, W/m.K | 7.52378E-02 | 1.0E-06 |
| | | Specific heat capacity, J/kg.K | 5.19450E+03 | 1.0E-01 |
| | | Density, kg/m$^3$ | 5.76353E+01 | 1.0E-03 |
| | | Viscosity, Pa.s | 2.05425E-05 | 1.0E-09 |
| A1_22 | 136.0 | Enthalpy, J/kg | 5.52672E+05 | 1.0E+01 |
| | | Thermal Conductivity, W/m.K | 6.38258E-01 | 1.0E-05 |
| | | Specific heat capacity, J/kg.K | 4.12991E+03 | 1.0E-01 |
| | | Density, kg/m$^3$ | 1.03784E+03 | 1.0E-01 |
| | | Viscosity, Pa.s | 2.39575E-04 | 1.0E-08 |
| | Saturation | Saturation temperature, °C | 3.26689E+02 | 1.0E-02 |
| | 333.0 | Enthalpy, J/kg | 2.53711E+06 | 1.0E+02 |
| | | Thermal Conductivity, W/m.K | 9.03124E-02 | 1.0E-06 |
| | | Specific heat capacity, J/kg.K | 6.69632E+03 | 1.0E-01 |
| | | Density, kg/m$^3$ | 7.78401E+01 | 1.0E-03 |
| | | Viscosity, Pa.s | 2.13215E-05 | 1.0E-09 |

**Table A.3. Test Cases A02_01 and A07_01 – Solid Properties and Nucleate Boiling Model**

| Test Case | Reference Time, s | Output Parameter | Anticipated Output Value | Tolerance |
|---|---|---|---|---|
| A02_01 | 9.90621E-01 | Reactor power, MW | 1.19325E+01 | 1.0E-03 |
| | | Max. cladding surface temp., °C | 1.1911E+02 | 1.0E-01 |
| | | Peak fuel temp., °C | 1.3399E+02 | 1.0E-01 |
| | 1.03963E+00 | Reactor power, MW | 4.13284E+01 | 1.0E-03 |
| | | Max. cladding surface temp., °C | 1.6454E+02 | 1.0E-01 |
| | | Peak fuel temp., °C | 2.0560E+02 | 1.0E-01 |
| | 1.13963E+00 | Reactor power, MW | 2.89987E+01 | 1.0E-03 |
| | | Max. cladding surface temp., °C | 1.7753E+02 | 1.0E-01 |
| | | Peak fuel temp., °C | 2.1214E+02 | 1.0E-01 |
| | 1.50000E+00 | Reactor power, MW | 3.22650E+01 | 1.0E-03 |
| | | Max. cladding surface temp., °C | 1.7921E+02 | 1.0E-01 |
| | | Peak fuel temp., °C | 2.1747E+02 | 1.0E-01 |
| | 2.00000E+00 | Reactor power, MW | 1.38861E+00 | 1.0E-04 |
| | | Max. cladding surface temp., °C | 6.3435E+01 | 1.0E-02 |
| | | Peak fuel temp., °C | 6.5366E+01 | 1.0E-02 |
| A07_01 | 9.90621E-01 | Reactor power, MW | 1.19325E+01 | 1.0E-03 |
| | | Max. cladding surface temp., °C | 1.1911E+02 | 1.0E-01 |
| | | Peak fuel temp., °C | 1.3399E+02 | 1.0E-01 |
| | 1.03963E+00 | Reactor power, MW | 4.13284E+01 | 1.0E-03 |
| | | Max. cladding surface temp., °C | 1.6455E+02 | 1.0E-01 |
| | | Peak fuel temp., °C | 2.0560E+02 | 1.0E-01 |
| | 1.13963E+00 | Reactor power, MW | 2.89987E+01 | 1.0E-03 |
| | | Max. cladding surface temp., °C | 1.8406E+02 | 1.0E-01 |
| | | Peak fuel temp., °C | 2.1844E+02 | 1.0E-01 |
| | 1.50000E+00 | Reactor power, MW | 3.22650E+01 | 1.0E-03 |
| | | Max. cladding surface temp., °C | 1.8638E+02 | 1.0E-01 |
| | | Peak fuel temp., °C | 2.2432E+02 | 1.0E-01 |
| | 2.00000E+00 | Reactor power, MW | 1.38861E+00 | 1.0E-04 |
| | | Max. cladding surface temp., °C | 6.3438E+01 | 1.0E-02 |
| | | Peak fuel temp., °C | 6.5370E+01 | 1.0E-02 |

*Note: Although these two capabilities are classified as steady-state, the transient test cases need to be used for the code-to-code comparison. Hence, the channel output files (*.out.ch02) are used for the acceptance test.*

**Table A.4. Test Cases A07_02 and A07_03 - Transition Boiling Heat Transfer**

| Test Case | Axial Node | Output Parameter | Anticipated Output Value | Tolerance |
|---|---|---|---|---|
| A07_02 | 2 | Heat Transfer Coefficient W/m$^2$.K | 32229.97 | 1.0E-01 |
| | | Cladding surface temp., °C | 330.42 | 1.0E-01 |
| | | Peak fuel temp., °C | 429.80 | 1.0E-01 |
| | 4 | Heat Transfer Coefficient W/m$^2$.K | 49534.78 | 1.0E-01 |
| | | Cladding surface temp., °C | 355.76 | 1.0E-01 |
| | | Peak fuel temp., °C | 526.46 | 1.0E-01 |
| | 6 | Heat Transfer Coefficient W/m$^2$.K | 55731.10 | 1.0E-01 |
| | | Cladding surface temp., °C | 364.96 | 1.0E-01 |
| | | Peak fuel temp., °C | 580.63 | 1.0E-01 |
| A07_03 | 1 | Heat Transfer Coefficient W/m$^2$.K | 32073.94 | 1.0E-01 |
| | | Cladding surface temp., °C | 313.81 | 1.0E-01 |
| | | Peak fuel temp., °C | 391.78 | 1.0E-01 |
| | 3 | Heat Transfer Coefficient W/m$^2$.K | 34852.19 | 1.0E-01 |
| | | Cladding surface temp., °C | 351.86 | 1.0E-01 |
| | | Peak fuel temp., °C | 480.96 | 1.0E-01 |
| | 5 | Heat Transfer Coefficient W/m$^2$.K | 35318.51 | 1.0E-01 |
| | | Cladding surface temp., °C | 378.66 | 1.0E-01 |
| | | Peak fuel temp., °C | 560.12 | 1.0E-01 |

*Note: Data are obtained at time 0.135 s for channel 3*

**Table A.5. Test Cases A03_01, A03_02, and A03_03 – Geometry Options**

| Output Parameter | | Anticipated Output Value | | | Tolerance |
|---|---|---|---|---|---|
| | | A03_01 | A03_02 | A03_03 | |
| Channel 1 | Power, MW | 7.50000E-01 | 1.50000E-01 | 7.49969E-01 | 1.00E-05 |
| | Flowrate, kg/s | 4.80000E+01 | 1.05547E+01 | 4.79986E+01 | 1.00E-03 |
| | Outlet temperature, °C | 2.37319E+01 | 2.33926E+01 | 2.37319E+01 | 1.00E-03 |
| | Surface heat flux, W/m$^2$ | 2.083333E+06 | 1.105354E+06 | 2.083306E+06 | 1.00E+02 |
| Channel 2 | Power, MW | 2.50000E-01 | 5.00000E-02 | 2.50031E-01 | 1.00E-05 |
| | Flowrate, kg/s | 8.00000E+00 | 1.63346E+00 | 8.00000E+00 | 1.00E-03 |
| | Outlet temperature, °C | 2.74826E+01 | 2.73290E+01 | 2.74836E+01 | 1.00E-03 |
| | Surface heat flux, W/m$^2$ | 2.083333E+06 | 1.105354E+06 | 2.083594E+06 | 1.00E+02 |
| Full Core | Power, MW | 1.00000E+00 | 2.00000E-01 | 1.00000E+00 | 1.00E-05 |
| | Flowrate, kg/s | 5.60000E+01 | 1.21882E+01 | 5.59986E+01 | 1.00E-03 |

**Table A.6. Test Cases A04_01, A04_02, A04_03, and A04_05 – Flow Options**

| Output Parameter | Anticipated Output Value | | | | Tolerance |
|---|---|---|---|---|---|
| | A04_01 | A04_02 | A04_03 | A04_05 | |
| Channel mass flux, kg/m$^2$s | 1.2789E+02 | 1.2789E+02 | 1.2789E+02 | 1.2789E+02 | 1.0E-02 |
| Outlet temperature, °C | 7.69202E+01 | 7.69212E+01 | 7.69202E+01 | 7.69209E+01 | 1.0E-03 |
| $\Delta P_{friction}$, Pa | 1.0309E-01 | 1.0309E-01 | 1.0309E-01 | 1.0309E-01 | 1.0E-05 |
| $\Delta P_{buoyancy}$, Pa | N/A | 1.00126E+02 | 1.00125E+02 | 1.00126E+02 | 1.0E-02 |

**Table A.7. Test Cases A05_01 to A5_10 – Single-phase Heat Transfer**

| Test Case | Anticipated Output Value | | Tolerance |
|---|---|---|---|
| | Reynolds Number | Heat Transfer Coefficient W/m$^2$.K | |
| A05_01 | 1987.01 | 2475.74 | 1.0E-01 |
| A05_02 | 1987.01 | 1165.77 | 1.0E-01 |
| A05_03 | 1987.01 | 1414.24 | 1.0E-01 |
| A05_04 | 3233.62 | 1936.89 | 1.0E-01 |
| A05_05 | 35464.75 | 7950.65 | 1.0E-01 |
| A05_06 | 35464.75 | 9475.26 | 1.0E-01 |
| A05_07 | 35464.75 | 10269.84 | 1.0E-01 |
| A05_08 | 63882.57 | 9294.79 | 1.0E-01 |
| A05_09 | 35464.75 | 9725.77 | 1.0E-01 |
| A05_10 | 35464.75 | 8884.06 | 1.0E-01 |
| A05_16 | 77451.69 | 42490.94 | 1.0E-01 |

*Note: Data are obtained at outlet axial node*

**Table A.8. Test Cases A05_11 to A05_15 – Transient Heat Transfer (Rosenthal & Miller) Options**

| Test Case | Reference Time, s | Output Parameter | Anticipated Output Value | Tolerance |
|---|---|---|---|---|
| A05_11 | 0.201 | Heat Transfer Coefficient W/m$^2$.K | 10267.59 | 1.0E-01 |
| A05_12 | 0.201 | Heat Transfer Coefficient W/m$^2$.K | 10267.59 | 1.0E-01 |
| A05_13 | 0.201 | Heat Transfer Coefficient W/m$^2$.K | 3810.74 | 1.0E-01 |
| A05_14 | 0.201 | Heat Transfer Coefficient W/m$^2$.K | 1623.88 | 1.0E-01 |
| A05_15 | 0.099 | Heat Transfer Coefficient W/m$^2$.K | 27304.54 | 1.0E-01 |

*Note: Data are obtained at node 1 of channel 1*

**Table A.9. Test Cases A06_01 and A6_02 – Fin or Bundle Effect**

| Test Case | Anticipated Output Value for Heat Transfer Coefficient, W/m$^2$.K | Tolerance |
|---|---|---|
| A06_01 | 19876.61 | 1.0E-01 |
| A06_02 | 22208.39 | 1.0E-01 |

*Note: Data are obtained at outlet axial node*

**Table A.10. Test Cases A08_01 to A08_04 – Friction Factor**

| Test Case | Anticipated Output Value for Friction Factor | Tolerance |
|---|---|---|
| A08_01 | 0.060933 | 1.0E-05 |
| A08_02 | 0.050778 | 1.0E-05 |
| A08_03 | 0.018682 | 1.0E-05 |
| A08_04 | 0.017343 | 1.0E-05 |

**Table A.11. Test Cases B01_05, B01_21, and B01_29 – Point Kinetic Model**

| Test Case | Reference Time, s | Anticipated Output Value for Reactor Power, MW | Tolerance |
|---|---|---|---|
| B01_05 (Step insertion) | 20.000 | 8.10772E-89 | 1.0E-93 |
| | 40.000 | 2.55936E-87 | 1.0E-91 |
| | 60.000 | 8.06436E-86 | 1.0E-90 |
| | 80.000 | 2.54095E-84 | 1.0E-88 |
| | 100.00 | 8.00614E-83 | 1.0E-87 |
| B01_21 (Ramp insertion) | 4.000 | 2.22844E-30 | 1.0E-34 |
| | 6.000 | 5.58205E-30 | 1.0E-34 |
| | 8.000 | 4.27863E-29 | 1.0E-33 |
| | 10.000 | 4.51164E-25 | 1.0E-29 |
| | 11.000 | 1.79221E-14 | 1.0E-18 |
| B01_29 (With feedback | 0.0500 | 1.20503E+01 | 1.0E-03 |
| | 1.0000 | 1.32499E+01 | 1.0E-03 |
| | 1.0412 | 4.07394E+01 | 1.0E-03 |
| | 1.1360 | 2.92622E+01 | 1.0E-03 |
| | 1.5000 | 3.24356E+01 | 1.0E-03 |

**Table A.12. Test Cases B02_01, B02_06, and B02_09 – Reactivity Feedback**

| Test Case | Reference Time, s | Output Parameter | Anticipated Output Value | Tolerance |
|---|---|---|---|---|
| B02_01 (Moderator) | 9.5000 | Reactor power, MW | 1.00129E+01 | 1.0E-03 |
| | | Total Reactivity, $ | 7.3181E-04 | 1.0E-07 |
| | 10.0000 | Reactor power, MW | 1.00137E+01 | 1.0E-03 |
| | | Total Reactivity, $ | 7.2701E-04 | 1.0E-07 |
| | 10.0900 | Reactor power, MW | 1.31707E+01 | 1.0E-03 |
| | | Total Reactivity, $ | 2.3786E-01 | 1.0E-04 |
| | 10.8000 | Reactor power, MW | 8.93769E-01 | 1.0E-05 |
| | | Total Reactivity, $ | -8.3796E+00 | 1.0E-03 |
| B02_06 (Doppler Effect) | 0.0500 | Reactor power, MW | 3.59685E+00 | 1.0E-04 |
| | | Total Reactivity, $ | 7.4951E-01 | 1.0E-04 |
| | 0.0860 | Reactor power, MW | 4.98817E+01 | 1.0E-03 |
| | | Total Reactivity, $ | 1.2839E+00 | 1.0E-03 |
| | 0.1243 | Reactor power, MW | 1.55893E+03 | 1.0E-01 |
| | | Total Reactivity, $ | 9.8598E-01 | 1.0E-04 |
| | 0.1500 | Reactor power, MW | 1.72169E+02 | 1.0E-02 |
| | | Total Reactivity, $ | 5.2295E-01 | 1.0E-04 |
| B02_09 (Thermal expansion) | 0.2000 | Reactor power, MW | 2.31344E-06 | 1.0E-10 |
| | | Total Reactivity, $ | 6.0000E-01 | 1.0E-04 |
| | 0.5000 | Reactor power, MW | 6.93118E-03 | 1.0E-07 |
| | | Total Reactivity, $ | 1.5000E+00 | 1.0E-03 |
| | 0.6000 | Reactor power, MW | 6.73889E+00 | 1.0E-04 |
| | | Total Reactivity, $ | 1.4982E+00 | 1.0E-03 |
| | 0.6400 | Reactor power, MW | 9.47129E+01 | 1.0E-03 |
| | | Total Reactivity, $ | 1.3409E+00 | 1.0E-03 |

**Table A.13. Test Cases B03_01 to B03_04 – Reactor Trip and Delay Time**

| Test Case | Reference Time, s | Output Parameter | Anticipated Output Value | Tolerance |
|---|---|---|---|---|
| B03_01 (Power trip) | 1.000 | Reactor power, MW | 3.20000E+01 | 1.0E-03 |
| | | Total Reactivity, $ | -2.8692E-08 | 1.0E-11 |
| | 1.052 | Reactor power, MW | 3.83999E+01 | 1.0E-03 |
| | | Total Reactivity, $ | 4.9780E-01 | 1.0E-04 |
| | 1.062 | Reactor power, MW | 3.94649E+01 | 1.0E-03 |
| | | Total Reactivity, $ | 4.9642E-01 | 1.0E-04 |
| | 1.072 | Reactor power, MW | 3.99618E+01 | 1.0E-03 |
| | | Total Reactivity, $ | 1.9409E-01 | 1.0E-04 |
| | 1.800 | Reactor power, MW | 3.47661E+00 | 1.0E-04 |
| | | Total Reactivity, $ | -1.4435E+01 | 1.0E-02 |
| B03_02 (Period trip) | 1.000 | Reactor power, MW | 3.20000E+01 | 1.0E-03 |
| | | Reactor period, s | 1.4254E+07 | 1.0E+04 |
| | 1.002 | Reactor power, MW | 3.22752E+01 | 1.0E-03 |
| | | Reactor period, s | 1.8798E-01 | 1.0E-04 |
| | 1.032 | Reactor power, MW | 3.61158E+01 | 1.0E-03 |
| | | Reactor period, s | 2.8380E-01 | 1.0E-04 |
| | 1.044 | Reactor power, MW | 3.68287E+01 | 1.0E-03 |
| | | Reactor period, s | 6.5878E+00 | 1.0E-03 |
| | 1.800 | Reactor power, MW | 3.45457E+00 | 1.0E-04 |
| | | Reactor period, s | -3.7924E+00 | 1.0E-03 |
| B03_03 (Flow trip) | 0.010 | Reactor power, MW | 3.20000E+01 | 1.0E-03 |
| | | Mass flux, kg/m2s | -8.1308E+03 | 1.0E+00 |
| | 0.800 | Reactor power, MW | 3.08944E+01 | 1.0E-03 |
| | | Mass flux, kg/m2s | -4.9143E+03 | 1.0E+00 |
| | 0.810 | Reactor power, MW | 3.08482E+01 | 1.0E-03 |
| | | Mass flux, kg/m2s | -4.7943E+03 | 1.0E+00 |
| | 1.400 | Reactor power, MW | 3.53737E+00 | 1.0E-04 |
| | | Mass flux, kg/m2s | -2.4530E+03 | 1.0E+00 |
| | 1.800 | Reactor power, MW | 3.32192E+00 | 1.0E-04 |
| | | Mass flux, kg/m2s | -8.1355E+02 | 1.0E-01 |
| B03_04 (Flow trip) | 4.000 | Reactor power, MW | 2.95275E+00 | 1.0E-04 |
| | | Mass flux, kg/m2s | -2.3301E+03 | 1.0E+00 |
| | 4.093 | Reactor power, MW | 2.95098E+00 | 1.0E-04 |
| | | Mass flux, kg/m2s | -2.3210E+03 | 1.0E+00 |
| | 4.113 | Reactor power, MW | 2.95059E+00 | 1.0E-04 |
| | | Mass flux, kg/m2s | -2.3191E+03 | 1.0E+00 |
| | 4.400 | Reactor power, MW | 1.07544E+00 | 1.0E-04 |
| | | Mass flux, kg/m2s | -2.2921E+03 | 1.0E+00 |
| | 10.000 | Reactor power, MW | 2.61430E-01 | 1.0E-05 |
| | | Mass flux, kg/m2s | -1.8305E+03 | 1.0E+00 |

**Table A.14. Test Cases B04_01 – Control Rod Reactivity**

| Reference Time, s | Output Parameter | Anticipated Output Value | Tolerance |
|---|---|---|---|
| 1.000 | Reactor power, MW | 3.20000E+01 | 1.0E-03 |
| | Total Reactivity, $ | 0.0000E+00 | 1.0E-03 |
| 1.052 | Reactor power, MW | 3.84065E+01 | 1.0E-03 |
| | Total Reactivity, $ | 5.0000E-01 | 1.0E-04 |
| 1.062 | Reactor power, MW | 3.94806E+01 | 1.0E-03 |
| | Total Reactivity, $ | 4.9824E-01 | 1.0E-04 |
| 1.072 | Reactor power, MW | 3.99852E+01 | 1.0E-03 |
| | Total Reactivity, $ | 1.9744E-01 | 1.0E-04 |
| 1.562 | Reactor power, MW | 3.63778E+00 | 1.0E-04 |
| | Total Reactivity, $ | -1.4540E+01 | 1.0E-02 |

**Table A.15. Test Cases B05_05 and B05_06 – Decay Heat**

| Test Case | Reference Time, s | Anticipated Output Value for Reactor Power, MW | Tolerance |
|---|---|---|---|
| B05_05 (ANS 2005) | 0.001 | 3.20000E+01 | 1.0E-03 |
| | 1.000 | 3.20000E+01 | 1.0E-03 |
| | 1.072 | 3.99618E+01 | 1.0E-03 |
| | 40.000 | 1.27221E+00 | 1.0E-04 |
| B05_06 (ANS 1973) | 0.001 | 3.20000E+01 | 1.0E-03 |
| | 1.000 | 3.20000E+01 | 1.0E-03 |
| | 1.072 | 3.99632E+01 | 1.0E-03 |
| | 40.000 | 1.34948E+00 | 1.0E-04 |

*Note: As the calculation of fission power can be confirmed by the previous test cases (B01_xx, B02_xx, B03_xx, and B04_xx), the checking of total power in these two cases is enough to ensure the calculation of decay heat using ANS2005 and ANS193 decay models.*

**Table A.16. Test Cases B06_03 – Power-Driven Mode**

| Reference Time, s | Output Parameter | Anticipated Output Value | Tolerance |
|---|---|---|---|
| 1.0000 | Reactor power, MW | 1.32499E+01 | 1.0E-03 |
| | Peak Fuel Temp., °C | 1.1338E+02 | 1.0E-01 |
| 1.0400 | Reactor power, MW | 4.07249E+01 | 1.0E-03 |
| | Peak Fuel Temp., °C | 1.6102E+02 | 1.0E-01 |
| 1.1400 | Reactor power, MW | 2.92730E+01 | 1.0E-03 |
| | Peak Fuel Temp., °C | 1.8275E+02 | 1.0E-01 |
| 1.5000 | Reactor power, MW | 3.24356E+01 | 1.0E-03 |
| | Peak Fuel Temp., °C | 1.9023E+02 | 1.0E-01 |
| 2.0000 | Reactor power, MW | 1.86803E+00 | 1.0E-03 |
| | Peak Fuel Temp., °C | 6.4078E+01 | 1.0E-02 |

**Table A.17. Test Cases C01_01 to C01_05 – SPERT-IV Experiments Validations**

| Test Case | Reference Time, s | Output Parameter | Anticipated Output Value | Tolerance |
|---|---|---|---|---|
| C01_01 | 0.676090 | Reactor power, MW | 5.90669E+01 | 1.0E-03 |
| | | Max. cladding surface temp., °C | 159.63 | 1.0E-01 |
| | | Peak fuel temp., °C | 180.92 | 1.0E-01 |
| | 0.748090 | Reactor power, MW | 1.03559E+01 | 1.0E-03 |
| | | Max. cladding surface temp., °C | 147.89 | 1.0E-01 |
| | | Peak fuel temp., °C | 156.21 | 1.0E-01 |
| C01_02 | 0.666 | Reactor power, MW | 8.00058E+01 | 1.0E-03 |
| | | Max. cladding surface temp., °C | 174.48 | 1.0E-01 |
| | | Peak fuel temp., °C | 199.29 | 1.0E-01 |
| | 0.852 | Reactor power, MW | 3.77723E+00 | 1.0E-03 |
| | | Max. cladding surface temp., °C | 129.84 | 1.0E-01 |
| | | Peak fuel temp., °C | 131.65 | 1.0E-01 |
| C01_03 | 0.676 | Reactor power, MW | 6.01123E+01 | 1.0E-03 |
| | | Max. cladding surface temp., °C | 157.35 | 1.0E-01 |
| | | Peak fuel temp., °C | 180.16 | 1.0E-01 |
| | 0.811 | Reactor power, MW | 4.83916E+00 | 1.0E-03 |
| | | Max. cladding surface temp., °C | 133.05 | 1.0E-01 |
| | | Peak fuel temp., °C | 135.44 | 1.0E-01 |
| C01_04 | 0.684 | Reactor power, MW | 6.44672E+01 | 1.0E-03 |
| | | Max. cladding surface temp., °C | 158.24 | 1.0E-01 |
| | | Peak fuel temp., °C | 183.74 | 1.0E-01 |
| | 0.70 | Reactor power, MW | 5.88059E+01 | 1.0E-03 |
| | | Max. cladding surface temp., °C | 167.09 | 1.0E-01 |
| | | Peak fuel temp., °C | 189.37 | 1.0E-01 |
| C01_05 | 0.681001 | Reactor power, MW | 6.02342E+01 | 1.0E-03 |
| | | Max. cladding surface temp., °C | 156.42 | 1.0E-01 |
| | | Peak fuel temp., °C | 180.06 | 1.0E-01 |
| | 0.891001 | Reactor power, MW | 1.46627E+01 | 1.0E-03 |
| | | Max. cladding surface temp., °C | 115.94 | 1.0E-01 |
| | | Peak fuel temp., °C | 121.76 | 1.0E-01 |

**Nuclear Science & Engineering Division**
Argonne National Laboratory
9700 South Cass Avenue, Bldg. 208
Argonne, IL 60439

www.anl.gov

Argonne National Laboratory is a U.S. Department of Energy laboratory managed by UChicago Argonne, LLC